RAPID STRENGTHENING OF SHORT-SPAN REINFORCED CONCRETE T-BEAMS WITH UNBONDED CARBON FIBRE REINFORCED POLYMER STRAPS

RENFORCEMENT RAPIDE DE POUTRES EN T EN BÉTON ARMÉ ET À COURTE PORTÉE AVEC DES BANDES DE POLYMÈRES RENFORCÉS DE FIBRES DE CARBONE LAMINÉES NON COLLÉES

A Thesis Submitted to the Division of Graduate Studies of the Royal Military College of Canada
by

Renée-Anne Paquet
Major

In Partial Fulfillment of the Requirements for the Degree of
Master of Applied Science in Civil Engineering

April 2025

Acknowledgments

The author would like to extend their heartfelt gratitude to her supervisors, Dr. R.G. Wight and Dr. M.-A. Dagenais for the invaluable guidance, advice, and support throughout the duration of this project.

The author also wishes to acknowledge the hard work done by the RMCC staff, with special thanks to Mrs. K. Mattson and Mr. A. Watson for their invaluable assistance. An even bigger thank you is extended to Mr. D. Gaskin, whose technical expertise and valuable suggestions greatly contributed to this research. His patience enduring the author's presence on a daily basis over several months, was appreciated. A huge thank you also goes to the O'Kelly Squadron Cadets: OCdts Nault-Robinson, Turner, and Donald, for their incredible hard work and dedication during this project. Finally, the author expresses gratitude to Capt. J. Kim and Ms. R. Starycki for generously taking time away from their own thesis work to provide help when it was needed the most.

The financial support of the Directorate of Combat Support Equipment Management (DCSEM 3) was appreciated as this worked formed a small portion of the larger effort regarding RMC support to military bridging for Canada and our allies.

Lastly, I would also like to express my deepest gratitude to my spouse Major Thomas van Beurden for his unwavering support and patience throughout this journey, especially during moments of anxiety. His encouragement and willingness to take on the role of the project's official photographer and sounding board made a world of difference, and this accomplishment would not have been possible without him.

Abstract

The ability to rapidly strengthen reinforced concrete structures is critical for military and emergency applications, where conventional strengthening techniques may be impractical due to time constraints. Military operations often rely on existing infrastructure, including short-span bridges in remote or less-traveled routes, which may be inadequate for supporting the heavy loads of military vehicles. Strengthening techniques for military engineers must allow for rapid implementation, use easily transportable materials, require minimal specialized tools and heavy equipment, and offer flexibility across various bridge conditions and configurations

This research evaluates the effectiveness of unbonded carbon fibre reinforced polymer (CFRP) straps with mechanical anchors as a rapid strengthening technique for simply supported short-span reinforced concrete bridges. An experimental program was conducted using six 6 m long T-beams that included two control specimens and four strengthened beams with single or double layers of CFRP straps and variations of a custom-designed mechanical anchor. The addition of tensioners during the application contributed to a more uniform strain distribution across the CFRP straps. The results demonstrated that unbonded CFRP systems can enhance load-carrying capacity, with strength increases of up to 22% with a double layer configuration. Additionally, the strengthening system improved serviceability by reducing deflections at high loads.

A numerical model was developed to predict the load-deflection response of the strengthened beams. The model appropriately represented overall trends and provided valuable insights into the structural behaviour despite some minor discrepancies that were observed when comparing the experimental results to the model.

The study confirms that unbonded CFRP using proper mechanical anchorage system is a viable technique for the rapid strengthening of short-span concrete T-beams, offering a practical alternative to bonded CFRP systems in time-sensitive applications. However, while the technique was proven effective, further research is recommended to optimize the anchor designs, integrate prestressing when appropriate, refine the numerical model to better capture nonlinear behaviour, and assess long-term performance under cyclic loading conditions.

Résumé

La capacité à rapidement renforcer les structures en béton armé est essentielle pour les applications militaires et d'urgence, où les techniques de renforcement conventionnelles peuvent s'avérer impraticables en raison de contraintes de temps. Les opérations militaires dépendent fréquemment des infrastructures existantes, notamment des ponts de courte portée situés sur des routes isolées ou peu fréquentées, qui peuvent être inadéquats pour supporter les charges lourdes des véhicules militaires. Les techniques de renforcement utilisées par les ingénieurs militaires doivent permettre une mise en œuvre rapide, utiliser des matériaux facilement transportables, nécessiter un minimum d'outils spécialisés et d'équipement lourd, et offrir une flexibilité d'adaptation selon l'état du pont.

Cette recherche évalue l'efficacité des bandes de polymère renforcé de fibres de carbone laminées (PRFC) non collées avec ancrages mécaniques comme technique de renforcement rapide des ponts en béton armé de courte portée simplement appuyés. Un programme expérimental a été réalisé avec six poutres de 6 mètres de long, comprenant deux spécimens de contrôles et quatre poutres renforcées avec une ou deux couches de bandes en PRFC et des variations d'un ancrage mécanique conçu sur mesure. L'ajout de tendeurs a contribué à une répartition plus uniforme des contraintes de déformations dans les bandes en PRFC. Les résultats ont démontré que les systèmes en PRFC non collées peuvent améliorer la capacité portante d'une poutre, avec une augmentation allant jusqu'à 22% avec la configuration à double couche. De plus, le système de renforcement a amélioré le comportement en service en réduisant la déflexion sous des charges plus élevées.

Un modèle numérique a été développé pour prédire la réponse charge-déflexion des poutres renforcées. Ce modèle a représenté de manière appropriée les tendances générales de la poutre en T et a fourni des informations utiles sur son comportement structurel. Cependant, certaines divergences ont été observées lors de la comparaison entre les résultats expérimentaux et le modèle.

L'étude confirme que l'utilisation des bandes de PRFC non collées avec un ancrage mécanique approprié est une technique viable pour le renforcement rapide des poutres en T béton armé de courte portée simplement appuyé, offrant une alternative pratique aux systèmes PRFC collés dans les applications sensibles au temps. Bien que cette technique ait prouvé son efficacité, des recherches supplémentaires sont recommandées pour optimiser la conception des ancrages, intégrer la précontrainte lorsque cela est approprié, affiner le modèle numérique afin de mieux capturer le comportement non linéaire et évaluer les performances à long terme dans des conditions de chargement cyclique.

Co-Authorship Statement

This thesis has been written in the manuscript-based format as outlined in the Royal Military College of Canada Thesis Preparation Guidelines. The author of this thesis, Major Renée-Anne Paquet, was the main contributor to the manuscript, with the co-authors providing guidance, advice, and feedback. As the author plans to submit the manuscript for publication in peer-reviewed journals, the manuscript will include both supervisors as co-authors.

Table of Contents

List of Figures

List of Tables

List of Symbols

b_f	width of the beam flange (mm)
b_w	width of the beam web (mm)
E_c	elastic modulus of concrete (MPa)
E_f	elastic modulus of CFRP (GPa)
E_s	elastic modulus of steel (GPa)
f_{fu}	tensile strength of CFRP (MPa)
f_r	concrete tensile strength (MPa)
f_y	yield strength of reinforcement steel (MPa)
F_u	ultimate strength of reinforcement steel (MPa)
f'_c	concrete compressive strength (MPa)
h_f	height of the flange (mm)
h_w	height of the web (mm)
I_{cr}	moment of inertia of the cracked cross-section (mm^4)
I_g	moment of inertia of the gross cross-section (mm^4)
M	bending moment (kN-m)
ε_c	strain of concrete (mm/mm)
ε_f	strain of CFRP (mm/mm)
ε_{sh}	strain of steel at hardening (mm/mm)
ε_u	strain of steel at ultimate (mm/mm)
ε_{xx}	longitudinal strain on the surface (mm/mm)
δ	deflection at mid-span (m)
φ	curvature (1/m)
ρ_{bal}	maximum reinforcement ratio
γ_c	density of concrete (kg/m^3)

List of Abbreviations

3D	Three-dimensional
ACI	American Concrete Institute
AFRP	Aramid Fibre Reinforced Polymer
CAF	Canadian Armed Forces
CB	Control Beam
CFRP	Carbon Fibre Reinforced Polymer
CSA	Canadian Standards Association
DIC	Digital Image Correlation
EB-FRP	Externally Bonded Fibre Reinforced Polymer
FRP	Fibre Reinforced Polymer
GFRP	Glass Fibre Reinforced Polymer
LVDT	Linear Variable Differential Transformer
NSM	Near-Surface Mounted
NSMR	Near-Surface Mounted Reinforcement
RC	Reinforced Concrete
RMCC	Royal Military College of Canada
SB	Strengthened Beam
UHPC	Ultra-High Performance Concrete

Chapter 1 - Introduction

1.1 General

When the Canadian military operates in theatre, whether for conflict, peacekeeping missions, training of foreign military, or disaster relief, safely reaching their destination is essential (North Atlantic Treaty Organization, 2019). In many foreign countries, Canadian military vehicles or allied military vehicles might exceed the load capacity of existing bridges, posing logistical and operational risks (MacDonald & Wight, 2022). Military forces typically maintain an inventory of standard bridges that can be rapidly assembled by military engineers. These resources, while invaluable, are both extremely limited and aging. Modernization initiatives, such as the procurement of advanced bridging systems are being implemented, however they are best used to overcome structures that have been severely damaged or destroyed or to cross gaps where no bridge exists (Department of National Defence, 2023). Consequently, the ability to rapidly strengthen existing bridges that may be understrength or lightly damaged becomes crucial. Appropriately designed and applied strengthening techniques may allow heavy vehicles to cross bridges technically rated as having insufficient capacity, increasing a commander's flexibility for manoeuvre and potentially saving time by shortening logistical supply routes.

The importance of effectively strengthening short-span bridges cannot be overstated, as these structures play an essential role in enabling access across all types of terrain. Smaller bridges on less traveled routes were the main focus of this research, as they are the most likely to be understrength and the easiest to strengthen. To meet military engineering requirements, any strengthening solution should meet the following criteria:

- **Rapid implementation.** The tempo of military operations is high, and strengthening techniques that can be applied within one working shift (one day or one night of work) are preferable.
- **Use easily transportable materials.** Materials should be lightweight and compact, suitable for air transport as well as occupying minimal space in military vehicles.
- **Involve minimal equipment and specialized tools/knowledge.** During military operations, heavy equipment resources are limited, therefore lightweight materials are preferred. Strengthening techniques that can be applied with simple and widely available tools, and limited specialized trade knowledge are also preferred.
- **Require limited access to the bridge structure.** During military operations, specialized equipment such as bridge access platforms are very limited resources that may be unavailable. Strengthening techniques that only require access to the region of the abutment (and/or pier) can significantly simplify that application process and facilitate rapid application.
- **Flexibility in application.** Bridges details vary and therefore techniques that can be applied in most situations (e.g. bridges of different span lengths, bridges with damage to concrete cover, bridges with pre-existing curvature, etc.) are preferred.

Effectively enhancing the structural integrity of bridges is a task that requires significant technical expertise and innovation (BMCDP, 2018). Over the years, a variety of strengthening techniques have been developed, however they may not have been proven to be suitable for implementation during military operations. These methods are often tailored to specific construction styles and materials. Similarly, the intent of this research was to investigate a rapid, field-applicable method, suitable for a military environment, to strengthen short-span simply supported concrete T-beams bridges and increase their capacity within a single working shift.

Fibre reinforced polymer (FRP) materials offer an attractive solution for strengthening because they are lightweight, reducing the need for heavy equipment, have a high strength-to-weight ratio, and are relatively easy to apply, requiring few specialized skills (Wight et al., 2001) (Polymer Process, n.d.). Traditional bonded carbon fibre reinforced polymer (CFRP) methods have been widely studied for bridge strengthening and the design and application of this strengthening technique is codified (CSA, 2021; CSA, 2019) but may require extensive surface preparation (Ostrowski & Furtak, 2021), extensive access to the soffits of the bridge structure, and significant curing time for the epoxy, which may be impractical in time-sensitive military settings. In contrast, unbonded CFRP would bring out the best qualities of bonded CFRP while eliminating time-consuming disadvantages. The performance of bridges largely depends on the condition and properties of the concrete beams and girders, which are important load-carrying elements (Wight et al., 2001). By using unbonded CFRP, this strengthening method becomes applicable not only to understrength bridge but also to damaged ones (ACI 440, 2023). The absence of bonding would effectively eliminate the need to repair the concrete before strengthening the structure. The applicability of unbonded CFRP for bridge strengthening is inherently limited by its span, given that the portion of load carried by the CFRP will decrease as the span increases. For longer spans, effective strengthening can be achieved through the application of prestressing techniques (Motavalli et al., 2011). Considering the critical role that strengthening short-span bridges can play in military operations, unbonded and non-prestressed applications was the focus of this research.

This research builds on limited existing studies on unbonded CFRP applications (Wang et al., 2024), as bonded methods are typically the norm for strengthening with CFRP, thus addressing a key gap in the field of rapid bridge strengthening. By researching and testing this technique, the study aims not only to expedite the strengthening process but to also ensure that military operations can proceed without significant delays, enhancing the operational capabilities of the Canadian Armed Forces and allies.

1.2 Aim and Objectives of the Research

The aim of this research was to investigate a rapid strengthening method for simply supported short-span reinforced concrete (RC) T-beam bridges, enhancing their load-carrying capacity and serviceability to support military operations. Given the Canadian Armed Forces' (CAF) limited capacity for over-bridging operations, this study seeks to address a critical need for time-efficient solutions that enable the safe and reliable passage of military vehicles. To achieve this aim, the research focused on two key objectives:

1) Developing and applying a rapid strengthening method using unbonded CFRP straps to reinforce short-span reinforced concrete T-beams; and
2) Assessing the effectiveness of the technique by evaluating its impact on the serviceability and load-carrying capacity of the strengthened structures.

1.3 Scope

To achieve the aim and objectives of this research, a comprehensive literature review was conducted on the subject of strengthening concrete structures. Based on the findings, an experimental program was developed. An existing bridge design was used to determine an appropriate beam specimen aspect ratio and size, leading to the design of six large-scale reinforced concrete T-beams (0.5 m high × 1 m wide × 6 m long) to ensure realistic testing conditions. All six beams were constructed identically, and anchors were designed with a focus on time efficiency and ease of application.

The level of strengthening targeted during this experimental program was a 12 to 15% increase in ultimate load capacity of the strengthened beam. This level was pursued to ensure that the strengthening technique, if applied in a field situation, would significantly increase the range of military traffic that could traverse a structure and sufficiently warrant the time and effort invested. The level was also chosen to ensure that the risk of over-reinforcement, loss of ductility or an unexpected mode of failure was low.

The strengthening approach needed to be time-efficient and logistically feasible, eliminating the need for scaffolding or epoxy bonding, which are both time-consuming and resource-intensive. Given the constraints of limited time and manpower, the research specifically focused on short-span structures and non-prestressed applications. These structures were selected due to their relatively simple access to abutments, as well as the absence of piers, both of which simplify the overall strengthening process.

All beams were tested under identical conditions to assess their ultimate load capacity and load-deflection behavior. The experimental program included two control beams and four strengthened beams. Additionally, tensile tests of the reinforcement bars and concrete compressive tests were conducted to ensure that accurate material properties would be used in the predictive model that was also developed. This simple predictive model was developed to provide insight into how a beam's load-deflection behaviour would respond when strengthened using unbonded CFRP straps.

The scope of this research was limited to short single-span structures, strengthened using materials readily available to CAF Engineers, with the exception of the CFRP. By focusing on these elements, this research aims to provide practical, rapid-strengthening solutions that enhance the operational capabilities of the Canadian Armed Forces while minimizing downtime and resource expenditure.

1.4 Contents

Five chapters are included in this document, following the manuscript-based format guideline laid out by the Royal Military College of Canada (RMCC). The current chapter, Chapter 1, covers the background, aim and scope of this research project. Chapter 2 is a literature review of some of the existing strengthening techniques and anchorage systems that currently exist on the market. Chapter 3 is a stand-alone paper that covers the experimental program, including the specimens and strengthening details and the results of the beam testing. This chapter also includes the application of a numerical predictive model representing the behaviour of the strengthened beams. Chapter 4 provides a summary of the research project and includes recommendations for future research on the subject. All cited sources and references used throughout the document can be found in Chapter 5.

Appendices follow Chapter 5. They include additional information, pictures and drawings on the design and construction of the beams and strengthening process. Background information on the theory behind the predictive model can also be found in the appendices.

Chapter 2 - Literature Review

2.1 General

The primary objective of this experimental program, as outlined in Chapter 1, was to develop a rapid strengthening technique for short-span reinforced concrete (RC) T-beams. The technique was specifically selected to be suitable for military operations, where resources such as manpower, equipment and time are limited. With proper preparation, it is anticipated that a team of military engineers should be able to complete the essential work required for strengthening in less than a day.

This chapter offers a summary of relevant background information to give readers a broad understanding of topics that are not directly discussed within the manuscript of Chapter 3. It provides an overview of essential terminology and explores some of the existing strengthening techniques for flexural members that are currently employed globally, in particular, the use of Fibre Reinforced Polymers (FRP) as a strengthening material. Methods discussed include external prestressed tendons, externally bonded FRP sheets and Near Surface Mounted Reinforcement (NSMR) which are widely accepted strengthening techniques and are used in practical applications. The use of prestressed bonded FRP sheets is a technique less developed but is of great interest as a method to efficiently and effectively use the FRP and the very limited existing and related work on unbonded FRPs, the focus of the research work in this thesis, is also covered. Non-FRP strengthening methods, such a steel plate bonding and Ultra-High Performance Concrete (UHPC) jacketing, are briefly introduced. Additionally, this chapter includes a short review of different types of anchors available on the market or in research applications, which are used to hold CFRP plates or straps and are integral to strengthening processes similar to the one applied in this research.

2.2 Terminology

The terms "repair," "retrofit," "rehabilitation," and "strengthening" are often used interchangeably in the context of concrete structures. However, each refers to distinct interventions that address different aspects of a structure’s performance and condition. Repair and rehabilitation are the two main categories while retrofitting and strengthening are subsets of rehabilitation. When none of these measures are sufficient, a structure may need to be replaced, though this option is costly and time-consuming (Vp, 2023).

According to the ACI Concrete Terminology page (ACI, 2013), the term "repair" or "restore" refers to action taken to address damaged, deteriorated, or faulty elements or materials of a concrete structure, without making any improvement over the initial design. The primary focus of repair is to restore structure’s integrity and bring it back to a serviceable state, preventing further deterioration and extending its lifespan (Ganesh & Murthy, 2019). Common repair techniques include patching cracks, replacing spalled concrete, injecting epoxy resin, or repairing reinforcement corrosion.

In contrast to repair, rehabilitation involves not just restoring a structure but also enhancing its performance and mechanical properties beyond the original design specifications and bringing it to a desired condition (ACI 562, 2016) This process may include retrofitting and strengthening measures to improve compressive, flexural, or shear strength, addressing issues like durability and resistance to environmental factors, as well as enhancing the service life and load-carrying capacity. Rehabilitation is often used when a structure is showing signs of age or wear, and simply repairing the damage would not be sufficient to meet modern standards. It might involve replacing old materials, upgrading to more durable ones, or enhancing resistance to forces like fatigue, seismic activity, or thermal stresses (Roy & Saha, 2024).

Retrofitting is a subset of rehabilitation that involves modifying an existing structure to improve its performance, safety, and functionality. These modifications are normally necessary to meet updated codes or design standards and often include the addition of new components such as beams, columns, shear walls, or seismic resilience features, as well as jacketing (Khode, 2019).The goal of retrofitting is to enhance the overall functionality, resilience, and serviceability of a structure, particularly when it must comply with new regulations or adapt to the requirements of modern safety, environmental, or load standards. Retrofitting can involve substantial changes that elevate the structure's performance beyond its original design (Alaee & Karihaloo, 2003); (Ganesh & Murthy, 2019).

Strengthening, the topic of this document, focuses on increasing the load-bearing capacity of a structure beyond its original design limits (ACI 562, 2016). This can be required when a structure must be adapted to new usage or when additional loads are anticipated, such as in the case of increased traffic for bridges or additional floors in buildings. Strengthening normally involves the addition of materials such as FRP, steel plates, or concrete overlays, or even structural modifications like the installation of braces, shear walls, or additional reinforcement. Strengthening ensures that a structure can carry higher loads and perform safely under extreme conditions. This process is often used when the existing structure is structurally sound but requires enhanced capabilities to meet current or future demands (Ganesh & Murthy, 2019), however strengthening can still be used for damaged structures when cost is an issue (Heiza et al., 2014) or when it is essential for operational needs to use the damaged structure.

2.3 Existing strengthening techniques

Strengthening RC structures is essential for improving their load-bearing capacity, durability, and overall performance. Over time, various techniques have been developed and refined to address the new needs of a structure. This section provides an overview of some of the most widely used and effective methods, including external prestressed steel tendons, FRPs in bonded, unbonded, and prestressed forms, as well as other commonly used techniques such as steel plate bonding and jacketing. Each method offers distinct advantages and challenges, making them essential tools in structural engineering.

2.3.1 External Prestressed Tendons

External prestressing is a widely used strengthening and rehabilitation technique initially developed for bridges but also applicable to other structures (Harajli, 1993). This method involves placing tendons outside the structure, which are then prestressed and anchored at the ends, sometimes with deviators along the length of the structure, to alter the tendon profile and improve force transfer, as illustrated in Figure 2-1. The primary advantage of this method is its simplicity and cost-effectiveness, making it a popular choice for enhancing the load-carrying capacity of concrete, steel, and timber structures (Nordin, 2004).

In this system, the prestressing force is transferred through the anchors and deviators rather than relying on direct bond with the concrete. This is an advantage for aging infrastructure, as the tendons can be installed without requiring extensive repairs (Preto, 2014). However, since the tendons are located away from the center of mass of the concrete beams, the anchorage of the tendons create major shear forces (Virgoleux, 1990). Steel tendons can be adjusted over time to compensate for losses in prestress or adapt to changing loading conditions (Nordin, 2004).

The prestressing tendons are usually made of high-strength steel, a widely used and robust material. However, FRP tendons are also an option. Compared to high-strength steel tendons, FRP tendons offer advantages such as higher resistance against corrosion and fatigue, and a high strength-to-weight ratio. However, their cost is higher, their resistance to UV radiation is lower, they are much more difficult to anchor, and they present a linear behavior up to failure, lacking the ductility of steel (Preto, 2014; Burningham et al., 2014).

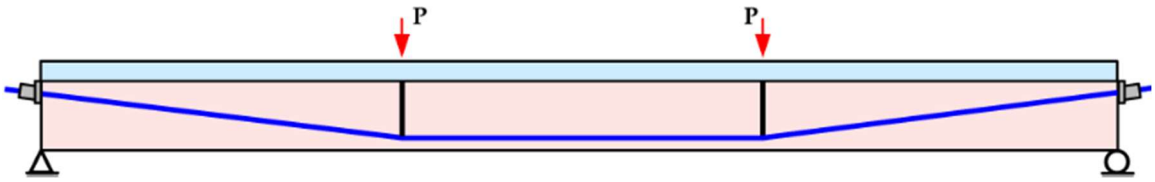

Figure 2-1. Example of an Externally Prestressed Beam (Yan, Chen, Han, Xie, & Sun, 2022)

Above and beyond the benefits in flexural strengthening, adding tensile reinforcement can also enhance shear resistance by improving crack control in the strengthened beam. If the additional tensile reinforcement is prestressed during the strengthening process, even greater concurrent enhancements in both flexural and shear behavior can be achieved (Porteous, 2001).

2.3.2 Fibre Reinforced Polymers

Various types of FRPs exist, most commonly including Carbon Fibre Reinforced Polymer (CFRP), Glass Fibre Reinforced Polymer (GFRP), and Aramid Fibre Reinforced Polymer (AFRP). These composite materials are highly versatile and have been utilized in a range of industries before gaining widespread popularity in structural engineering. Their ability to provide high-strength reinforcement without significantly increasing the weight of structures makes them ideal for strengthening and retrofitting (Ganesh & Murthy, 2019).

In Figure 2-2, the stress-strain curve of CFRP, GFRP and ARFP is compared to those of reinforcement steel and prestressed steel. The curves demonstrate that CFRP, GFRP, and AFRP materials exhibit high strength and a linear-elastic non-ductile behaviour until failure. Stiffnesses of FRP vary from moderate to high stiffness for CFRPs. The non-prestressed CFRP's high stiffness and strength is comparable to prestressed steel, highlighting its potential as effective alternative for structural strengthening.

FRPs are commonly used to reinforce existing buildings, bridges, and other infrastructure to improve their performance and extend their lifespan, as they stand out as some of the most effective strengthening methods to enhance the ultimate load-bearing capacity of existing RC structures (Panahi et al., 2021). The versatility and durability of FRP materials make them a popular choice for addressing challenges in structural engineering, offering solutions for both new constructions and the rehabilitation of aging infrastructure (Zhang et al., 2020). They also offer a resistance to chemicals and corrosion, and low thermal expansion (Bhatt & Goe, 2017).

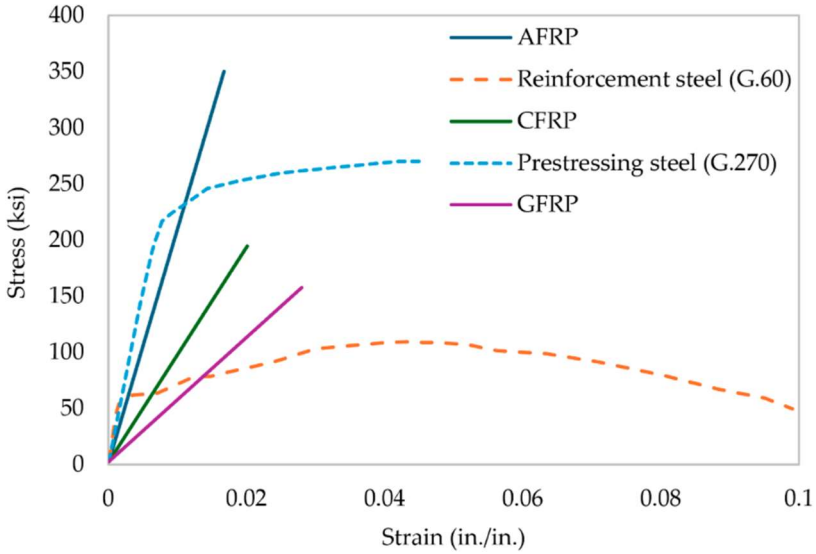

Figure 2-2. Comparison of steel with different FRP materials (Saeed, 2016)

2.3.2.1 Bonded FRP

Bonded FRP systems can be put into two distinct categories, externally bonded and near-surface mounted (NSM). Each method strengthens reinforced concrete elements by enhancing their flexural and shear resistance, but they differ in application, failure modes, and practical considerations.

Externally Bonded FRP

As shown on Figure 2-3, the externally bonded FRP (EB-FRP) method involves bonding one or more layer of FRP sheets or laminates to the concrete surface in order to increase the flexural or shear strength. CFRP sheets are the most commonly used material for the externally bonded

technique. In Canada, the design of these bonded FRP strengthening techniques for reinforced concrete is fully codified for buildings (CSA S806-12 (R2021)) and for bridges (CSA, S6-19).

The EB-FRP systems provide an additional layer of reinforcement that works in conjunction with the existing concrete, improving its structural performance under various loading conditions (Panahi et al., 2021). The FRP sheets help distribute loads more effectively, enhancing both flexural and shear strength, making structures more resilient, while also helping to control crack propagation by reducing the width and number of cracks in the concrete (Hammad et al., 2024).

However, the performance of EB-FRP systems depends significantly on proper surface preparation. The concrete substrate must be clean, roughened, and free of contaminants to ensure optimal bond strength. Inadequate surface preparation can lead to premature debonding and reduced strengthening efficiency. Additionally, EB-FRP sheets are sensitive to moisture and UV exposure, often requiring protective coatings when applied in outdoor environments (ACI 440, 2023).

A major limitation of EB-FRP systems is their reliance on epoxy, which requires precise application and has a time-temperature-dependent curing process (ACI 440, 2023). This can extend construction timelines, making the method less ideal for projects requiring rapid execution. Additionally, applying epoxy in confined or overhead spaces adds complexity, making the process labor-intensive and sometimes messy.

The primary mode of failure for externally bonded FRP systems, as highlighted in ACI 440.2-23, is premature debonding, especially in areas of high flexural or shear stress. This typically happens when laminates peel away from the concrete surface due to stress concentrations. It can occur as intermediate crack debonding, where it starts with a flexural crack and propagates along the bond interface or an end debonding, where it starts at the end of the CFRP and propagates towards the mid-span (Teng et al., 2003). The CFRP can also fail when its tensile strength is exceeded. Anchorage failure is the third most common type of failure for CFRP systems, where the inadequate anchorage leads to detachment.

Near-Surface Mounted (NSM) FRP

The NSM technique consists of embedding glass, aramid or carbon FRP bars (or plates) into pre-cut grooves filled with high-strength epoxy to securely bond the bars (or plates) to three sides of the structure, as shown in Figure 2-3. This configuration reduces the stress concentrations at the bond interface, decreasing the likelihood of debonding (El-Hacha & Rizkalla, 2004). Compared to EB-FRP, NSM is particularly advantageous when there are space limitations or when aesthetic considerations are important, as the FRP bars are embedded in the concrete, leaving the surface cleaner and less prone to damage. It is also less susceptible to environmental degradation, offering a better protection against moisture and UV exposure (Panahi et al., 2021). In different studies, it is shown that NSM-reinforced (NSMR) concrete elements exhibit lower deflection and smaller crack widths, with further reductions as the reinforcement ratio increases. However, while NSM reinforcement generally maintains ductility, excessive reinforcement may lead to a reduction in ductile behavior (Hammad et al., 2024).

The effectiveness of NSMR depends on the bond properties of the epoxy with the reinforcement bars themselves and the surrounding concrete in the groove (Hassan, 2002). The primary mode of failure for NSMR systems is also debonding. However, unlike externally bonded FRP, the debonding in NSMR systems generally occurs at the epoxy-concrete interface rather than directly between the FRP and concrete. This failure is primarily due to shear stress concentration and is influenced by the groove dimensions and mechanical properties of the materials. The second type of failure is influenced by high tensile stresses at the interface and groove dimensions. This failure is initiated by splitting of the epoxy, which progresses to the CFRP-epoxy interface. The CFRP in NSMR system can also fail due to tensile rupture at midspan. Similarly to the externally bonded applications, this failure indicates that the tensile capacity of the bars is exceeded (El-Hacha & Rizkalla, 2004). Despite these challenges, NSMR offers advantages such as better bond performance, improved tensile strength utilization, protection against environmental conditions, and reduced risk of premature debonding (Hammad et al., 2024).

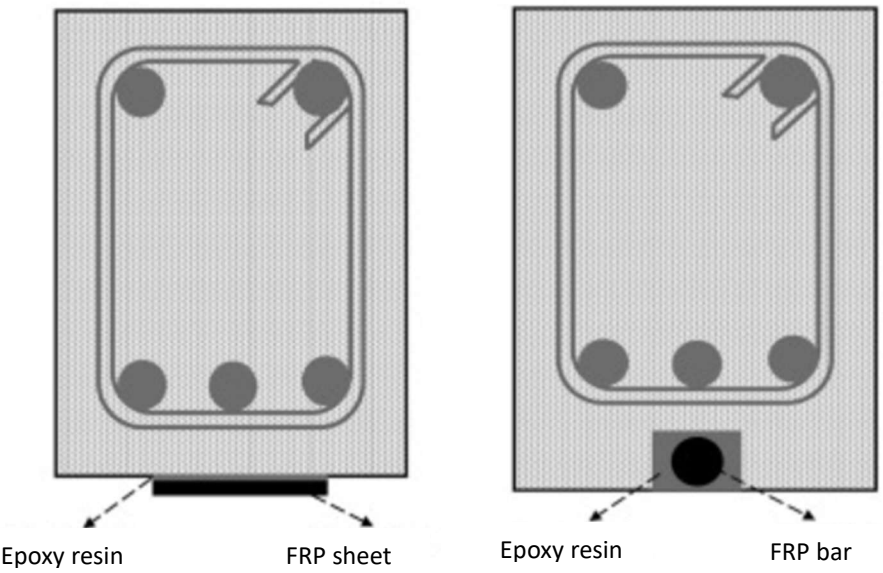

Figure 2-3. Strengthening of RC beam with bonded FRP material (Panahi, Zareei, & Izadi, 2021)

Limitations Bonded Methods

The bonded sheets or NSMR methods, while effective, present several challenges that need to be addressed during both the planning and execution phases to ensure that the bond between the FRP and concrete remains strong and durable over time. Both methods require curing, extending the construction timeline, which can be a drawback in projects that require quick turnaround times. The liquid nature of the epoxy requires precision during application, especially when working in confined or difficult-to-reach areas, such as underneath the structure. A key challenge with the externally bonded FRP techniques is the use of epoxy, which not only requires careful application

but also has a time-temperature-dependent curing time, as noted in ACI 440.2-23. This makes the method time-consuming and messy, despite its relative simplicity.

Traditional bonded FRP systems may not be ideal for military applications, not only due to their time-consuming installation but also because of their dependence on specific weather conditions. Epoxy adhesives, which are critical to the bonding process, are highly sensitive to temperature and humidity levels, often requiring controlled environments for proper application. Additionally, the proper storage of epoxy materials is essential to maintain their effectiveness, which may not be feasible in the field under unpredictable or harsh conditions. Furthermore, the bonded systems rely on the quality of the concrete cover. In zones of operations and in developing areas, it is likely that the concrete cover may be of lower quality or significanly damaged, potentially reducing the effectiveness and reliability of bonded strengtheneing techniques. These practical limitations make bonded systems less suitable for many scenarios encountered in military operations.

2.3.2.1.1Prestressed CFRP Sheets and Laminates

Prestressed CFRP is a subset of bonded CFRP and has been investigated in the early 1990s (Saadatmanesh & Ehsani, 1991) (Triantafillou & Deskovic, 1991) since bonded CFRP without prestressing utilizes only about 20% to 50% of their tensile strength (Piatek et al., 2020). When prestressing CFRP, it can significantly enhance the serviceability and durability of a RC structure by reducing crack widths and delaying their onset, minimizing deflections and curvature failures. Similar to the non-prestressed version, these sheets improve load-bearing capacity, efficiently utilizing CFRP's high tensile strength and increasing structural resilience, using the material more efficiently and engaging a higher portion of their strength compared to non-prestressed material (Motavalli et al., 2011). The prestressing process also reduces tensile stresses in the reinforcement and delays yielding (Wight et al., 2001). In contrast to non-prestressed bonded system, it helps close existing crack, which can help prevent moisture ingress and further improve the durability of the structure (El-Hacha et al., 2001).

However, the transfer of prestress to concrete can induce severe shear stresses at the interface between the FRP and the beam, requiring additional strengthening to prevent premature debonding failures (Motavalli et al., 2011). The application of prestressed CFRP involves careful preparation, specialized equipment, and labor-intensive procedures, making it a complex and costly process (El-Hacha, Wight, & Green, 2001). The implementation of a prestressed CFRP system necessitates the development of a suitable anchorage solution (Jumaat et al., 2011). Despite these challenges, its effectiveness in enhancing the load capacity and durability of RC structures makes it a valuable strengthening solution. However, the application of prestressed CFRP laminates in the field is more complex compared to non-prestressed methods, requiring careful planning and execution (Wight, 1998).

2.3.2.2 Unbonded CFRP

Unbonded CFRP systems, offer a viable alternative to traditional bonded CFRP methods. These systems differ by the absence of adhesives or fasteners, using only end anchorages to transfer loads.

This significantly reduces the risk of premature debonding failure, a common issue in bonded systems (Ganesh & Murthy, 2019).

In general, unbonded CFRP systems can enhance the load-carrying capacity of RC beams, although their effectiveness varies based on anchor design and CFRP configuration. Failure modes are often associated with CFRP slippage or localized stress concentrations at anchor points, rather than debonding failures seen in bonded systems. Despite these challenges, such as anchorage design and stress concentration management, unbonded CFRP systems present advantages in terms of flexibility, durability, and ease of maintenance. Ongoing research and experimental validation continue to refine this technique, making it a promising solution for structural rehabilitation (Wang, et al., 2024).

While Hosseini et al. (2018) researched the efficacy of prestressed unbonded CFRP plates on steel members, an investigation into strengthening of RC beams using unbonded CFRP plates was recently carried out by Wang, et al (2024) in China with promising results. The investigation aimed to compare bonded and unbonded prestressed CFRP plates using both developed and commercially available anchors. Although the study looked at both type of anchors, Figure 2-4 presents the results specifically for beams using the developed anchor. The results show that for the same beam, both bonded (PB) and unbonded (PU) strengthening achieved similar ultimate loading capacity, with an increase of up to 50% (β_u) when compared to the control beam (B0). Notably, the unbonded version achieved a slightly higher ultimate load (F_u) than the bonded version, despite having a lower yield point (F_y). This highlights the effectiveness of FRP materials, bonded and unbonded, in enhancing the load-bearing capacity of RC structures, making them viable alternatives to traditional materials.

Specimen	F_{cr} (kN)	β_{cr} (%)	F_y (kN)	β_y (%)	F_u (kN)	β_u (%)	Δ_u	Failure mode
B0	16	/	193.3	/	221.3	/	157.8	Concrete crushing
PB-30	42	162.5	266.9	38.1	323.4	46.1	124.9	Concrete crushing
PB-45	52	225.0	287.6	48.8	327.3	47.9	94.4	CFRP fracture
PU-30	40	150.0	257.1	33.0	330.9	49.5	123.7	Concrete crushing
PU-45	50	212.5	273.1	41.3	329.5	48.9	93.6	CFRP fracture

Figure 2-4. Summary of Main Test Results comparing Bonded and Unbonded Plates (Wang, et al., 2024)

2.3.3 Other common techniques

In addition to the widely used methods previously discussed, there are several other effective techniques for strengthening RC structures. These techniques have been utilized for decades and continue to play a crucial role in enhancing the structural performance and durability of RC members. The following sections provide an overview of these techniques, their applications, and their advantages and challenges.

2.3.3.1 Steel plate bonding

This method has been described as a viable technique at the end of the 1960s (Fleming & King, 1967) and has been widely used since the 1970s with the purpose of increasing the structural performance and stiffness of concrete beams or slabs, particularly by improving the flexural and shear capacity of distressed concrete elements. It consists simply of bonding steel plates to the concrete surface using epoxy adhesive, with additional fastening such as dowels or bolts, if required, as shown in Figure 2-5 (Heiza et al., 2014).

Steel plate bonding is cost-effective, causes minimal disruption, and has barely any effect on clearances making it a popular choice for strengthening. However, the success of this method depends heavily on ensuring strong bond integrity to avoid issues like premature debonding, which can lead to brittle failure (Ganesh & Murthy, 2019). Premature bonding may also occur over time if corrosion occurs at the steel concrete bond location. Additionally, the method can be time-consuming, particularly when factoring in curing time and transportation of material. Furthermore, whether they are used as a strengthening method for concrete or steel structures, steel plates have a poor strength-to-weight ratio, which complicates handling and installation (Yossef, 2015).

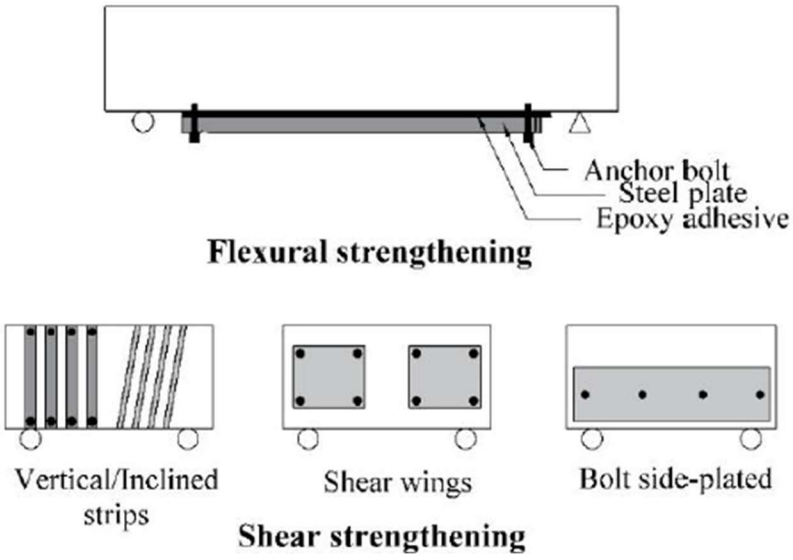

Figure 2-5. Example of Strengthening Using Externally Bonded Steel Plates (Adhikary & Mutsuyoshi, 2006)

2.3.3.2 Jacketing

Jacketing, also known as section enlargement, is a traditional retrofitting technique used to improve the performance of concrete structure. This method involves confining the original structural element with a reinforced concrete jacket as illustrated in Figure 2-6, enhancing the load-carrying capacity and stiffness of the structure. While section enlargement can effectively strengthen concrete, it has some drawbacks, such as the increase in member size, which may pose clearance issues, and the need for additional formwork and curing time. Although it is a relatively low-cost strengthening solution, it often requires significant labor investment (Heiza et al., 2014).

In recent years, ultra-high-performance concrete (UHPC) jacketing has emerged as an advanced alternative to traditional section enlargement, offering enhanced performance for retrofitting aging or RC structures. UHPC jacketing enhances shear and flexural strength while shifting the failure mode from brittle shear failure to a ductile flexural failure. This change significantly increases the safety and durability of the structure (Li & Aoude, 2023). Unlike traditional jacketing, UHPC provides superior bonding strength, reducing the risk of premature debonding and offering better long-term performance. This makes UHPC an ideal choice for structures requiring substantial reinforcement without the downsides of increased member size or extensive labor in application (Li & Aoude, 2023).

Both traditional and UHPC jacketing can be time-consuming due to the labor-intensive process of preparing the beam for retrofitting and curing time of the new concrete.

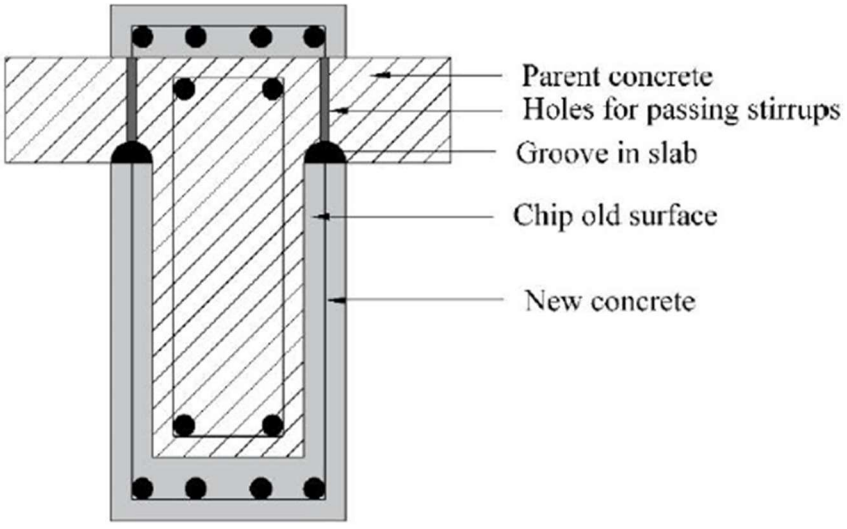

Figure 2-6. Typical Strengthening by section enlargement/concrete jacketing (Cheong & MacAlevey, 2000)

2.4 Type of anchors

One of the main challenges in using CFRP laminates for structural strengthening is ensuring proper anchorage to the structure. Without a secure grip, the laminates are likely to slip, reducing their effectiveness. To prevent this, it is necessary to firmly secure the ends of the laminates with an anchor system. Anchors not only keep the CFRP laminates attached to the structure, they can also

be designed to facilitate prestressing, which utilizes the high ultimate tensile strength of the material. A well-designed CFRP anchor is critical to the overall success of the strengthening method and must be carefully considered during the design process (Mohee et al., 2016).

Several anchors have been developed for CFRP laminates, with epoxy-based, and mechanical anchors having been widely studied (Deng et al., 2022). However, designing effective anchors remains challenging, with ongoing research focused on improving anchorage systems and understanding failure mechanisms (Mohee et al., 2016).

Regardless of the type of anchor used, various failure mechanisms can occur. These include debonding of the anchor, tensile rupture of the CFRP outside the anchor, localized cracking and crushing of the CFRP within the anchor due to stress concentrations, and slippage, as shown in Figure 2-7.

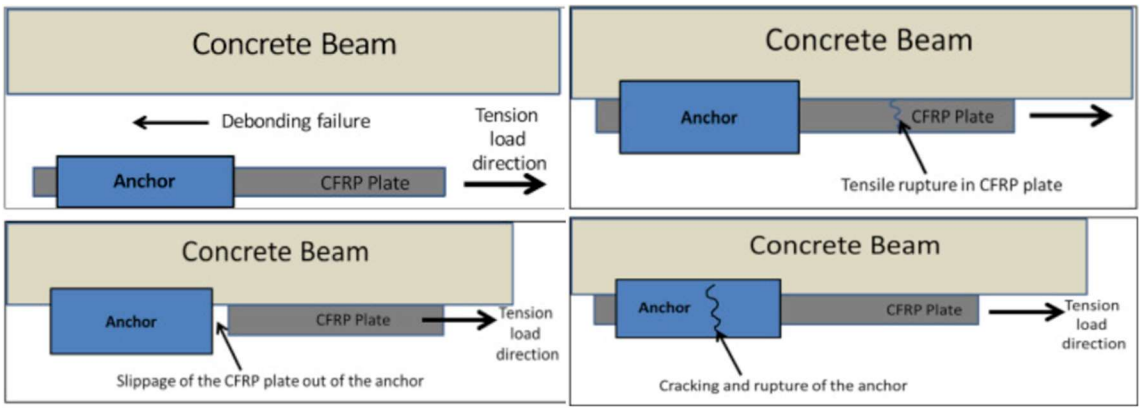

Figure 2-7. Potential Failure Mechanism (Mohee, Al-Mayah, & Plumtree, 2016)

2.4.1 Mechanical Anchors

Mechanical anchors use bolts or friction to grip the plates and provide more reliable prestressing capabilities (Li et al., 2019). They offer several advantages over epoxy-based anchors, including higher reliability in prestressing. However, challenges include localized stress concentrations and the need for precise installation to avoid affecting the internal reinforcement (Mohee et al., 2016).

Mechanical anchors can be further divided into two categories; friction-based anchors (left) and wedge anchors (right), as seen in Figure 2-8. Friction-based anchors utilize the friction between the CFRP and the anchorage system to provide grip. These anchors are often easier to install and do not require curing time. As the name indicates, wedge anchors use wedges to grip the CFRP laminate. This method has shown high efficiency in prestressing application, however can create localized stress concentrations.

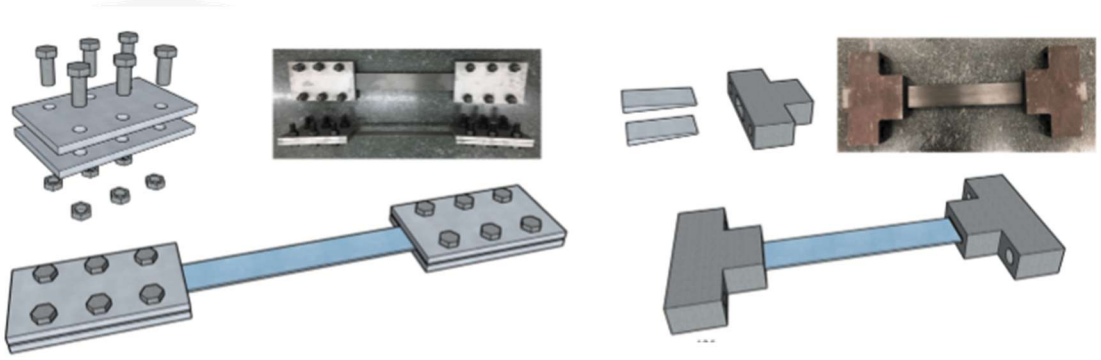

Figure 2-8. Example of Friction-Based and Wedge Anchors (Deng, Zhong, Zheng, & Zhu, 2022)

2.4.2 Epoxy Anchors

Epoxy-based anchors typically involve using adhesives to secure CFRP plates to the structure, but they often carry only a fraction of the ultimate tensile strength of the plates (Li et al., 2019). This method is time-consuming due to the curing process of the epoxy and requires larger anchorage lengths and potentially costly heat-treatment equipment for the installation of the epoxy-base gradient anchor (Mohee et al., 2016). Epoxy anchors are mostly used for plate bonding, whether with steel or CFRP laminates. The L-shape end anchor developed by Jumaat and Alam is one example of the epoxy-based anchor and is illustrated in Figure 2-9.

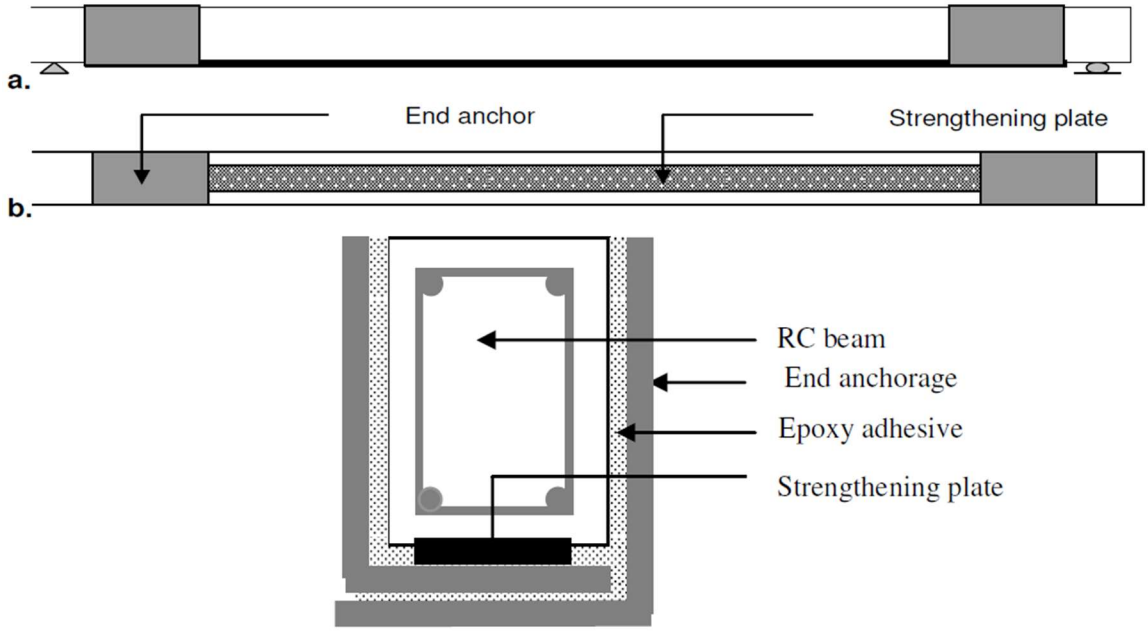

Figure 2-9. L-Shape Epoxy-Based Anchor (Jumaat & Ashraful Alam, 2010)

2.4.3 Hybrid Anchors

Hybrid anchors combine elements of both mechanical and epoxy-based anchors but are more commonly used with bonded systems. Several hybrid anchor designs have been investigated. Figure 2-10(a) illustrates a hybrid anchor that utilizes epoxy directly applied at the CFRP-wedge interface (Burtscher, 2008). Another variation, studied by Wu & Huang (2008), follows the bonded FRP technique, where a layer of epoxy is used to adhere the FRP to the concrete surface. Once the epoxy hardens, a second coat is applied, followed by the installation of specialized mechanical fasteners along the FRP reinforcement at specified intervals. These fasteners consist of metal pieces with two nails on either side, as shown in Figure 2-10(b) (Wu & Huang, 2008). A hybrid anchor was researched and tested by Blazewicz for use with prestressed CFRP strips. The system includes a dead-end anchor and a live-end with a tensioning device included, as illustrated in Figure 2-11, and utilized epoxy bonding along the entire length of the strip to improve load efficiency. The main difference between the live-end and dead-end is the inclusion of additional holes near the dashed separating the external and internal areas on the picture, which allow for the installation of the tensioning device at the live-end. Unlike the design proposed by Wu & Huang, this hybrid anchor incorporates additional mechanical fasteners embedded through the CFRP (rivets or bolts in Figure 2-11), combining adhesive bonding and gripping to minimize slippage and enhance load transfer (Piatek et al., 2020).

These anchors aim to provide reliable prestressing capabilities while minimizing the drawbacks associated with each individual method. Ongoing research focuses on optimizing hybrid anchor designs to improve their performance and practicality in various structural applications (Mohee et al., 2016).

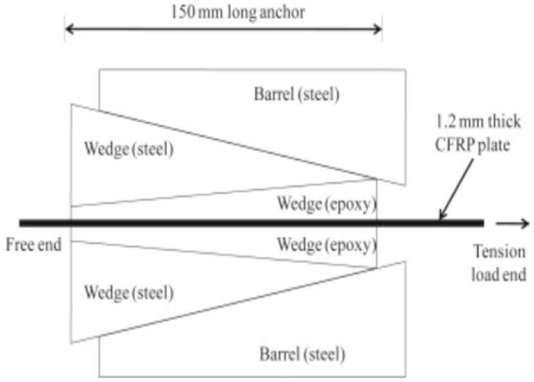

(a) Example of Hybrid Anchor (Mohee, Al-Mayah, & Plumtree, 2016)

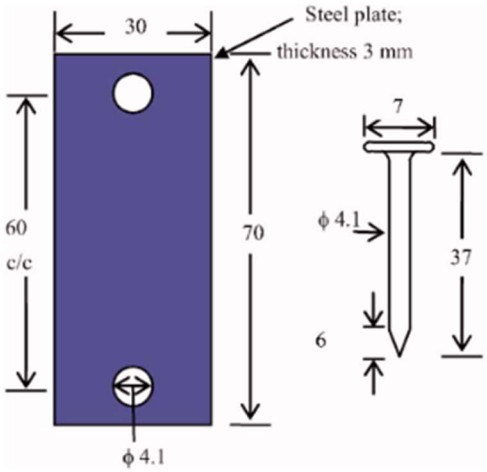

(b) Details of a Mechanical Fastener for Hybrid Anchor (Wu & Huang, 2008)

Figure 2-10. Hybrid Anchors – Examples 1 and 2

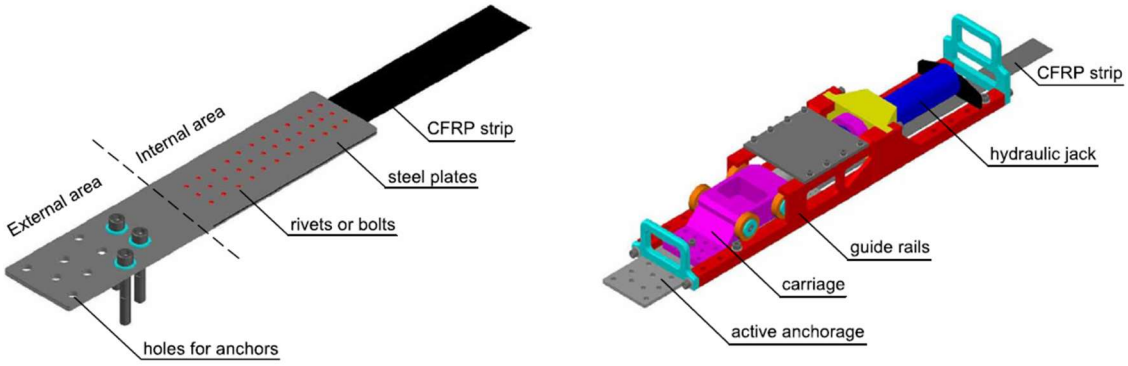

(a) Dead-End Anchor

(b) Schematic of Tensioning Device on Live-End Anchor

Figure 2-11. Hybrid Anchors Example 3 (Piatek, Siwowski, Michalowski, & Blazewicz, 2020)

2.5 Summary

The literature review highlights that while traditional bonded CFRP systems have been proven effective, their reliance on extensive surface preparation, adhesive application, and curing times limits their practicality in time-sensitive scenarios. Similarly, non-FRP methods such as prestressing steel tendons, steel plate bonding, and UHPC jacketing are also effective but require heavy materials, specialized equipment, and time-consuming installation. In contrast, unbonded CFRP systems paired with mechanical anchorages offer a promising alternative for the rapid strengthening of reinforced concrete structures, particularly in military applications, by eliminating many of these time-consuming steps.

Despite their potential, research on unbonded CFRP remains limited, particularly in military and emergency applications, where speed and challenging site conditions can be critical. This gap in knowledge motivated the experimental study presented in Chapter 3, which investigates the performance of unbonded CFRP straps with mechanical anchors when used to strengthen simply supported short-span reinforced concrete T-beams.

.

Chapter 3 – Manuscript: "Rapid Strengthening of Short Span Reinforced Concrete T-beams with Unbonded Carbon Fibre Reinforced Polymer Straps"

3.1 Abstract

The ability to rapidly strengthen reinforced concrete structures is critical for military and emergency applications, where conventional strengthening techniques may be impractical due to time constraints. This research evaluates the effectiveness of unbonded carbon fibre reinforced polymer (CFRP) straps installed with mechanical anchors as a rapid strengthening technique for simply supported short-span reinforced concrete bridges.

An experimental program was conducted using six 6 m long beams that include two control specimens and four strengthened beams with single or double layers of CFRP straps and variations of a custom-designed mechanical anchor. The addition of tensioners contributed to a more uniform strain distribution across the CFRP straps. The results demonstrated that unbonded CFRP strap systems can enhance load-carrying capacity, with strength increases of up to 22% with a double layer configuration. Additionally, the strengthening system improved serviceability by reducing deflections at high loads. A numerical model was developed to predict the load-deflection response of the strengthened beams.

The study confirms that the application of unbonded CFRP straps, using proper mechanical anchorage is a viable technique for the rapid strengthening of short-span simply supported concrete T-beams, offering a practical alternative to bonded CFRP systems in time-sensitive applications.

3.2 Introduction

The ability to rapidly strengthen existing concrete bridges is crucial for diverse types of military operations, including conflict, peacekeeping, disaster relief, and training missions, where existing bridges may not support the heavy loads of military vehicles. Military engineers require solutions that are not only effective but also deployable within tight operational timeframes, particularly in scenarios with logistical constraints. Standard bridging resources used by military forces are limited (Department of National Defence, 2023) and therefore viable strengthening techniques are required. One situation likely to be encountered and well-suited for strengthening are short-span bridges with inadequate capacity that are likely to exist on more remote and less travelled secondary routes. This research explores the use of unbonded carbon fibre reinforced polymer (CFRP) straps with mechanical anchors as a rapid strengthening technique to increase the load carrying capacity of simply supported short span reinforced concrete (RC) T-beams within a single working shift (day or night). The aim was to achieve a target increase in ultimate load capacity of at least 12 to 15%, ensuring the strengthening technique would justify the time and resources required for implementation in military operations.

Bonded and prestressed CFRP techniques have been widely studied since the early 1990s (Saadatmanesh & Ehsani, 1991; Triantafillou & Deskovic, 1991) and applied to strengthen concrete structures due to their superior strength-to-weight ratio (Yossef, 2015), relatively easy application process requiring few specialized skills (Wight, Green, & Erki, 2001), and superior effectiveness in enhancing load capacity and crack control (Panahi, Zareei, & Izadi, 2021; (Hammad et al., 2024). However, bonded systems may rely heavily on extensive surface preparation and epoxy application, combined with prolonged curing times, and repair of damaged concrete if required (ACI 440, 2023), which may make them unsuitable for time-sensitive scenarios. Additionally, traditionally bonded CFRP systems that are not prestressed have been shown to utilize only 20% to 50% of their tensile strength before failure occurs, significantly limiting their effectiveness (Piatek et al., 2020). Prestressing can improve this efficiency by engaging more of the CFRP's tensile capacity, but it adds another step to an already time-consuming process. Traditional bonded FRP systems may not be suitable for military applications not only due to their time-consuming installation but also because epoxy adhesives are weather-dependent and require proper storage, making them impractical in unpredictable field conditions.

Different types of anchors, such as mechanical, epoxy-based, and hybrid, are available and have been used with traditional bonded CFRP and each have their unique benefits and limitations. Mechanical and friction-based anchors can provide reliable anchorage and prestressing but can cause localized stress concentrations (Li et al., 2019). Epoxy-based anchors, while capable, require extensive curing time to be effective. Hybrid anchors combine features of both methods, aiming to reduce their individual drawbacks but still require further optimization (Mohee, Al-Mayah, & Plumtree, 2017). In general, anchors have demonstrated reliability in prestressing applications, however, their use has been predominantly associated with bonded CFRP systems (Brigante, 2014; Jumaat et al., 2011). Unbonded CFRP eliminates most of the time-intensive steps, especially when relying on mechanical anchors, providing a more efficient alternative for rapid deployment in military environments, however limited research has been done on unbonded anchored non-prestressed strengthening.

Bonded CFRP systems typically fail due to intermediate crack debonding, end debonding, or anchorage failures (ACI 440, 2023; El-Hacha & Rizkalla, 2004; Teng et al., 2003). In contrast, unbonded systems primarily experience slippage or localized stress concentrations which can create challenges at anchor points (Wang, et al., 2024), rather than the more common premature debonding failure seen in bonded systems (Ganesh & Murthy, 2019). Research by Wang et al. (2024) demonstrated that unbonded CFRP systems, when paired with well-designed mechanical anchors, can achieve similar or even greater ultimate load capacities compared to bonded systems, while also mitigating the risk of premature debonding failure. Their experimental results showed an increase in ultimate load capacity of up to 50% in reinforced concrete beams, with unbonded CFRP even outperforming bonded systems under specific conditions.

With limited existing research on unbonded CFRP applications, this study seeks to address a significant gap by exploring an unbonded CFRP strengthening technique, aiming to expedite rapid

bridge strengthening and support military operational readiness. Through an experimental program involving six 6 m long reinforced concrete T-beams, the research aimed to validate the efficacy of CFRP straps with custom-designed mechanical anchors for improving the load-carrying capacity of simply supported short-span bridges. The approach was intended to provide a concept for a rapid, practical solution for enhancing the operational readiness of the military forces while minimizing logistical delays.

3.3 Experimental Program

The aim of this research was to investigate a concept to rapidly strengthen simply supported single span concrete T-beams, focusing on increasing the flexural resistance. Six experimental beams were constructed following the same design plans and construction methods. Two beams were tested without any strengthening as control beams and the other four beams were tested with various strengthening methods using CFRP straps.

3.3.1 Specimens

The experimental program involved casting six RC beams, based on the same design. The beams were cast on two different occasions, therefore creating two groups of beams with their respective control to compare to the strengthened beams, as outlined in Table 3-1. CB refers to the control beams, whereas SB denotes the various strengthened beams. The naming convention for strengthened beams follows the format SB-X.Y, where X represents the number of CFRP layers and Y indicates the test number. For example, SB-1.1 corresponds to test number 1 of a beam strengthened with one layer of CFRP, while SB-1.2 refers to the same configuration tested on a second beam.

Table 3-1. Summary of Sample Beams

Group	Beam	Age at test	Strengthened Method
1	CB-1	99 days	-
	SB-1.1	138 days	Single layer of CFRP
	SB-1.2	166 days	Single layer of CFRP with tensioners
2	CB-2	68 days	-
	SB-2.1	147 days	Two layers of CFRP with tensioners
	SB-2.2	170 days	Two layers of CFRP with tensioners

The design of the T-beam was based on a review of existing short span T-beam bridges. The overall intention for the design was to have a realistic height to width ratio based on realistic spacings of webs while still having an appropriate height to span ratio. The height to span ratio was taken into consideration to avoid short beam behaviour, in which shear behaviour could have dominated. The thickness of the flange was chosen to be representative of a trafficked beam deck and to accommodate reinforcement details. The finalized design specified a 6000 mm long beam, a total

height of 500 mm including a flange thickness of 140mm, and flange and web widths to be respectively 1000 mm and 200 mm wide. The cross-section of the beam is shown in Figure 3-1.

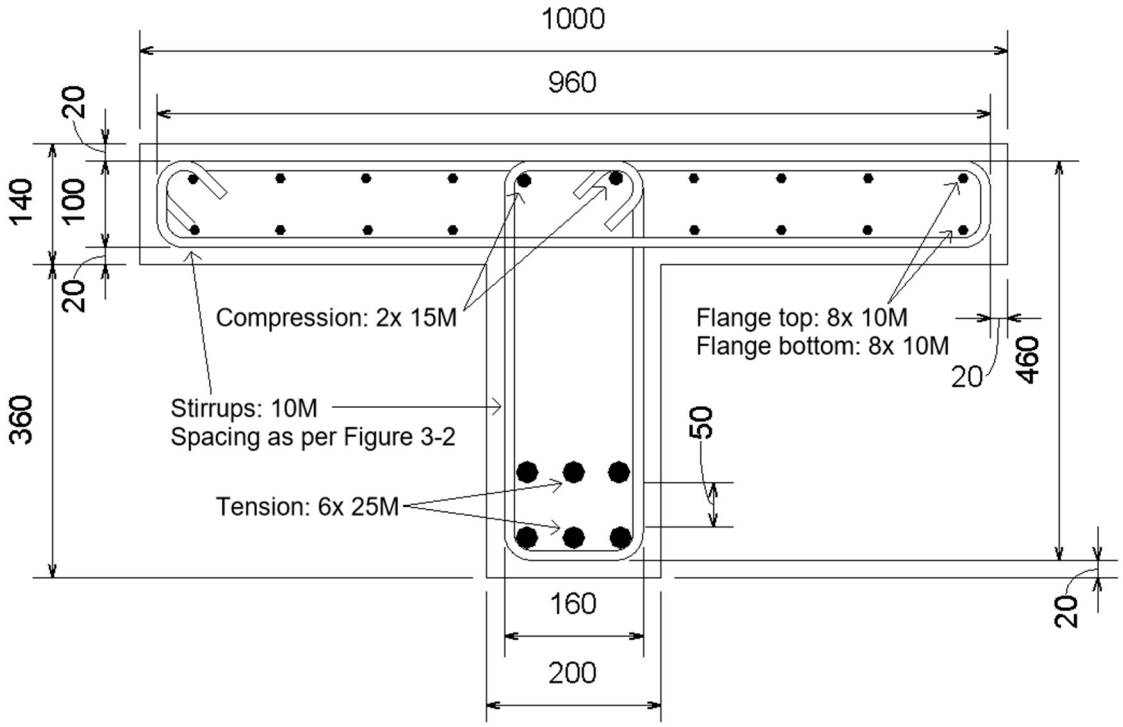

Figure 3-1. Cross-Section - Reinforcement and Beams

The beam was designed to be under-reinforced with a steel ratio of approximately 20% of the balanced reinforcement ratio ρ_{bal}. For the longitudinal reinforcement, six 25M Grade 400 reinforcement bars were arranged in two layers in the tension zone for a reinforcement ratio of 0.72% and two 15M Grade 400 reinforcement bars were used in the compression zone. The flange was also reinforced with eight 10M Grade 400 reinforcement bars at the bottom and top of the flange to provide crack control and represent typical reinforcement that may be present in a regular bridge deck. A cover of 20 mm was maintained all around by using plastic reinforcement bar chairs. The beams were reinforced in shear in a way that the beams would be able to sustain a moving load that was consistent with the two point-loads as applied in the experimental setup. Therefore, the beams were heavily reinforced in shear, with the original shear design capacity being 20% higher than the demand, which significantly reduced the risk of a shear failure when the beams were strengthened and subjected to the loading applied near mid-span. As shown in Figure 3-2, the spacing, center-to-center, of the 10M stirrups varied from 100 mm to 233 mm at mid-span. Appendix A provides additional details regarding the construction of the specimens. A screenshot of the design spreadsheet for the beams that was used to determine the appropriate under-reinforced percentage of steel is shown in Annex B.

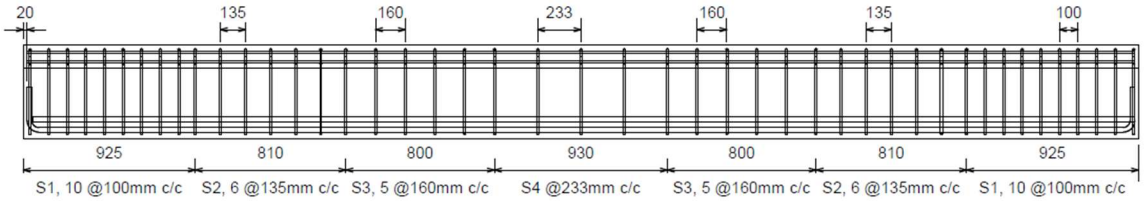

Figure 3-2. Side View - Reinforcement

3.3.2 Material

Concrete cylinders were cast with the beams and their compression tests were conducted concurrently with beam testing. Coupons from the principal 25M reinforcement bars, were tested to determine representative yield and ultimate strengths suitable for use in the moment-curvature model discussed in Section 3.5. Appendix A explains in detail the construction method of the specimens and the lessons learned during the construction of the beams, as well as for the construction of the anchors and the tensioners.

Ready-mix concrete from a local supplier was used to pour the beams. The concrete used was a 35 MPa non-air entrained mix with a 10mm maximum aggregate size and sufficient superplasticizer for a 150 mm slump. Concrete samples were cast alongside the beams in 100 mm diameter plastic cylinders with a height to width ratio of 2:1, with 24 cylinders for each pour. Despite similar specifications, the concrete strength differed slightly between pours, averaging 49 MPa with a standard deviation of 2.33 MPa for Group 1 and 43 MPa with a standard deviation of 3.37 MPa for Group 2. Concrete samples were tested according to the CSA 23.2-9c standards concurrently with corresponding beam tests to determine the compressive strength to use in the model. Table 3-2 summarizes the characteristics of the concrete used for each beam in the model, with the Elastic Modulus calculated using the formula specified in the CSA A23.3.

Table 3-2. Concrete Properties per Beam (as per CSA 23.2-9c)

Property	CB-1	SB-1.1	SB-1.2	CB-2	SB-2.1	SB-2.2
Compressive strength (MPa)	49	49	49	42	44	45
Elastic Modulus (GPa)	31.0	31.0	31.0	29.2	29.5	30.0

Three different sizes of Grade 400 reinforcement were used: 10M, 15M, and 25M. Stirrups were bent by the manufacturer, while other reinforcement was cut and assembled on site. Test samples from the 25M bars was tested according to ASTM Standard A370-24, yielding a 456 MPa yield strength and 557 MPa ultimate strength. All other reinforcement bars were assumed to have the same yield strength.

CSS V-Wrap CUCL Unidirectional Carbon Laminate (CFRP) from Simpson Strong-Tie was selected for its high strength, stiffness, and lightweight properties. The chosen straps were 1.4 mm thick and 90 mm wide, with each layer composed of two straps installed side by side equally spaced from the web centreline. The CFRP straps were left unbonded for all tests. The manufacturer's

design specifications for the CFRP straps are presented in Table 3-3, with the stress-strain curve used to represent the CFRP properties shown in Figure 3-3 with the stress in MPa and strain in mm/mm.

Table 3-3. CFRP Material Properties - As per the manufacturer

Property	Design Value per ICC-ES AC125	Design Value per ISO 527
Tensile Strength	1250 MPa (181,000 psi)	2800 MPa (400,000 psi)
Tensile Modulus	163 GPa (23,600 ksi)	165 GPa (24,000 ksi)
Elongation at Break	0.8%	1.7%

ICC-ES AC125 accounts for practical application conditions, including safety factors and environmental durability, which result in more conservative values. ISO 527, on the other hand, measures the material's intrinsic properties in controlled laboratory settings, providing higher theoretical values that do not consider real-world constraints. For this research, values closer to the ISO standard were chosen due to the controlled experimental settings and the aim of accurately predicting the actual behavior of the strengthened beams.

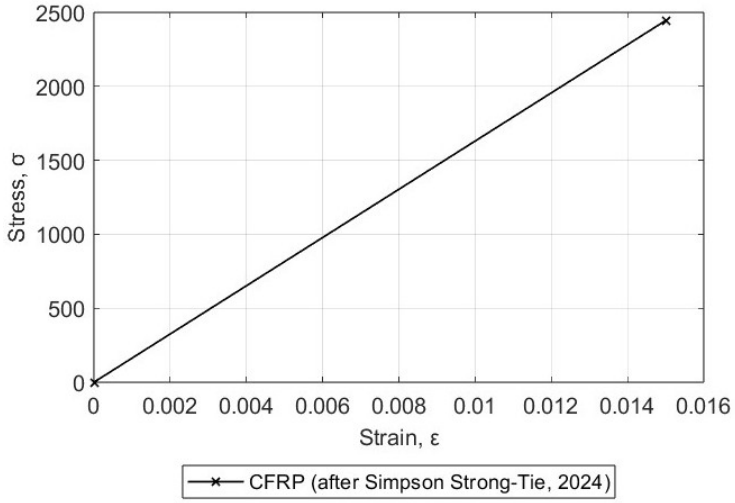

Figure 3-3. Stress-Strain Relationship of the CFRP

3.3.2.1 Anchors

The CFRP straps were installed on the beams using custom-designed mechanical anchors that were built specifically for this research project. Various concepts of anchors were considered and designed as part of this project, including an adjustable dead-end anchor, a live-end anchor, and two U-shaped dead anchors, with single and double layers. However, only the two U-shaped anchors were used for the non-prestressed tests outline in this manuscript. A close-up of the installed CFRP straps in the anchor is shown in Figure 3-4, while the initial design concept of the

single-layer U-shaped anchor is depicted in the 3D drawing in Figure 3-5. Finally, a clearer view of the installed anchor and CFRP can be seen in Figure 3-6.

Figure 3-4. Close-up of CFRP Installed on SB-2.2

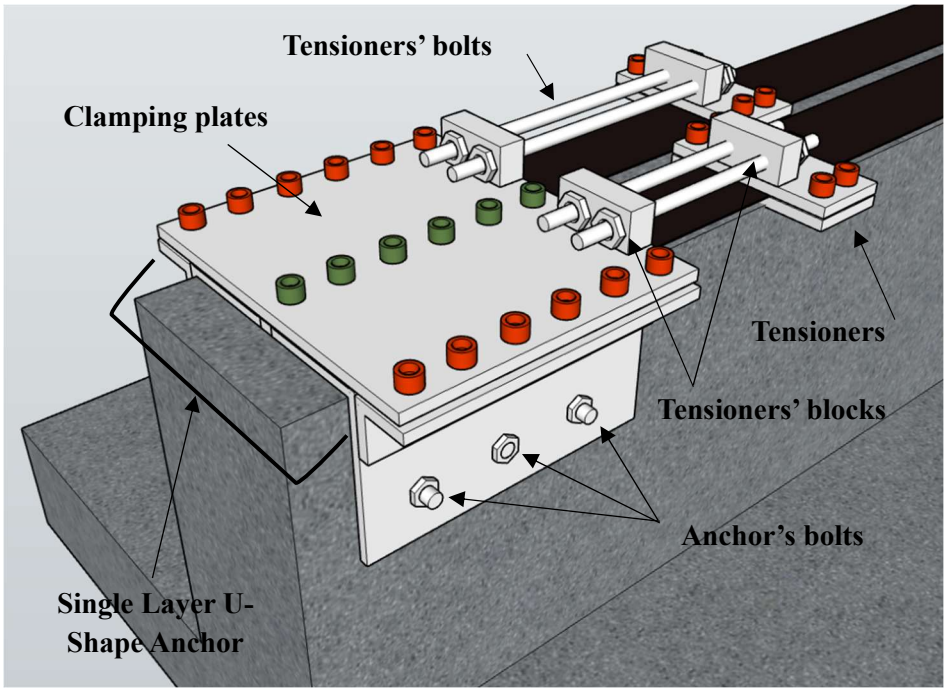

Figure 3-5. Upside Down 3D Drawing of the Single Layer U-Shape Anchor

Figure 3-6. CFRP Installed on SB-2.2

Design work was completed on a series of anchors that were not used to strengthen the beams in this study. The first of these was an adjustable anchor, designed for on-site assembly, which allows for direct adjustment with metal plates, angle irons, threaded rods, and bolts. The second anchor, known as the live end anchor, was a modified version of the previous adjustable anchor. It was designed to hold a hydraulic jack for prestressing the CFRP strap and could potentially be refined for future prestressed applications. However, it should be noted that these two anchor designs were purely conceptual and were never physically constructed. Three-dimensional drawings of both theoretical anchors can be found in Appendix C.

The following anchors were designed, built, and tested as part of this study. The U-shape anchor was selected to strengthen the beams due to the limited amount of clearance under the beam and the consistent dimensions of all beams used in the experiment. Precise knowledge of the reinforcement bar and stirrup locations allowed for the anchor to be built and installed as one piece. The double-layer dead anchor, based on the U-shaped design, accommodates two CFRP layers, requiring an extra steel layer. Modifications were done after every test to ensure better tension retention and to address shear cracking. All anchors featured perpendicular raised welds for improved CFRP grip and glued rubber to prevent strap damage. The final version of the anchor can be seen in Figure 3-7 (a), while the grip plate is presented in Figure 3-7 (b).

The modifications made to the anchors, from the first to the final version, included the addition of tightening bolts on the clamping plates, adjustments to the torque applied to these bolts, extra components at the back of the anchor to counteract twisting under load and thereby limit shear cracks, and adjustments to the welded lines to reduce slippage and prevent transversal breaks in the anchors.

All bolts on the anchor were torqued to 68 Nm (50 ft -lb.) for SB-1.1 and SB-1.2. As for SB-2.1 and SB-2.2, outside bolts were torqued to 81 Nm (60 ft-lb) and center bolts to 95 Nm (70 ft-lb). These torque values were determined through testing the effects of the clamping plates on 600 mm samples of the CFRP strap. The tests showed that the welds caused dents in the CFRP strap, which were desirable for improving grip. However, adjustments were made to the spacing, shape, and height of the welded lines to prevent excessive pressure at single points, which could risk cutting the straps. Additionally, a tightening pattern was established to control the stress distribution on the straps.

Appendix C includes drawings of the anchors used and three-dimensional models of the designed but untested anchors.

(a) Anchor Installed on SB-2.2 (b) Example of Grip Plate

Figure 3-7. Anchors

It was determined that 11.1 mm (7/16 in.) thick clamping plates were required to limit bending of the anchor under large loads. This ensures that the anchors maintain their integrity and performance even under significant stress.

3.3.2.1.1Tensioners

After the execution of test SB-1.1, it became apparent that the manual installation of the straps resulted in irregular tensioning and uneven distribution of loads. To address this, a tensioner was designed. This tensioner consisted of two small rubber-faced plates gripping the straps. The plates were then connected to the anchors through metal blocks joined by bolts. Because of the limited space, the tensioning devices were installed slightly offset, one in front of the other, instead of side by side. Both tensioning devices were upgraded to an improved version for SB-2.2, enhancing performance and accuracy. The initial (a) and improved (b) version are shown in Figure 3-8. The upgraded version features several enhancements: larger tightening bolts and bigger blocks for improved performance, a thinner upper plate to reduce the weight, and the ability to accommodate a hammer drill for tightening bolts instead of relying on a wrench. Detailed drawings and models for all anchors and tensioners can be found in Appendix C.

To streamline the application process, the CFRP straps were pre-cut to the correct length prior to installation. Each strap was measured to span from end to end of the anchors, with an additional 50 mm added, 25 mm on each side, to facilitate proper spacing and placement during installation. This additional length not only ensured accurate alignment within the anchors but also provided a clear visual reference during testing to monitor potential strap slippage. These preparatory steps significantly reduced the time required for strap installation and improved overall efficiency.

(a) Tensioners Version 1 (b) Tensioners Version 3

Figure 3-8. Tensioners

An initial tensioning was done until both straps produced a similar acoustic response when lightly vibrated, and strain gauges were then used to refine and measure the final tensioning, to ensure similar tension levels. While the actual level of tensioning applied was not precisely known, this process ensured that adjacent straps achieved similar tension levels. It is worth noting that it may be theoretically possible to estimate the strain in CFRP straps by analyzing the sound they produce when tensioned, similar to determining stress in vibrating strings, though further experimental validation would be needed for such an approach.

3.3.2.2 Installation of the strengthening system

To ensure the rapid installation of the unbonded system, the process was optimized for efficiency. Anchors were preassembled as single units whenever possible. Precise knowledge of the reinforcement bar and stirrup locations allowed for accurate marking and placement of anchor bolts, minimizing the need for on-site adjustments. The beam was marked in advance to guide the accurate positioning of the anchor bolts. During installation, the anchor was held in place as the beam was drilled, and bolts were secured immediately afterward.

The installation process of the CFRP straps started with inserting the straps between the two clamping plates that do not hold the tensioners. After confirming that the straps were straight and properly spaced, they were tightly secured within the plates. The straps were then inserted into the clamping plates at the opposite end of the beam and tightened using the experiment-specific

tensioners, shown in Figure 3-8. Once tensioning was completed, the straps were firmly secured within the second anchor and the tensioners were removed. When required, the process was repeated for the second layer CFRP strap. With the upgraded version of the tensioners, the installation process became significantly faster, as power tools could now be used to tighten the straps efficiently and evenly.

When the correct tools are employed and precise measurements have been taken, the installation can be completed quickly and effectively. Accurate beam measurements are essential since there are two possibilities to mount the anchor if it happens to be too small: modify the anchor or remove part of the beam's concrete cover to accommodate the installation properly. Both options would introduce significant delays in the installation process, with the latter risking potential consequential damage to the beam.

Additionally, the proper placement of the anchor bolts relative to the beam's reinforcement is critical during installation. For this experiment, drawings of the beam were available, which facilitated bolt placement. However, one stirrup was found to interfere slightly, necessitating extra time to drill through the web. This highlights the importance of thorough pre-installation investigation to identify the exact location of reinforcement and avoid delays.

The entire system installation process typically takes two to three hours per beam, provided that thorough reconnaissance of the beam dimensions and reinforcement locations has been conducted and the appropriate tools are utilized. The process could be further streamlined by using high-strength wedge anchors with limited depth drilling into the web. Although this would require more wedge anchors per beam and result in additional holes to be drilled, the advantage of not needing perfect alignment for the holes would simplify and expedite the installation.

For field applications, initial preparation is essential to ensure the effectiveness of the strengthening method. This includes conducting reconnaissance to determine the dimensions of the beams and identifying the location of internal reinforcement, such as stirrups using reinforcement bar locators. This is critical to enable proper alignment and installation of the anchors, minimizing on-site adjustments, and reducing delays.

3.3.3 Instrumentation

Strain gauges were bonded to the reinforcement steel and embedded into the concrete. A total of 14 strain gauges were installed on the reinforcement cage. Six strain gauges were also installed on the top flange, directly on the concrete to monitor concrete strain up to failure; three Concrete gauges at the Mid-Span (CM) and the other three Concrete gauges at a specified Distance (CD), as shown in Figure 3-9. CM labeled strain gauges are located directly at the mid-span, with one on each of the left and right flange and one on the transversal centerline of the beam. As for CD labeled strain gauges, they are located at a distance of h/2 from an applied load, where h is the total height of the beam. Explanation of the nomenclature is shown Figure 3-9. An additional six gauges were installed on the CFRP straps, in order to not only monitor the equal tensioning of the straps but also to monitor the tension in the straps during the test.

Linear variable differential transformers (LVDTs) were also installed at key locations along the beams to monitor their vertical displacement, and also to assess the differential movement between the flanges, the elongation of the lower portion of the beam during testing and to monitor the movement of the anchors.

All loads, displacements and strain data were recorded in real time using an HBM MGCplus data acquisition system (DAQ). It supported multiple synchronized input channels, allowing simultaneous data acquisitions from load cells, LVDTs, and strain gauges. The DAQ collected the data at a rate of 2.0 Hz, ensuring precise monitoring throughout the test. The system was integrated with catman 5.4.2 software, which facilitated efficient data processing, visualization, and analysis.

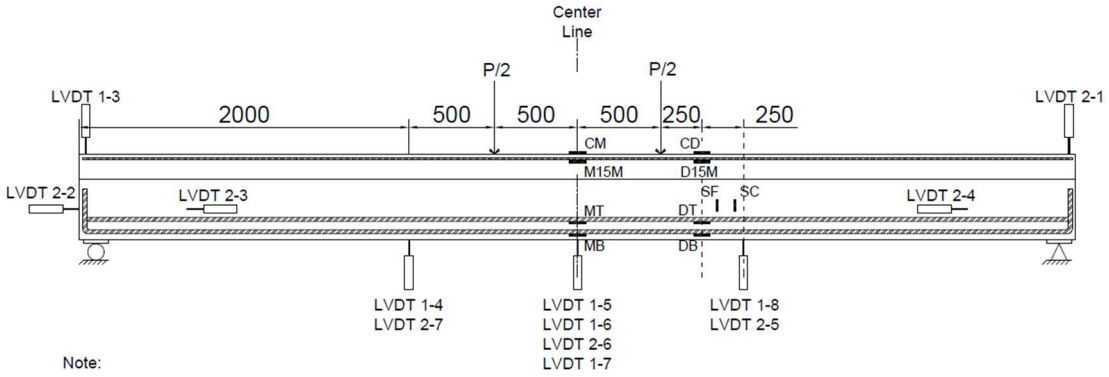

Note:

Only the longitudinal rebars in compression and tension are represented in this drawing

Not to scale

Legend:

Displacements

LVDT 1-3 & 2-1:	Vertical displacement of the extremities
LVDT 2-2:	Elongation of the beam
LVDT 2-3 & 2-4:	Movement of the anchors
LVDT 1-4 & 2-7:	Vertical displacement at half-height away from the left point load
LVDT 1-6 & 2-6:	Vertical displacement at mid-span
LVDT 1-8 & 2-5:	Vertical displacement at half-height away from the right point load

Strain Gauges

CM, M15M, MT, MB:	Mid-span
CD, D15M, DT, DB:	Half-height of the beam away from the right point load
SC, SF:	Stirrup

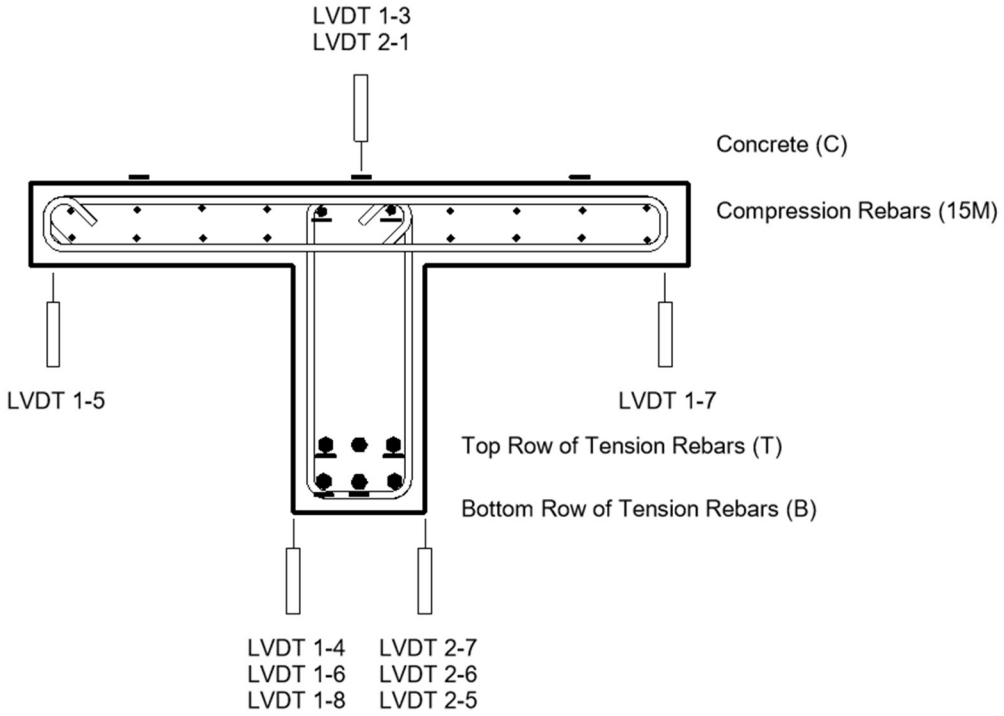

Figure 3-9. Instrumentation

Digital Image Correlation (DIC) was used to monitor crack formation and propagation with high precision. Unlike strain gauges, which provide point-specific measurements, the DIC enables a detailed comparison of crack widths and their evolution throughout the test for an entire area of the surface.

Using Figure 3-10, the placement of the DIC cameras was determined to ensure optimal coverage of the constant moment zone while accounting for obstructions caused by the testing frame. This setup maximized crack and displacement data collection while mitigating potential visibility issues. The yellow section shows the field of view for camera 1, while the red section is for camera 2. The section that overlaps in orange is the image data that can be processed by the software. Since the main field of view was looking at the web, the orange section that would be on the flange is smaller, as seen in Section 3.4.3.

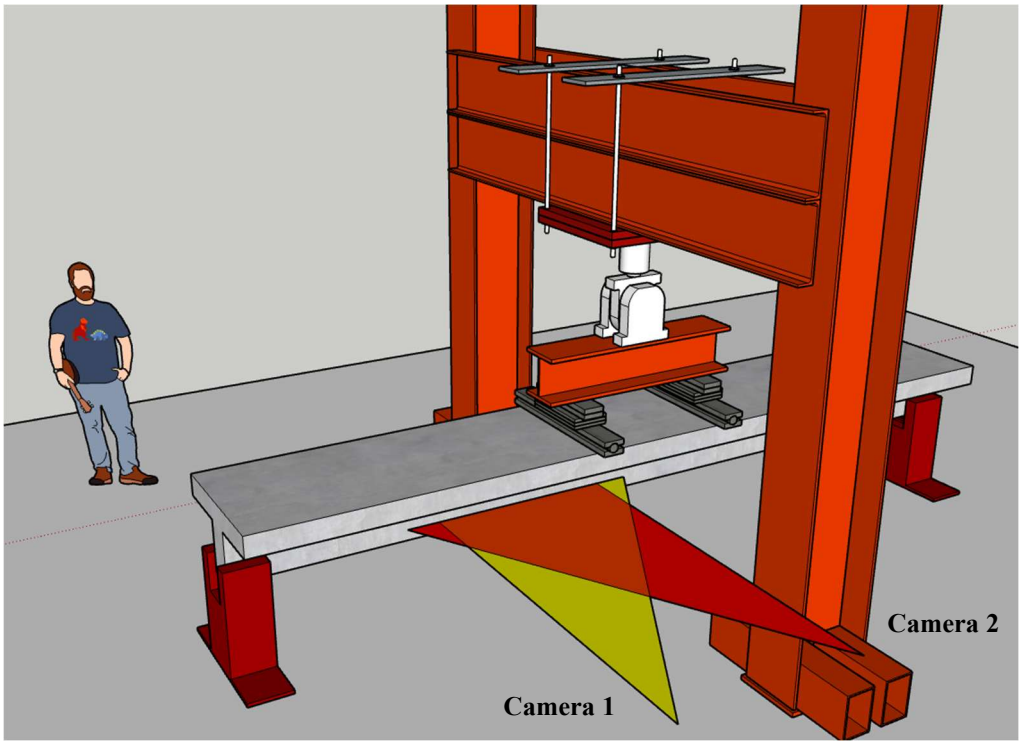

Figure 3-10. Camera Setup

3.3.4 Test Setup and Loading Procedure

To evaluate the flexural performance of the strengthened beams, all specimens were tested under four-point bending using a custom-built testing frame. This setup was chosen because it creates a constant moment region between the two applied loads, allowing for a more controlled assessment of flexural behavior**.** The setup also provides insights into the effectiveness of CFRP strengthening

in enhancing the beam load-bearing capacity, by monitoring load-deflection behavior and crack formation.

The testing frame was built using two stiffened I-beams connected together at the top with two pairs of C-channel. A 1000 kN actuator controlled by an MTS Flex 40 Station Manager 793 was installed in between the C-channels, with a heavily stiffened I-beam attached to the actuator serving as a loading beam. This loading beam applied force through two separate sets of metal plates, generating two point loads spaced 1000 mm apart. The beams were supported at both ends by pedestals, with one pedestal providing a pinned support, while the other functioned as a roller. Figure 3-11 presents a scaled three-dimensional (3D) model of the testing setup, with a reference person measuring 1.83 m

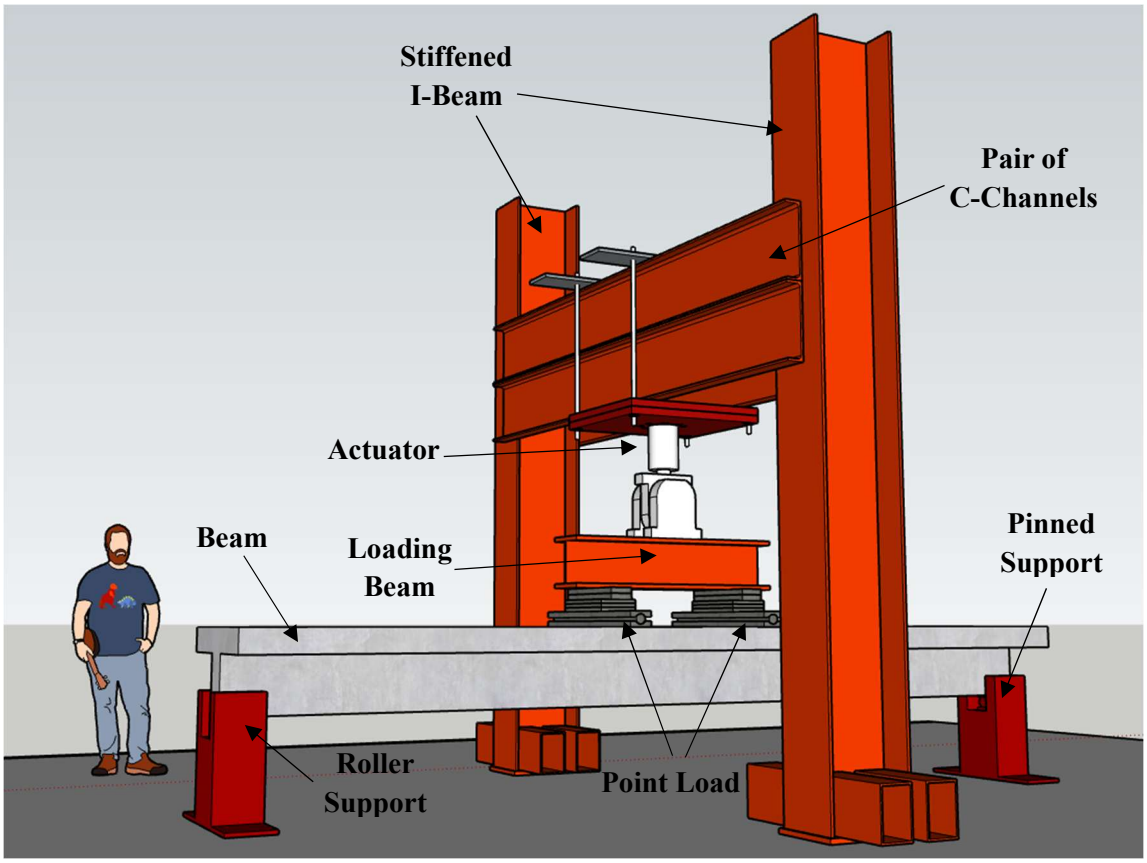

Figure 3-11. 3D Model of Experimental Setup

All six beams were carefully positioned on the pedestals in a consistent manner, ensuring that the web of each beam was situated identically across all tests. The pinned and roller support pieces were installed on the pedestal 100 mm away from the beam ends. In addition to the concept shown in Figure 3-11, the four-point bending setup dimensions, shown in Figure 3-12, was used for all tests. The applied loads were positioned 1000 mm apart, with each point load located 500 mm from the center of the beam. To ensure uniform contact between the loading plates and the beam surface,

self-leveling cement was used under the metal plates at the loading points. The dead weight applied on the concrete beam included the metal plates that created the basis for the point load, as well as the loading beam and part of the actuator itself. These components added up to approximately 8 kN.

For experimental loading to failure, the actuator was set to a displacement-controlled loading rate of 2 mm/min.

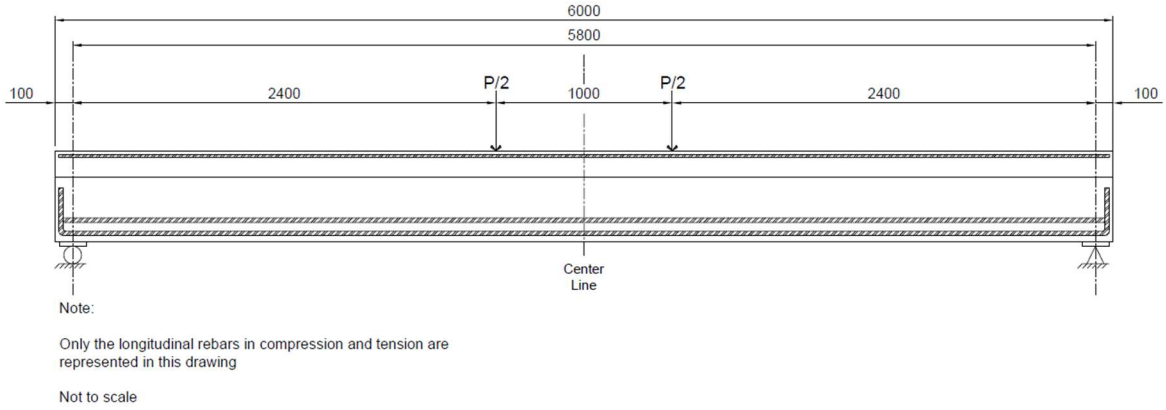

Figure 3-12. Location of Loads

Crack formation and propagation were visually inspected and documented throughout the test. After failure, the DAQ system continued to monitor all instrumentation, recording data until the load was fully removed from the beam, capturing any residual deformations and evaluating whether the beam retained any elastic behavior. Additionally, crack widths and patterns were measured and assessed post-test. The CFRP straps and mechanical anchors were also examined to evaluate their performance and identify any issues. Photos and notes were taken before, during and after each test for further analysis.

3.4 Test Results

The results for all tested beams are summarized in Table 3-4, which includes details on the strengthening method, failure mode, ultimate load, and the percentage increase in load capacity compared to the control beam. As expected, the beams strengthened with two layers of CFRP and tensioners achieved the highest loads with an increase of up to 22%. While the amount of CFRP played a significant role, the use of tensioners had a notable impact on the overall effectiveness of the strengthening, as seen between SB-1.1 and SB-1.2.

Table 3-4. Summary of Beams Failure

Beam	Strengthened Method	Failure Mode	Ultimate Load (kN)	% increase
CB-1	-	Concrete crushing	543	-
SB-1.1	Single layer (SB-1) of CFRP	Concrete crushing with all straps broken	563	3.7%
SB-1.2	Single layer (SB-1) of CFRP with tensioners	Concrete crushing with all straps broken	583	7.4%
CB-2	-	Concrete crushing	548	-
SB-2.1	Two layers (SB-2) of CFRP with tensioners	Concrete crushing with one strap broken	670	22.3%
SB-2.2	Two layers (SB-2) of CFRP with tensioners	Concrete crushing with all straps broken	651	18.6%

Note: For all beams, the final failure mode was preceded by the yielding of the main tension reinforcement.

3.4.1 General Observations

During experimental loading of the beam SB-1.1, the actuator gradually applied pressure to the beam until the first audible cracking in the strap was heard at 321 kN. This was followed by a more significant crack occurring at 510 kN, which caused a transverse break that reduced the working area of the strap. Post-experiment observations showed that both straps slipped by approximately 90 mm during loading. The first strengthening attempt was challenging and highlighted the need for improvements.

Improvements made to the raised weld pattern in the anchors and the addition of the tensioners for SB-1.2 positively impacted the straps behaviour. The first cracking sound in the straps was heard at 525 kN. Post-experiment observation showed that the straps slipped between 70 mm and 80 mm during the test, with a noticeable decrease in the number of transverse breaks observed in the straps when compared to previous tests. These findings suggest that the modification to the anchorage system enhanced the straps' performance.

Even though SB-2.1 was pre-cracked before the test, likely due to prolonged storage under another specimen, this did not affect the overall behaviour of the beam. Significant inward shifting of both anchors was noted during loading, likely caused by the shear cracks propagating through the anchors' bolts, as shown in Figure 3-13. This led to more damage to the concrete when compared to all the other tests. The first and only significant crack in the CFRP occurred at 579 kN. Post-experiment observations showed that the other three straps remained intact, with an average slippage of 20 mm.

(a) During the experiment (b) After removal of the anchor

Figure 3-13. SB-2.1 Shear Crack

Improvements made to SB-2.2, included the addition of a piece of metal extending vertically up the back end of the anchor, as shown in Figure 3-14. This modification effectively prevented shear cracks from propagating through the anchors' bolts. Although slight rotation of the anchor was observed, as illustrated in Figure 3-14(b), no shear cracks were present, indicating that this improvement worked as intended.

The first noticeable crack in the straps occurred at 570 kN. At 645 kN, the portion of one strap extending beyond the face of the web completely broke off, effectively weakening the overall strength of the strap. This weakening likely occurred because the portion of the strap that broke off no longer contributed to the resistance of the applied load, reducing the effective load-bearing area of the strap. Post-experiment observations revealed limited transverse breaks in the straps, but all straps cracked longitudinally. Unlike a significant transverse break, a longitudinal crack does not necessarily indicate failure, as the straps, while divided into multiple smaller segments, remain anchored and continue to function effectively as load-bearing components. The slippage of the straps in the anchors varied between 14 and 20 mm. These findings suggest that even with all the improvements made, the anchors still did not fully prevent the slipping of the straps.

(a) Anchor on SB-2.2 before testing (b) Anchor on SB-2.2 after testing

Figure 3-14. Anchors on SB-2.2, before and after

Post-test observations revealed that when the beams were cut into thirds for disposal, the end sections reverted to a straight shape, while the middle section remained bent. This confirms the plastic hinge formation was confined to the central high moment region of the beams.

3.4.2 Load-Deflection Behaviour

The load-deflection curves of all the specimens are shown in Figure 3-15, providing valuable insight into the behavior of the beams under varying loads, as well as the benefits of strengthening. The variation in the slopes between the beams highlights differences in their stiffness. In the figure, indicators "A" and "B" define the slopes before and after yield, respectively. Slope "B" reflects the post-yield stiffness of the beam and plays a crucial role in assessing its deformation behavior after the steel reinforcement has yielded.

The strengthened beams, particularly SB-2.1 and SB-2.2, demonstrate increased post-yield stiffness due to the strengthening measures. While this improved stiffness may limit excessive deflection which in turn is good for serviceability, excessive strengthening could restrict plastic deformation, increasing the risk of brittle failure in some cases. Finding the right balance between stiffness and ductility is essential to avoid overly brittle behavior.

In addition to ultimate load performance, limiting the overall deflection under a certain load plays a key role in improving serviceability. Reduced deflection minimizes damage to secondary structural elements and helps maintain the beam’s functionality. This becomes particularly relevant in SB-2.1 and SB-2.2, where the combination of increased stiffness and reduced deformation enhances their serviceability under operational loads.

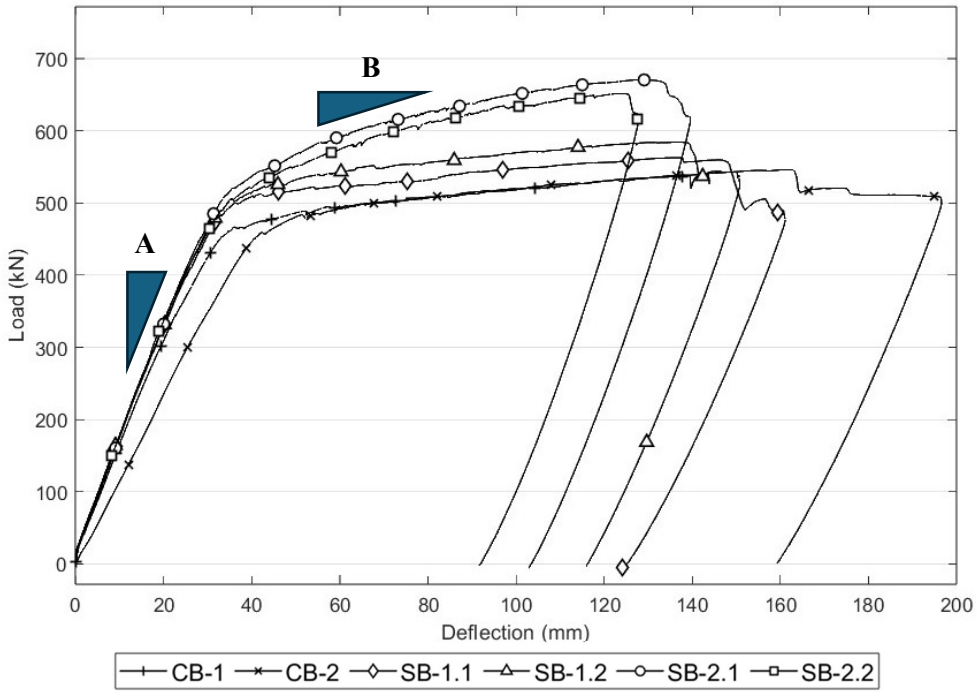

Figure 3-15. Load-Deflection Curves

In Table 3-5, significant values characterizing the beams are summarized. Both control beams exhibit typical behavior for an under-reinforced concrete beam. Adding one layer of CFRP enhances the ultimate load by 3.7% and 7.4%, while adding two layers significantly improves the beam's ultimate load capacity up to 22.3%. A summary of the increase percentage can be found in Table 3-4. Since the strengthening is unbonded, its effect on the first crack is negligeable and primarily based on the concrete material properties (Wight, Green, & Erki, 2001). When comparing CB-2 and SB-2.1, the mid-span displacement at ultimate load was reduced by 24.8%.

Table 3-5. Beam Behaviour Details

Beam	**First Crack**		**Yielding**		**Ultimate**	
	Load (kN)	Displacement at mid-span (mm)	Load (kN)	Displacement at mid-span (mm)	Load (kN)	Displacement at mid-span (mm)
CB-1	24	1	462	35	543	154
SB-1.1	23	1	499	34	563	136
SB-1.2	26	1	505	35	583	129
CB-2	18	1	457	42	548	161
SB-2.1	N/A	N/A	516	35	670	129
SB-2.2	27	1	505	35	651	123

Both control beams, CB-1 and CB-2, exhibited similar behavior during testing, with the exception of their flexural rigidity up to the yield point. This variation could partially be attributed to CB-1 having a higher compressive strength than CB-2. Additionally, CB-2 exhibited a significantly lower

first crack load compared to CB-1, as shown in Table 3-5. Although there was bulging of the formwork during the Group 2 pour, leading to additional concrete compared to the designed beam, both control beams reached the same yield point of 457 kN. This suggests that the addition of extra concrete did not have a significant impact on the beam's load-carrying capacity. Instead, the difference in the concrete's compressive strength may have influenced its stiffness, and when combined with the effect of the lower cracking strength, caused the load-displacement curve to shift further to the right compared to CB-1.

As shown in Figure 3-15, the flexural stiffness of the single layer strengthened beam, SB-1.1 and SB-1.2, was similar. Both beams exhibited a delayed yield point compared to the control beams, with an increase of approximately 40 kN. After the yield point, it becomes evident that when the straps work concurrently (SB-1.2), as opposed to being loaded sequentially (SB-1.1), the difference in deformation under similar loads is noticeable. As expected, this suggests that the straps working in tandem, as observed in SB-1.2 significantly impact the overall performance of the beam, since the ultimate load was increased by 20 kN for 7 mm less of deflection.

The second layer of CFRP significantly increased the load-bearing capacity when compared to SB-1.1 and SB-1.2, although it also made the beams less ductile, as shown in Figure 3-15. The yield point of SB-2.1 is similar to that of SB-1.1 and SB-1.2, while SB-2.2 had a yield point almost 60 kN higher than the control.

Figure 3-16 to Figure 3-18 provide a visual indication of the beams' performance after the test when all the applied loads were removed. These images are composites, created by stitching multiple photos together to avoid obstructions caused by the loading frame during photography. They are intended to facilitate comparisons of the cracking patterns and residual deflection observed in the beams. Figure 3-16 shows CB-1 after the test, exhibiting significant cracks and high deformation. Figure 3-17, depicting SB-1.1, shows a slight improvement in handling the load when compared to the deflection of the control beam, with fewer and less severe cracks. In Figure 3-18 3-18, representing SB-2.1, the improvements are even more noticeable, with less deformation and even fewer cracks. The number of vertical cracks for half the span went from 29 for CB-1, down to 27 for SB-1.1, while SB-2.1 has 24. While the applied loads increased significantly from CB-1 to SB-2.1, the reduction in the number of cracks highlights the effectiveness of the strengthening technique and was successful in enhancing the serviceability which may, in turn, improve the durability of the beams.

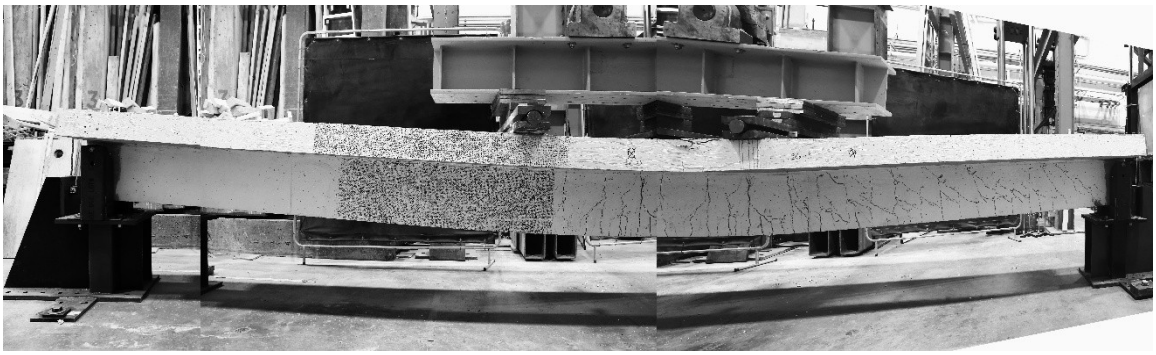

Figure 3-16. CB-1 control beam at failure

Figure 3-17. SB-1.1 single layer at failure

Figure 3-18. SB-2.1 double layer at failure

3.4.3 DIC

On Figure 3-19, the longitudinal strains (ε_{xx}) on the surface of the beams are shown, highlighting areas where cracks have already formed or are about to form. These images, all captured using the same camera setup described in Section 3.3.3 and at an applied load of 535kN, which was near the ultimate load of the control beams, offer valuable insights into the deformation process of strengthened concrete T-beams.

The control beams, shown in Figure 3-19 (a) and (b), exhibit significant deformation and more pronounced surface cracking. SB-1.1 and SB-1.2 (Figure 3-19 (c) and (d)) show slight improvements, while SB-2.1 and SB-2.2 (Figure 3-19 (e) and (f)) demonstrate significantly reduced crack development, particularly near the loading point. This improved behavior is further

supported by the data in Table 3-6, which shows a reduction in deformation of up to 70% for the strengthened beams.

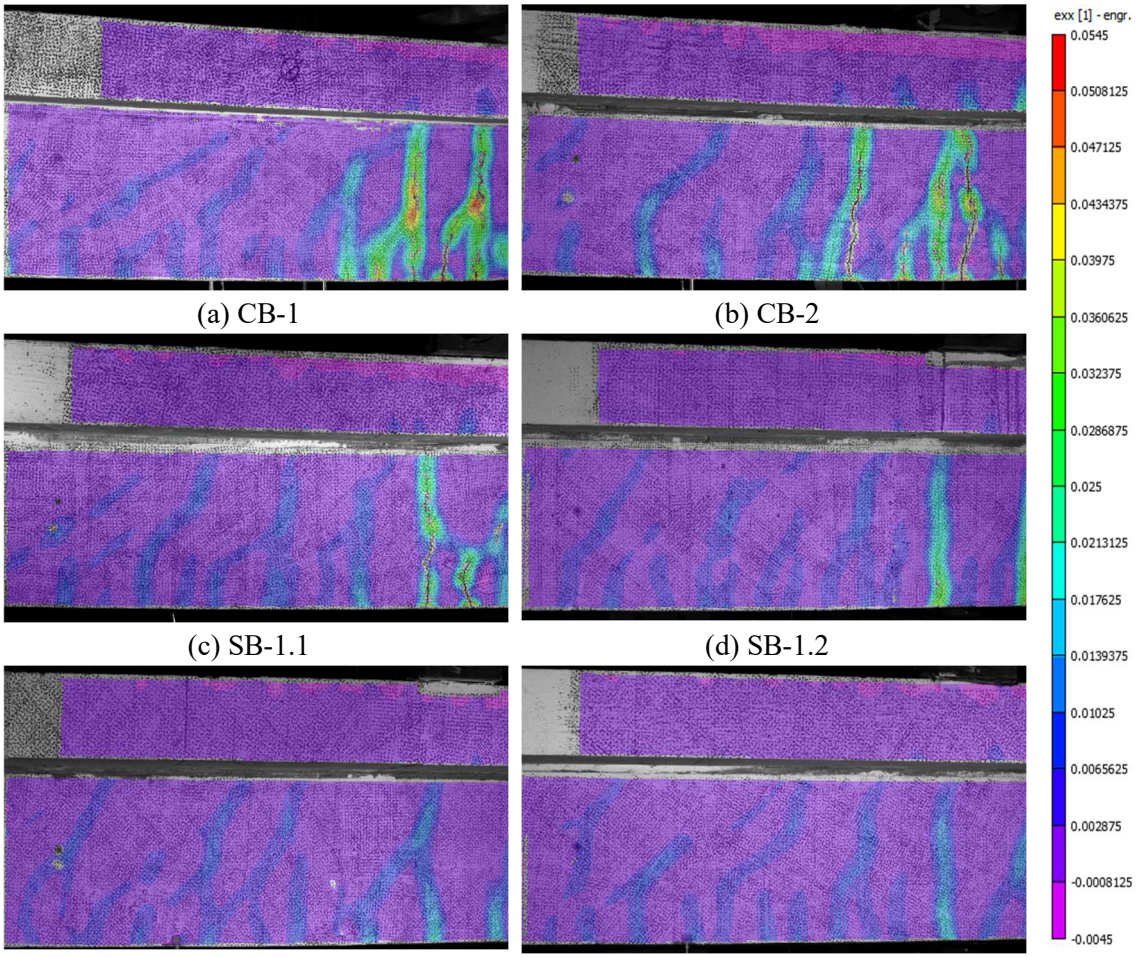

(a) CB-1 (b) CB-2

(c) SB-1.1 (d) SB-1.2

(e) SB-2.1 (f) SB-2.2

Figure 3-19. Digital Image Correlation (DIC) at 535 kN

Table 3-6. Summary of Deformation at 535 kN

Beam	Deformation at mid-span (mm)	Percentage of Reduction (Vs. CB-1)	Percentage of Reduction (Vs. CB-2)
CB-1	131	-	-
SB-1.1	82	37.4%	-
SB-1.2	51	61.1%	-
CB-2	130	-	-
SB-2.1	39	-	70.0%
SB-2.2	44	-	66.2%

These results highlight the effectiveness of CFRP straps in improving the performance of T-beams. By reducing crack formation, and increasing both durability and load-bearing capacity, the strengthening technique proves to be a reliable and practical solution for structural reinforcement. Furthermore, the use of two layers of CFRP straps enhances the efficiency of the system, making it a promising option with potential long-term maintenance benefits.

3.4.4 Strain of CFRP and Movement of Anchors

Figure 3-20 (strain vs. load) and Figure 3-21 (strain vs. displacement) provide insight into the behaviour of CFRP straps under increasing load. These graphs illustrate the initial linear strain response as the straps are loaded, followed by nonlinear deviations as the straps experience cracking and damage, slippage of the laminated sheet in the anchors or movement of the anchors.

In the legends, A1 and A3 refer to the first layer of CFRP positioned on the left and right sides of the beam, respectively, while B1 and B3 denote the second layer of CFRP, also positioned on the left and right sides as per the chosen viewpoint. For all tests, the strain values were zeroed at the beginning to ensure consistent evaluation of the CFRP behaviour.

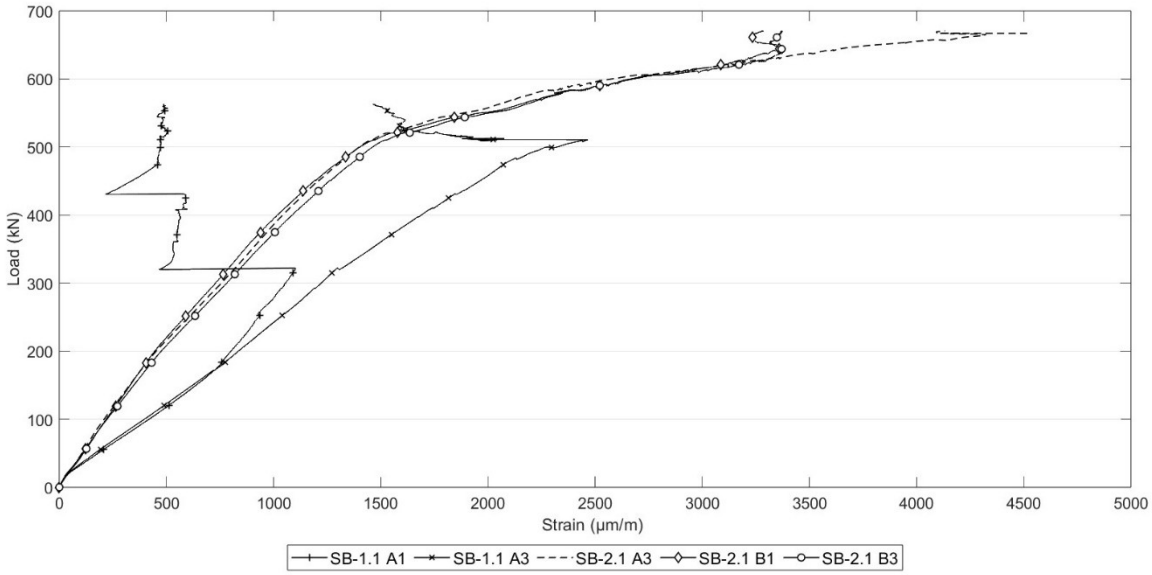

Figure 3-20. Strain of CFRP Straps vs. Load

Initially, the linear strain distribution aligns with the expected linear stress-strain response of CFRP. This suggests that the straps are effectively engaging with the applied load, sharing the increased tension in conjunction with the steel reinforcement and performing as intended, before yielding of the steel. After yielding, nonlinearity is visible in all curves, with SB-1.1 A1 displaying particularly distinct behavior before yielding, as discussed below. If the CFRP straps are evenly loaded and fully effective, and slipping or anchor movement is minimized, the CFRP laminated sheets will experience a significant increase in strain after the steel yields even with little additional load

applied. This increase in strain will lead to higher stress and tension forces in the CFRP straps, ultimately enhancing the moment capacity of the strengthened beams. This desired behavior is clearly demonstrated in SB-2.1, where the straps are particularly effective

The straps are less effective in SB-1.1, as evidenced by the first major deviation in SB-1.1 A1, which aligns with the first audible CFRP crack at 321 kN. This observation suggests that the sudden strain release was caused by localized damage, reducing the effectiveness of the straps. Beyond this point, the strap reengages, showing its ability to retain some load-carrying capacity even after being damaged. A subsequent sudden strain release is noticeable in the Figure 3-20 at approximately 430 kN, which could be attributed to additonal crack forming or significant anchor slippage.

Comparing SB-1.1 and SB-2.1 highlights the influence of the tensioners. SB-1.1 exhibits highly uneven strain distribution across its straps, indicating less effective force sharing. In contrast, SB-2.1 maintains a more consistent strain distribution, suggesting that the tensioners help evenly distribute loads and improve the overall utilization of CFRP strengthening.

The zone of nearly constant strain in Figure 3-21 could be attributed to continuous slippage of the CFRP withing the anchor. The straps remain active and do not fail as the beam deforms but they are not reaching their full load-carrying potential, nor are they increasing the load carrying capacity of the beam. This suggests that slippage prevents further strain accumulation in the straps, thereby limiting the overall efficiency of the strengthening system.

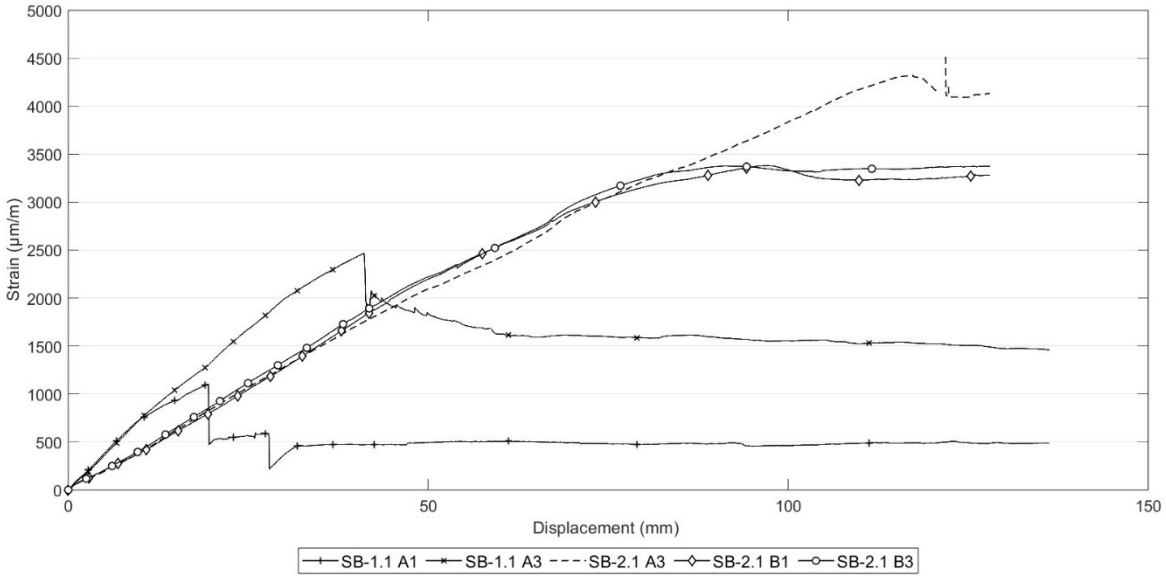

Figure 3-21. Strain of CFRP vs. Displacement

As described above, the observed nonlinearity of all three SB-2.1 straps in Figure 3-20 is the expected behaviour of an effective CFRP strap. Once the steel yields, the CFRP takes up most of

the additional load, while the steel contributes little to the final increase in beam's capacity. Consequently, the rate of straining in the CFRP increases significantly. Figure 3-22 suggests that at high loads the anchors are more likely to move, however in the case of SB-2.1, this significant movement, when compared to SB-1.1, did not negate the effectiveness of the strengthening system and may have contributed to retaining some ductility within the system. Controlling, limiting and better predicting anchor slip and movement is critical in maintaining the overall efficiency and effectiveness of the reinforcement system.

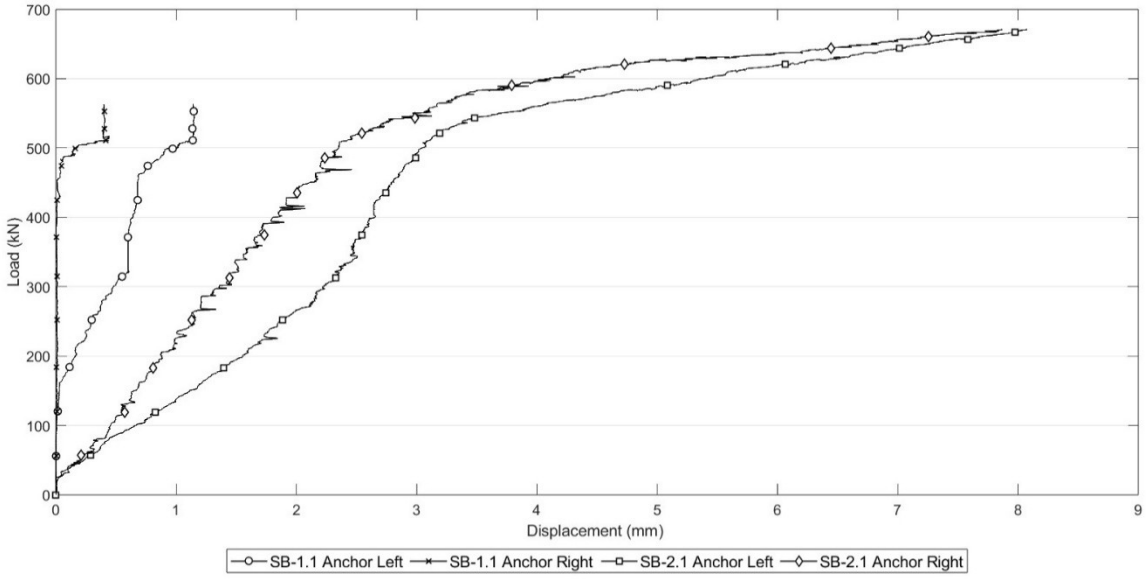

Figure 3-22. Movement of the anchors

These observations highlight the importance of proper anchoring and tensioning in order to optimize the performance of unbonded CFRP straps for strenghtening RC structures. While slippage within the anchor was initially considered a critical issue, a small amount of slippage may help stabilize strain levels in the straps, potentially preventing localized failures in the system. This is further supported by the post-experimental observations of SB-2.1, where three of its straps remained mostly intact, suggesting that controlled slippage did help prevent localized failures and possibly transverse breaks in the CFRP.

3.5 Numerical Model

This section presents a preliminary predictive model designed to represent the experimental beams' flexural behaviour. The model is based on the theoretical moment-curvature behaviour of concrete beams using a strain-compatibility approach. The load-deflection curve of each beam is then determined using the moment-curvature relationship along the length of the beam. Adjustments were made to the model to appropriately represent the unbonded CFRP straps. Once completed, the predictive model's results were compared with the experimental data to assess its accuracy and efficiency, identifying any discrepancies.

3.5.1 Theoretical Moment-Curvature Model

The model is based on the specified cross-sectional geometry of the beam. The model assumes that the shear reinforcement is adequate to sustain all loads, allowing the analysis to focus on flexural behaviour. The material properties used in the model align with those of the experimental beams, incorporating tested or calculated values where available. The tensile modulus of the CFRP straps was estimated within the ranges provided by the manufacturer, while a small level of prestressing force was achieved with the tensioners. Steel properties were based on the strength of the steel of the 25M Grade 400 reinforcement bar used in the construction of the beams and tested during the experimental program. The elastic modulus of the steel was set at E_s=200 GPa. The concrete properties stress-strain curve is based on a theoretical curve (Collins & Mitchell, 1997), but uses the properties from the tested cylinders. The CFRP properties, based on the manufacturer's coupon testing were used in the predictive model. This consisted of a modulus of elasticity of 163 GPa and a tensile strength of 2445 MPa (85% of the maximum manufacturer's coupon test value in Table 3-3).

The model divides the beam into 50 horizontal layers of equal thickness, in which the linear strain distribution theory is used to determine the strain of the concrete in all the layers. In this theory, the strain is assumed to vary linearly from the top to the bottom of the beam. Where reinforcement is located, the strain compatibility theory assumes that the reinforcement undergoes the same strain as the surrounding concrete. The model iterates to find when the sum of the forces in the horizontal direction caused by the sections in compression and in tension is equal to zero, effectively finding equilibrium in the structure. Once the internal forces are resolved, the internal resisting moments can be calculated.

Concrete tensile strength is also included in the model, in particular, to represent the beam behaviour before initial cracking. Additional details regarding the material properties, including steel reinforcement strength, concrete behaviour, and a screenshot of the Excel spreadsheet which was used to program and display the model are provided in Appendix C

3.5.1.1 Sectional Analysis Adjustment for Unbonded Strengthening

To account for the unbonded strengthening, the sectional analysis was modified based on theory and equations used for unbonded cables and tendons in strengthened structures. The omega factor, as described by Bouffard (1999) and Naaman (1991), and included in CSA-S806 (CSA, 2021) was necessary to compensate for the lack of bonding, between the CFRP and the concrete beam, which alters the load transfer mechanism between the two components. Without this bond, the transfer of forces from the concrete to the CFRP occurs only at the anchor, affecting the beam's overall stiffness and load-bearing capacity. The omega factor accounts for the incompatibility in strains at the bottom of the beam and in the CFRP. It reduces the strains of the CFRP straps predicted by the linear strain distribution method, leading to a more accurate prediction of the beam's deformation and performance under load. The following equations were used to calculate the omega factor, with Figure 3-23 specifying the appropriate coefficient to use at each stage.

$$\Omega = \frac{2}{3}$$

$$\Omega_{cr} = \Omega \frac{I_{cr}}{I_g}$$

$$\Omega_u = \frac{3}{(L/d_{ps})}$$

Equation 1. Omega Factors

It is worthwhile noting that the omega factor at ultimate Ω_u becomes much less effective as the beam becomes longer or as the aspect ration (L/d_{ps}) increases. This approximate equation implies that for the non-prestressed strengthening application of the CFRP strap, effective strengthening cases would most likely be limited to simply supported bridges with a span-to-heigh ratio of 20 or less. At aspect ratios greater than 20, Ω_u would be lower than 0.15 which the model implies would be insufficient for effective and efficient strengthening. For reference, the experimental beams in this study have an aspect ratio of 12. It should be emphasized that more testing is required to definitively establish the upper limits of this method's applicability as other factors including overall length and loading patterns will affect the effectiveness of the straps.

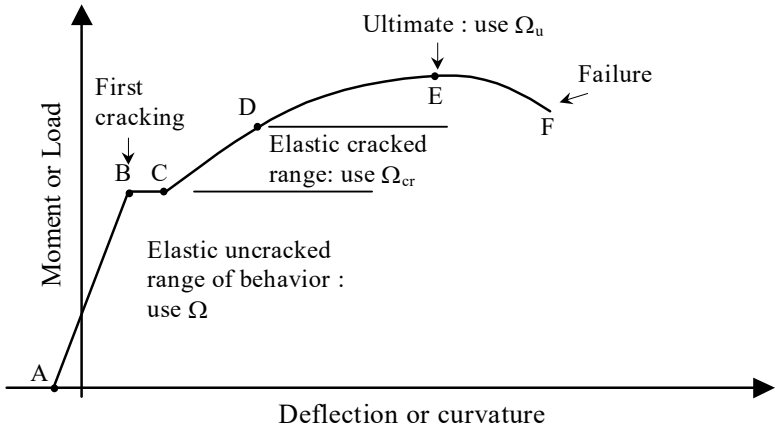

Figure 3-23. Applicability of bond reduction coefficients to the moment-curvature response (Bouffard, 1999)

3.5.2 Load-Displacement Model – Numerical Integration Method

The data from the moment-curvature model was used to create a theoretical load-deflection curve, which was then compared to the experimental results. The load-displacement model was based on the relationship between the curvature of a beam and its deflection under an applied load, providing insight into the structural behavior of loaded beams

The load-displacement model determined midspan deflection by numerically integrating curvature along the beam's length. The numeral integration method, shown in Equation 2, accounts for the

contribution of different sections along the beam, each defined by a moment arm in the equation. Accuracy of the model can be improved by increasing the number of sections used. To represent this experiment, moment arms were increased by 0.1m for each section, resulting in a total of 29 sections.

$$\delta = \left(\frac{\phi_1 x_1 + \phi_2 x_2}{2}\right)(x_2 - x_1) + \left(\frac{\phi_2 x_2 + \phi_3 x_3}{2}\right)(x_3 - x_2) + \cdots + \left(\frac{\phi_{n-1} x_{n-1} + \phi_n x_n}{2}\right)(x_n - x_{n-1})$$

Equation 2. Deflection at Midspan (Collins & Mitchell, 1997)

where,

δ is the deflection at midspan

φ is the curvature

x is the moment-arm or location along the length of the beam from the start of the beam of the section to integrate

In Figure 3-24, the predictive model is compared to CB-1, SB-1.2, and SB-2.1, which represent a control, a single-layer strengthened beam, and a double-layer strengthened beam, respectively. The theoretical curves, generated using the predictive model, show that the model overestimates stiffness and underestimates the yield point, but it generally captures the overall load-deflection behavior of a doubly reinforced concrete T-beam strengthened with unbonded CFRP. Table 3-7 provides a concise numerical summary of key values derived from Figure 3-24 at yielding and ultimate conditions, including load and mid-span displacement. The experimental results consistently show higher yield loads and displacements compared to the theoretical predictions, suggesting that the model underestimates the beams' initial capacity and deformation. Although ultimate load predictions align more closely with experimental data, discrepancies in displacement highlight the need for further refinement of the model.

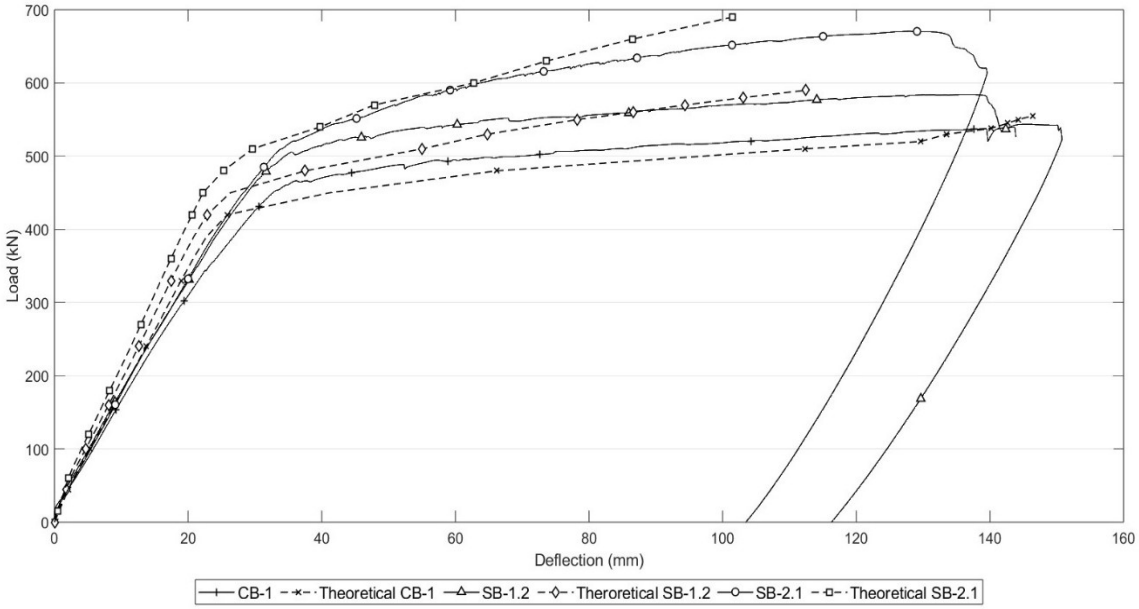

Figure 3-24. Comparison of Experimental Results with Predictive Model

Table 3-7. Comparison of Beam Behaviour - Theoretical Vs. Experimental

Beam	Type of Data	Yielding		Ultimate	
		Load (kN)	Displacement at mid-span (mm)	Load (kN)	Displacement at mid-span (mm)
CB-1	Theoretical	420	26	555	146
	Experimental	462	35	543	154
SB-1.2	Theoretical	450	26	590	112
	Experimental	505	35	583	129
SB-2.1	Theoretical	480	30	660	101
	Experimental	516	35	670	129

3.5.3 Linear Strain Distribution

As described in Section 3.5.1, the strain compatibility theory assumes a linear strain distribution under all loads. While the theoretical model accounts for strain differences between the layers and recognizes that yielding may initiate in one layer of steel before the other, experimental results suggest additional nonlinear effects, such as cracking and local force redistributions, contribute to the discrepancies observed between theoretical predictions (dashed lines) and experimental results (solid line). These discrepancies, illustrated in Figures 3-25 and 3-26, highlight the limitations of the theory in capturing and monitoring complex strain behaviors.

In Figures 3-25 and 3-26, additional points at the bottom of the graphs represent the strains in the CFRP straps at the specified load. For Figure 3-26, which involves two CFRP layers, the strain values for the experimental 245 kN load are not shown as they overlap with those of the theoretical CFRP at 39 kN. It is also important to note that the depth of the CFRP varies during the experiment until it comes in contact with the bottom of the beam. However, for clarity in the graphs, the strains are depicted at the original location of the straps. Despite this visual adjustment, the model accurately accounts for the changing distance of the straps as they move closer to the beam's surfaces.

As shown in Figure 3-25, at mid-span, the assumption of linear strain distribution remains valid up until yielding. However, beyond this point, deviations occur, particularly in the bottom layer of reinforcement, where nonlinear strain distribution develop. These discrepancies suggest limitations in the theoretical approach, and strain gauge monitoring, when capturing post-yield behaviour of section with multiple reinforcement layers in a highly cracked concrete environment.

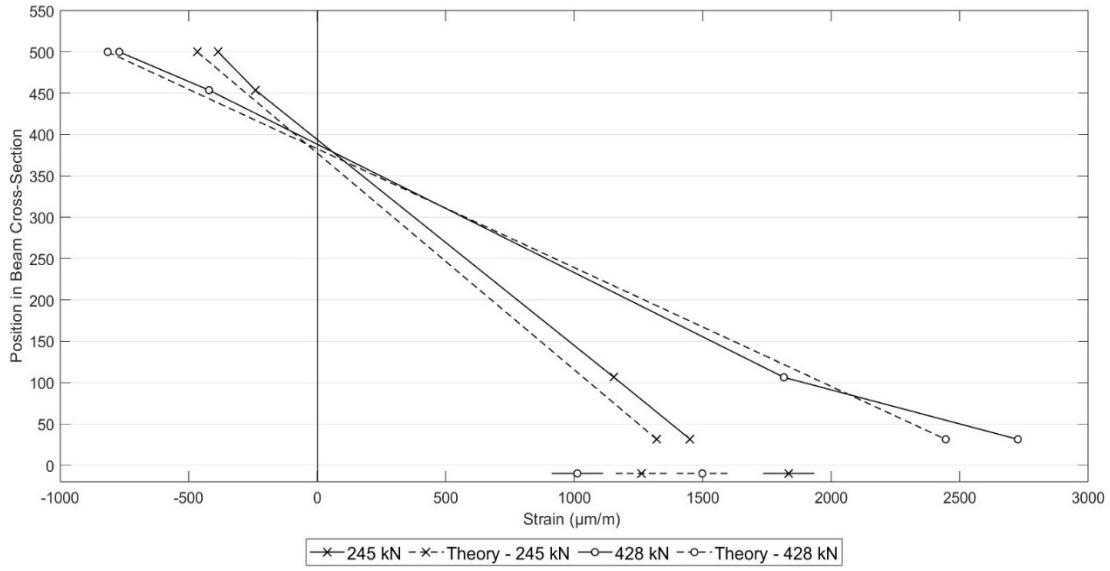

Figure 3-25. SB-1.1 Strain Distribution at Midspan

As illustrated in Figure 3-26, at 750 mm from mid-span; outside the zone of constant moment; the strain-profile remains consistently nonlinear throughout the experiment. This behaviour suggests that shear effects may also influence the strain response in regions where shear forces and inclined cracking are present, disrupting the expected linear strain distribution not only post-yielding as suggested by Figure 3-25 but at all load levels. Furthermore, as the applied load increases within the studied range, the discrepancies between theoretical predictions and experimental observations become more pronounced. This is particularly evident when comparing strain profiles across different load levels in Figure 3-25. While the behavior at loads beyond 560 kN remains uncertain

due to insufficient data, the observed trend within the studied range reinforces the assumption that regions outside the constant moment zone experience different force redistribution mechanisms, likely influenced by shear and local deformations.

When considering the CFRP, the model tends to overestimate the strain at higher loads, which can be seen in both Figures 3-25 and 3-26, while at lower loads, it underestimates the values as seen in Figure 3-26. This discrepancy may indicate that the omega factors used in the model are not fully accurate. However, it should be noted that the original strain of the CFRP before applying the omega factor is derived from the linear strain distribution theory which may already underestimate the strain at the bottom of the concrete. These findings suggest that while the model provides a reasonable approximation, its predictive accuracy could be improved with adjustments to better account for strain distribution and the variability of omega factors. Some of this difference could occur because of uneven stressing of the CFRP strap. This could be better monitored with additional instrumentation on the straps. Improvements to more evenly stress the straps, to limit slippage of the straps and anchors, and modifications to prevent damage to the straps may also improve the accuracy of predictions.

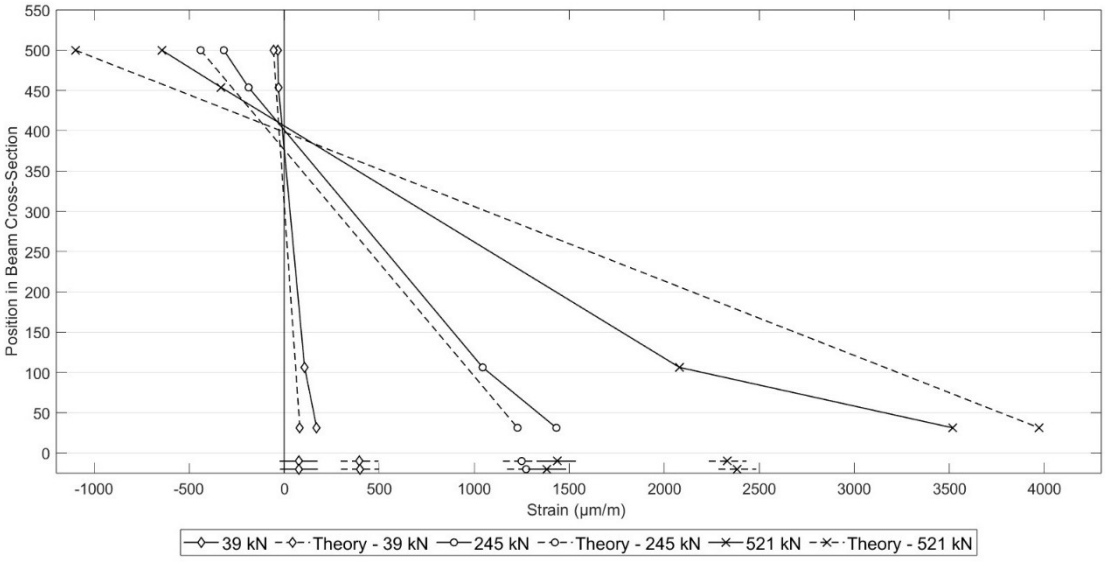

Figure 3-26. SB-2.2 Strain Distribution @ 750mm from Midspan

The experimental position of the neutral axis was calculated using data from the concrete and steel strain gauges installed on the beams. As shown in Table 3-7, the experimental and theoretical values for the neutral axis depth converge as the applied load increases. This suggests that while strain distribution may be nonlinear, as seen above, the neutral axis location is primarily governed by the

beam's overall curvature rather than strain distribution effects. This convergence suggests that a greater curvature in the beam enhances the model's predictive accuracy.

In this comparison, it was assumed that the depth of the neutral axis remained constant along the beam, despite the nonlinear behaviour discussed above. While variations in shear and bending moment outside the constant moment region can influence local stress distribution, as seen with the constant nonlinear behaviour discussed above, and potentially affect the neutral axis depth, the governing role of curvature remains unchanged.

As expected, the neutral axis shifts upward as the applied load increases, reflecting the transition toward a more plastified state in the tension reinforcement. Notably, this upward shift in the depth of the neutral axis is consistent across both the theoretical and experimental values, as demonstrated in Table 3-7.

Table 3-8. Comparison of the Depth of Neutral Axis

Beam	Load (kN)	Moment arm (m)	Bending Moment (kN-m)	Depth of Neutral axis (mm)	
				Theoretical	Experimental
SB-1.1	245	2.9	294	117.7	106.1
	428		514	112.5	111.7
SB-2.2	39	2.15	42	188.9	123.4
	245		264	119.9	99.2
	521		561	97.7	94.0

Despite its limitations, the theoretical model still holds value. The model provides a sufficiently accurate approximation of the strengthened beam's behavior, making it a valuable tool for understanding its structural response.

3.6 Conclusion

This research was designed to investigate the feasibility and effectiveness of unbonded CFRP strap systems combined with mechanical anchorages as a rapid strengthening technique for simply supported short-span reinforced concrete bridges.

The experimental results confirmed that this technique significantly improved the load-carrying capacity, with an increase of up to 22% compared to the control specimens, exceeding the initial minimal strengthening target of 12 to 15%. Furthermore, serviceability considerations revealed that the same strengthened beam exhibited reduced mid-span displacements at failure of 25% while still retaining significant ductility in the beam. The use of mechanical anchors facilitated a more efficient installation process compared to the traditional bonded CFRP systems, making this approach particularly suitable for time-sensitive applications, thereby addressing a key gap in the field.

The test results also highlighted the importance of anchor performance and proper tensioning in achieving optimal non-prestressed CFRP utilization. The introduction of tensioners led to a more uniform strain distribution across the CFRP straps, improving load-sharing efficiency. However, localized failures in the CFRP, non-uniform gripping and slippage in the anchors indicate that further refinement is needed to enhance the overall system performance. While controlled and limited CFRP slippage within the anchors may contribute to stabilizing strain levels and preventing localized failures, excessive movement can limit the straps' effectiveness.

The numerical model developed provides valuable insights into the load-deflection response of strengthened beams. While the model captured the general trends observed in the experiments, discrepancies in strain distribution and beam deformation suggest that refinements are needed to better account for the nonlinear behavior of reinforced concrete beams with more than one layer of tension reinforcement and the prediction of tension in the unbonded straps.

Overall, the study confirms that unbonded CFRP strengthening with mechanical anchors is a viable technique for rapidly increasing the load-bearing capacity of reinforced concrete T-beams. Future research should focus on optimizing anchor design to reduce slippage, refining numerical models to account for nonlinear strain behavior, and further assessment of the long-term performance of this strengthening technique under cyclic loading conditions.

3.7 References

American Concrete Institute Committee 440. (2018, March). Guide for the Design and Construction of Externally Bonded FRP Systems for. *ACI 440.2R-17*. American Concrete Institute.

Bouffard, P. B. (1999). *Externally Prestressing the Remianing Span of Severely Damaged Continuous Concrete Beams*. Kingston, Ontario: MEng Thesis, Royal Military College.

Brigante, D. (2014). *New composite materials. Selection, design and application.* Heidelberg: Springer International Publishing.

Collins, M. P., & Mitchell, D. (1997). *Prestressed Concrete Structures.* Response Publications.

Canadian Standards Association. (2021). CSA Standard S806. *Design and construction of building components with fibre-reinforced polymers* . Ontario, Toronto: CSA Group.

Department of National Defence. (2023, December). *Bridge and Gap Crossing Modernization*. Retrieved from Government of Canada: https://apps.forces.gc.ca/en/defence-capabilities-blueprint/project-details.asp?id=1015

El-Hacha, R., & Rizkalla, S. H. (2004). Near-Surface-Mounted Fiber-Reinforced Polymer Reinforcements for Flexural Strengthening of Concrete Structures. *ACI Structural Journal*, 717-726.

Ganesh, P., & Murthy, A. R. (2019). Repair, retrofitting and rehabilitation techniques for strengthening of reinforced concrete beam - A review. *Advances in concrete construction, 8(2)*, 101-117.

Hammad, M., Bahrami, A., Khushnood, R. A., & Khokhar, S. A. (2024). A State-of-the-Art Review on Structural Strengthening Techniques with FRPs: Effectiveness, Shortcomings, and Future Research Directions. *Materials, 17(6)*.

International Code Council Evaluation Service. (2022). AC125. *Acceptance criteria for concrete and reinforced and unreinforced masonry strengthening using externally bonded fiber-reinforced polymer composite systems*. ICBO Evaluation Service, Inc.

International Organization for Standardization. (2019). *ISO 527-1:2019 Plastics — Determination of tensile properties — Part 1: General principles.*

Jumaat, M. Z., Rahman, M. M., & Rahman, M. A. (2011). Review on bonding techniques of CFRP in strengthening concrete structures. *International Journal of the Physical Sciences, 6(15)*.

Li, F., Li, W., Lu, S., & Shen, L. (2019). Development of a Prestressing CFRP Laminate Anchorage System. *Advances in Materials Science and Engineering, 2019*.

MacDonald, A. J., & Wight, R. G. (2022, October 3). *Rapid military bridge evaluation software*. Retrieved from Canadian Army Today: https://canadianarmytoday.com/rapid-military-bridge-evaluation-software/?form=MG0AV3

MacGregor, J. G. (1988). *Reinforced Concrete: Mechanics and Design.* Prentice Hall.

Mohee, M. F., Al-Mayah, A., & Plumtree, A. (2017). Development of a novel prestressing anchor for CFRP plates:. *Composite Structures, 176*, 20-32.

Naaman, A. E., & Alkhairi, R. M. (1991). Stress at Ultimate in Unbonded Post-Tensioning Tendons: Part 2 - Proposed Methodology. *ACI Structural Journal, 8(6)*, 683-692.

North Atlantic Treaty Organization. (2019, February). Allied Joint Publication 3 (AJP-3). *Allied Joint Doctrine for the Conduct of Operations, UK Version*. NATO Standardization Office.

Piatek, B., Siwowski, T., Michalowski, J., & Blazewicz, S. (2020). Flexural Strengthening of RC Beams with Prestressed CFRP Strips: Development of Novel Anchor and Tensioning System. *Journal of Composites for Construction*.

Panahi, M., Zareei, S. A., & Izadi, A. (2021). Flexural strengthening of reinforced concrete beams through externally bonded FRP sheets and near surface mounted FRP bars. *Case Studies in Construction Materials, 15*.

Saadatmanesh, H., & Ehsani, M. R. (1991). RC Beams Strengthened with GFRP Plates. I: Experimental Study. *Journal of Structural Engineering, 117(11)*, 3417-3433.

Triantafillou, T. C., & Deskovic, N. (1991). Innovative Prestressing with FRP Sheets: Mechanics of Short-Term Behavior. *Journal of Engineering Mechanics, 117(7)*, 1652-1672.

Wang, H.-T., Liu, S.-S., Shi, J.-W., Xu, G.-W., Chen, M.-S., & Bian, Z.-N. (2024). Bonded and unbonded strengthening of RC beams with the prestressed CFRP plate system: An experimental study. *Construction and Building Materials, 438*.

Wight, R. G., Green, M. F., & Erki, M.-A. (2001). Prestressed FRP sheets for poststrengthening reinforced concrete beams. *Journal of Composites for Construction, 5(4)*, 214-220.

Yossef, N. M. (2015). Strenghtening Steel I-beams by Welding Steel Plates before or While Loading. *International Journal of Engineering Research and Technoclogy, 4(7)*, 545-550.

Chapter 4 – Conclusion and Recommendations

General

This research investigated the feasibility and effectiveness of unbonded CFRP strengthening systems with custom-designed mechanical anchors for the rapid strengthening of reinforced concrete T-beams, representing components of short-span simply supported concrete bridges. The study was motivated by the need for a practical, efficient, and rapidly deployable strengthening technique suitable for military applications. The research used experimental testing to assess the improvements of the load-bearing capacity, crack control, and serviceability benefits of this method. A numerical model was also created to predict the load-deflection behaviour of the strengthened beams.

Conclusions

The experimental results demonstrated that unbonded CFRP strengthening can significantly enhance the load-carrying capacity of simply supported reinforced concrete beams, with strength increases of up to 22% when using a double-layer configuration, confirming the effectiveness of the method and exceeding the initial strengthening target of 12 to 15%. The use of mechanical anchors facilitated rapid installation without the need for surface preparation or specialized adhesives, making this approach suitable for time-sensitive applications, such as military operations or disaster relief. Furthermore, the use of tensioners facilitated a more uniform strain distribution across the CFRP straps, improving load-sharing efficiency. However, the study highlighted that the non-uniform grip of the anchors remains a challenge, as localized failures and slippage were observed at high loads. Further refinement of the anchorage system is needed to minimize these inconsistencies.

Serviceability benefits were also observed, as strengthened beams exhibited reduced deflections under similar loads, with a reduction of up to 25%, which can contribute to prolonged structural integrity and improved performance under operational conditions. Crack development was also monitored, showing that the CFRP system helped control crack propagation and limit crack widths under the same load, which contributes to improved durability.

The numerical model developed in this study provided valuable insights into the load-deflection behavior of the strengthened beams, capturing the experimental trends with reasonable accuracy. However, due to its reliance on linear strain distribution assumptions, the model underestimated yielding and did not fully capture nonlinear effects present in reinforced beams with multiple layers of tension reinforcement and unbonded strengthening components.

Overall, the findings confirm that unbonded CFRP with mechanical anchorage is a viable and efficient method for the rapid strengthening of short-span simply supported reinforced concrete bridges and similar structures. This technique offers a promising alternative to bonded CFRP systems, particularly in scenarios where quick implementation and minimal surface preparation are required. Furthermore, as discussed in Chapter 1, to meet military engineering requirements, the

proposed strengthening method outlined in the document appropriately addressed the outlined criteria:

- **Rapid Implementation.** The use of the custom-designed mechanical anchors facilitated rapid installation within a single work shift. It eliminated the need for surface preparation or specialized adhesives, making this approach ideal for time-sensitive applications, such as military operations or disaster relief.
- **Use Easily Transportable Materials.** The CFRP straps used in this study are lightweight and compact, ensuring they are easily transportable by air or in military vehicles.
- **Minimal Equipment and Specialized Tools/Knowledge.** The strengthening technique employed requires limited equipment and involves a straightforward installation process. The use of mechanical anchors and tensioners simplifies the application, as the method can be carried out using commonly available tools and without the need for highly specialized trade knowledge.
- **Limited Access to the Bridge Structure.** By relying on mechanical anchors and unbonded CFRP, the technique requires access only to critical regions such as abutments and piers, eliminating the need for extensive bridge access platforms.
- **Flexibility in Application.** The unbonded system accommodates bridges with varying span lengths, damaged concrete, and existing deformation. It can be installed even on bridges with significant cracks or cover damage, demonstrating adaptability to diverse conditions

Recommendations for Future Research

Building on the findings of this study, the following areas are recommended for further investigation:

1. **Optimization of Dead-End Mechanical Anchors**. Enhance anchor grip to reduce slippage and improve force transfer efficiency in order to limit transversal breaks. Development and testing of the theoretical adjustable dead-end anchors could increase the adaptability and flexibility of the system to a variety of structural conditions, such as bridges with minor beam variations.

2. **Investigation of Live-End Mechanical Anchors for Prestressing.** Evaluate the effectiveness of live-end anchors to address limitations posed by the maximum height-to-span ratio or length restrictions likely to exist with non-prestressed CFRP strap strengthening. Prestressing is likely to make more efficient use of the strengthening material and is likely to delay crack initiation and reduce crack widths. This approach could further enhance the structural performance of beams, including improvements in serviceability

3. **Exploration of Additional CFRP Layers.** Investigate whether a third layer of CFRP could further enhance load capacity while avoiding excessive brittleness. Exploring

alternative configurations to balance strength gains and structural ductility is recommended.

4. **Enhancement of Strain Measurement Techniques.** Consider using fibre optic sensors instead of localized strain gauges to improve understanding of strain distribution and beam behavior. Fibre optic sensors offer continuous strain monitoring over larger areas, providing more comprehensive data and insights into the performance of CFRP systems and the overall beam response.

5. **Refinement of Numerical Models.** Incorporate nonlinear behaviour when using multiple layers of tension steel into the numerical model to improve its predictive accuracy as well as better representing the unbonded CFRP straps. Validation of these refinements will ensure that the simple model can more accurately represent the beam behaviour, particularly in the elastic-plastic range where only portions of the reinforcement bars have yielded.

6. **Alternative Installation Approaches.** Investigate the use of a single wider CFRP strap as an alternative to multiple narrower straps. This modification could simplify installation, eliminate the need to calibrate adjacent strap tensions, and reduce overall installation time. Additionally, if narrower straps are used, the feasibility of adding an extra layer of CFRP could be revisited. The reduced width may help mitigate potential brittleness concerns while also increasing the moment arm of the strap, potentially improving overall structural efficiency.

7. **Long-Term Performance Studies Under Cyclic Loading.** Assess the performance of unbonded CFRP systems under cyclic loading and varying environmental conditions. Testing for fatigue resistance, durability, and environmental exposure will ensure reliability in real-world applications

This study successfully demonstrated a rapid strengthening technique that enhances structural performance while meeting key military engineering requirements. By addressing the identified limitations and refining the system further, unbonded CFRP strengthening has the potential to become a standard solution for emergency and temporary bridge reinforcement.

Chapter 5 - References

Adhikary, B. B., & Mutsuyoshi, H. (2006). Shear strengthening of RC beams with web-bonded continuous steel plates. *Constr. Build. Mater., 20*, 296-307.

Alaee, F. J., & Karihaloo, B. L. (2003). Retrofitting of Reinforced Concrete Beams with CARDIFRC. *J. Compos. Constr., 7*, 174-186.

American Concrete Institute. (2013). ACI Concrete Terminology. *ACI CT-13*. American Concrete Institute.

American Concrete Institute Committee 440. (2018, March). ACI 440.2R-17. *Guide for the Design and Construction of Externally Bonded FRP Systems for Strengthening Concrete Structures*. American Concrete Institute.

American Concrete Institute Committee 562. (2016). ACI 562-16. *Code requirements for assessment, repair, and rehabilitation of existing concrete structures*. American Concrete Institute.

Bakis, C. E., Bank, L. C., Brown, V. L., Cosenza, E., Davalos, J. F., Lesko, J. J., . . . Triantafillou, T. C. (2002). Fiber-Reinforced Polymer Compositesfor Construction - State-of-the-Art Review. *Journal of Composites for Construction, 6(2)*, 73-87.

Bhatt, P., & Goe, A. (2017). Carbon fibres: production, properties, and potential use. *Material Science Research India, 14(1)*, 52-57.

BMCDP. (2018). *Bridge Rehabilitation and Strengthening Manual: Part 1.* Government of People's, Republic of Bangladesh Ministry of Road Transport and Bridges, Roads and Higways Department.

Bouffard, P. B. (1999). *Externally Prestressing the Remianing Span of Severely Damaged Continuous Concrete Beams*. Kingston, Ontario: MEng Thesis, Royal Military College.

Brigante, D. (2014). *New composite materials. Selection, design and application.* Heidelberg: Springer International Publishing.

Burningham, C. A., Pantelides, C. P., & Reaveley, L. D. (2014). New unibody clamp anchors for posttensioning carbon-fiber-reinforced polymer rods. *PCI Journal*, 103-113.

Burtscher, S. L. (2008). Wedge anchorage for CFRP strips. *J. Compos. Constr., 12(4)*, 446-453.

Canadian Army Today. (2022, October 3). *Rapid military bridge evaluation software*. Retrieved from Canadian Army Today: https://canadianarmytoday.com/rapid-military-bridge-evaluation-software/?form=MG0AV3

Canadian Standard Association. (2021). CSA Standard S6:19 (R2024). *Canadian Highway Bridge Design Code*. Ontario, Toronto: CSA Group.

Canadian Standards Association. (2020). CSA A23.3:19. *Design of Concrete Structures*. Toronto, ON: Standards Council of Canada.

Canadian Standards Association. (2021). CSA Standard S806-12. *Design and construction of building components with fibre-reinforced polymers*. Ontario, Toronto: CSA Group.

Cheong, H. K., & MacAlevey, N. (2000). Experimental behaviour of jacketed reinforced concrete beams. *J. Struct. Eng. 126(6)*, 692-699.

Collins, M. P., & Mitchell, D. (1997). *Prestressed Concrete Structures.* Response Publications.

Deng, J., Zhong, M., Zheng, Y., & Zhu, M. (2022). Experimental Study on the Durability of Steel Anchors for Prestressed CFRP Laminates under Accelerated Galvanostatic Corrosion. *Materials, 15(16)*.

Department of National Defence. (2023, December). *Bridge and Gap Crossing Modernization*. Retrieved from Government of Canada: https://apps.forces.gc.ca/en/defence-capabilities-blueprint/project-details.asp?id=1015

El-Hacha, R., & Rizkalla, S. H. (2004). Near-Surface-Mounted Fiber-Reinforced Polymer Reinforcements for Flexural Strengthening of Concrete Structures. *ACI Structural Journal*, 717-726.

El-Hacha, R., Wight, R. G., & Green, M. F. (2001). Prestressed fibre-reinforced polymer. *Prog. Struct. Engng Mater, 3*, 111-121.

Fleming, C. J., & King, G. E. (1967). The Development of Structural Adhesives for Three Original Uses in South Africa. *RILEM International Symposium, Synthetic Resins in Building Construction*, 75-92.

Ganesh, P., & Murthy, A. R. (2019). Repair, retrofitting and rehabilitation techniques for strengthening of reinforced concrete beam - A review. *Advances in concrete construction, 8(2)*, 101-117.

Hammad, M., Bahrami, A., Khushnood, R. A., & Khokhar, S. A. (2024). A State-of-the-Art Review on Structural Strengthening Techniques with FRPs: Effectiveness, Shortcomings, and Future Research Directions. *Materials, 17(6)*.

Harajli, M. H. (1993). Strenghtening of Concrete Beams by External Prestressing. *PCI Journal*, 76-88.

Hassan, T. K. (2002). Flexural Performance and Bond Characteristics of FRP Strengthening Techniques for Concrete Structures, PhD Thesis. Winnipeg, Manitoba: Department of Civil and Geological Engineering, University of Manitoba.

Heiza, K., Nabil, A., Meleka, N. N., & Tayel, M. (2014). *State-of-the Art Review: Strengthening of Reinforced Concrete Structures – Different Strengthening Techniques.*

Hosseini, A., Ghafoori, E., Motavalli, M., Nussbaumer, A., Zhao, X.-L., & Koller, R. (2018). Prestressed Unbonded Reinforcement System with Multiple CFRP Plates for Fatigue Strengthening of Steel Members. *Polymers, 10(3)*.

International Code Council Evaluation Service. (2022). AC125. *Acceptance criteria for concrete and reinforced and unreinforced masonry strengthening using externally bonded fiber-reinforced polymer composite systems*. ICBO Evaluation Service, Inc.

International Organization for Standardization. (2019). *ISO 527-1:2019 Plastics — Determination of tensile properties — Part 1: General principles.*

Jumaat, M. Z., & Ashraful Alam, M. D. (2010). Experimental and numerical analysis of end anchored steel plate and CFRP laminate flexurally strengthened reinforced concrete (r.c.) beams. *International Journal of the Physical Sciences, 5(2)*, 132-144.

Jumaat, M. Z., Rahman, M. M., & Rahman, M. A. (2011). Review on bonding techniques of CFRP in strengthening concrete structures. *International Journal of the Physical Sciences, 6(15)*.

Khode, H. S. (2019). Advanced Retrofitting Techniques for Reinforced Concrete Structures: A State of an Art Technical Review. *International Journal of Innovative Research in Science, Engineering and Technology, 8(10)*.

Li, C., & Aoude, H. (2023). Effect of UHPC jacketing on the shear and flexural behaviour of high-strength concrete beams. *Structures, 51*, 1972-1996.

Li, F., Li, W., Lu, S., & Shen, L. (2019). Development of a Prestressing CFRP Laminate Anchorage System. *Advances in Materials Science and Engineering, 2019*.

MacDonald, A. J., & Wight, R. G. (2022, October 3). *Rapid military bridge evaluation software*. Retrieved from Canadian Army Today: https://canadianarmytoday.com/rapid-military-bridge-evaluation-software/?form=MG0AV3

MacGregor, J. G. (1988). *Reinforced Concrete: Mechanics and Design.* Prentice Hall.

Mohee, F. M., Al-Mayah, A., & Plumtree, A. (2016). Anchors for CFRP plates: State-of-the-art review and future potential. *Composites Part B: Engineering, 90*, 432-442.

Mohee, M. F., Al-Mayah, A., & Plumtree, A. (2017). Development of a novel prestressing anchor for CFRP plates:. *Composite Structures, 176*, 20-32.

Motavalli, M., Czaderski, C., & Pfyl-Lang, K. (2011). Prestressed CFRP for Strengthening of Reinforced. *Journal of Composites for Construction, 15(2)*, 194-205.

MurtazaRasool, A., Khan, U., & Hammed, A. (2017). Assessment of internal and external prestressing of prestressed box girders. *International Journal of Technical Research & Science, 2(9)*, 536-547.

Naaman, A. E., & Alkhairi, R. M. (1991). Stress at Ultimate in Unbonded Post-Tensioning Tendons: Part 2 - Proposed Methodology. *ACI Structural Journal, 8(6)*, 683-692.

Nordin, H. (2004). *Strengthening structures with externally prestressed tendons, Laboratory tests.* Sweden: Luleå University of Technology.

North Atlantic Treaty Organization. (2019, February). Allied Joint Publication 3 (AJP-3). *Allied Joint Doctrine for the Conduct of Operations, UK Version*. NATO Standardization Office.

Ostrowski, K. A., & Furtak, K. (2021). The influence of concrete surface preparation on the effectiveness of reinforcement using carbon fibre-reinforced polymer in high-performance, self-compacting, fibre-reinforced concrete. *Composite Structures, 276*.

Panahi, M., Zareei, S. A., & Izadi, A. (2021). Flexural strengthening of reinforced concrete beams through externally bonded FRP sheets and near surface mounted FRP bars. *Case Studies in Construction Materials, 15*.

Piatek, B., Siwowski, T., Michalowski, J., & Blazewicz, S. (2020). Flexural Strengthening of RC Beams with Prestressed CFRP Strips: Development of Novel Anchor and Tensioning System. *Journal of Composites for Construction*.

Polymer Process. (n.d.). *Fiber Reinforced Polymer: Manufacturing Process and Use in Construction*. Retrieved from Polymer Process: https://polymer-process.com/fiber-reinforced-polymer/?form=MG0AV3

Porteous, J. E. (2001). Strengthening the remaining span of severely damaged shear-deficient two-span concrete beams.

Preto, P. B. (2014). *Guidelines for External Prestressing as Strengthening Technique for Concrete Structures.* Lisbon: Departamento de engenharia civil of Instituto Superior Técnico.

Roy, D., & Saha, S. (2024). Rehabilitation Techniques for Concrete Structures: An Overview of Modern Practices . *SSR Journal of Engineering and Technology, 1(1)*.

Saadatmanesh, H., & Ehsani, M. R. (1991). RC Beams Strengthened with GFRP Plates. I: Experimental Study. *Journal of Structural Engineering, 117(11)*, 3417-3433.

Saeed, Y. M. (2016). *Behavior of Prestressed Concrete Beams with CFRP Behavior of Prestressed Concrete Beams with CFRP Strands Strands. PhD. Dissertation, Portland State University*. Portland, Oregon, USA.

Teng, J. G., Smith, S. T., Yao, J., & Chen, J. F. (2003). Intermediate crack-induced debonding in RC beams and slabs. *Construction and Building Materials, 17(6-7)*, 447-462.

Triantafillou, T. C., & Deskovic, N. (1991). Innovative Prestressing with FRP Sheets: Mechanics of Short-Term Behavior. *Journal of Engineering Mechanics, 117(7)*, 1652-1672.

Virgoleux, M. P. (1990). External Prestressing: from Construction History to Modern Technique and Technology. *External Prestressing in Bridges, ACI Special Publication SP-120*, 1-60.

Vp, F. (2023, April 23). *Retrofitting of Concrete Reinforced Structure*. Retrieved from Linkedin: https://www.linkedin.com/pulse/retrofitting-concrete-reinforced-structure-fahiz-vp

Wang, H.-T., Liu, S.-S., Shi, J.-W., Xu, G.-W., Chen, M.-S., & Bian, Z.-N. (2024). Bonded and unbonded strengthening of RC beams with the prestressed CFRP plate system: An experimental study. *Construction and Building Materials, 438*.

Wight, R. G. (1998). *Strengthening concrete beams with prestressed fiber reinforced polymer sheets. Ph.D. Thesis: Queen's University, Department of Civil Engineering*. Kingston, Ontario.

Wight, R. G., Green, M. F., & Erki, M.-A. (2001). Prestressed FRP sheets for poststrengthening reinforced concrete beams. *Journal of Composites for Construction, 5(4)*, 214-220.

Wu, Y.-F., & Huang, Y. (2008). Hybrid Bonding of FRP to Reinforced Concrete Structures. *Journal of Compolsites for Construction, 12(3)*, 266-273.

Yan, W., Chen, L., Han, B., Xie, H., & Sun, Y. (2022). Flexural Analysis Model of Externally Prestressed Steel-Concrete Composite Beam with Nonlinear Interfacial Connection. *Applied Sciences, 12(9)*.

Yossef, N. M. (2015). Strenghtening Steel I-beams by Welding Steel Plates before or While Loading. *International Journal of Engineering Research and Technoclogy, 4(7)*, 545-550.

Zhang, X., Li, G., & Wu, H. (2020). Applications of FRP composites in retrofitting and strengthening of existing infrastructure. *Journal of Composites for Construction, 24(2)*.

Appendix A – Construction Details and Lessons Learned

Formwork

Due to limited space and personnel availability, two different pours were planned 40 days apart. Three concrete formworks were built on site following design specifications, and the formworks were reused for the second pour. Given the shape of the T-beam, side supports were also required to ensure that the flanges wouldn't fail or sag excessively under their own weight during the pour and the curing process, as shown in Figure A-1.

(a) Concrete formwork

(b) Removal of the beam

Figure A-1. Formwork

All beams and cylinders were left to cure in the same ambient conditions, and were removed from their forms a few days apart. All cylinders were tested in compression using a 1335 kN Rhiele compression testing machine, following the CSA 23.2-9c Standard, Compressive Strength of Cylindrical Concrete Specimens.

Reinforcement bars

All reinforcement steel were provided by a local supplier. Stirrups for the web were bent to shape by the manufacturer according to specifications. All other reinforcement was cut to the proper size on site. Reinforcement bar cages were built on site using jigs to make the construction faster and more consistent between each beam, as shown in Figures A-2 and A-3. Test samples were taken from the 25M reinforcement bar, shaped and tested according to the ASTM Standard A370-24, *Standard Test Methods and Definitions for Mechanical Testing of Steel Products* using a Tinius Olsen 133 kN (30,000 lb) Universal Testing Machine.

Figure A-2. Jigs for Reinforcement Bars Cages

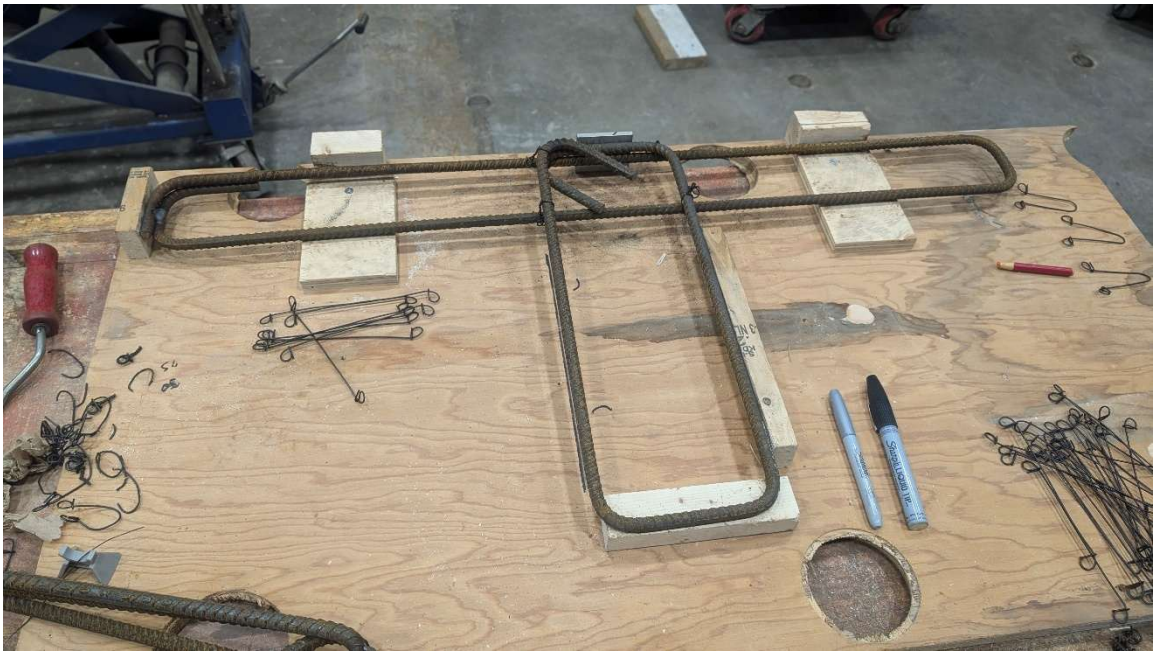

Figure A-3. Jigs for Stirrups

CFRP

CFRP was specifically chosen for its high strength-to-weight ratio, making it an ideal material for rapid field execution. The lightweight nature of CFRP means that it doesn't require an entire team to move, simplifying on-site logistics, as well as reducing the labor required. As illustrated in

Figure A-4, a single person can easily transport a 150 m roll of CFRP. However, to ensure the roll doesn't unroll and to accurately cut the CFRP to the proper length, a minimum of two people is required for this task. This property of CFRP not only simplifies handling but also accelerates the installation process, making it a highly efficient choice for strengthening applications.

Figure A-4. Demonstration of Lightweight Property of the CFRP

Anchor

The double-layer U-shape dead anchor underwent the most modifications throughout the experimental program. All adjustments made were based on the lessons learned from each previous test. In the single-layer version, six bolts were used over a 300 mm length, which was the maximum number possible without compromising the structural integrity of the plate. However, with the introduction of a second layer, the middle plate still utilized six bolts, but these bolts were divided; three connecting to the bottom plate and three connecting to the top plate. This redistribution of bolts per plate necessitated further changes to ensure sufficient mechanical anchorage. The overall length of the anchor was then increased by 50% compared to the single-layer dead anchor, bringing it to 450 mm long.

Initially, both layers remained independent while still sharing a common grip plate. During the preparation for SB-2.1, it was observed that plate number 3 was pulling on plate number 2, causing an unintended loss of tension in the first layer of CFRP. To address this issue in SB-2.2, six additional holes were added, allowing direct bolting from plate #1 to plate #3, preventing plate number 3 from transferring excessive force to plate #2, ensuring better tension retention in both CFRP layers. These six additional bolts were torqued before the bolts joining plate #3 to plate #2.

During the SB-2.1 experiment, shear cracks propagated from the support through the anchors' bolts. The force exerted on the anchor was so significant that it caused deformation of the bolts, as shown in Figure A-5. To address these issues, further modifications were made to the double-layer dead anchor. The extra piece, shown in Figure 3-6(a), was added to the anchors to provide extra shear support and limit rotation.

Figure A-5. Deformed Anchors' Bolts

Tensioners

The tensioners were designed to ensure that there would be no slack in the strap. While this device functions similarly to the live anchor prestressing technique, it operates on a smaller scale. Though it may not generate actual prestressing, it can tighten the straps more effectively than by hand.

In the drawings, the two small metal plates pinching the strap are referred to as a "Sandwich". These plates are secured with bolts torqued to 47.5 Nm (35 ft-lb), and threaded rods and bolts going through the blocks; one block bolted to the "sandwich" and the other one bolted to the anchor. Since the tensioners had to be installed one in front of the other, one tensioner used 9.5mm (3/8 in.) high strength bolts, while the other utilized 9.5 mm (3/8 in.) threaded rods. However, the 9.5mm (3/8 in.) threaded rod frequently bent under the applied force, causing the tensioning device to twist the strap. This twisting introduced inaccuracies in measuring the actual strain on the strap.

As shown in Figure A-6, even with high strength ½ in. bolts, the issue persisted, however to a lesser degree than with the 9.5 mm (3/8 in.) threaded rods.

Figure A-6. Tensioning Device Twisting the Strap

During the tensioning of SB-2.1, similar issues happened, exacerbated by the fact that parts were reused and the threaded rods had already been bent once. To address this, an improved tensioning device was developed. The updated design featured a thicker and wider block on both the anchor and the "sandwich," along with the replacement of threaded rods with 12.7 mm (½ in.) high-strength 305 mm (12 in.) bolts. The thicker block also allowed for the use of an impact gun for tensioning, streamlining the process and making it faster. For SB-2.2, both tensioning devices were upgraded to the thicker block design with 12.7 mm (½ in.) bolts.

Appendix B – Design Spreadsheet

This excerpt from the design spreadsheet presents the calculation of the steel ratio for the beams and confirms that the neutral axis is located within the slab. The inputted T-beam geometry follows the design specifications, while the material properties define the key characteristics of concrete and steel as requested to the manufacturer.

The calculations confirms that the beam is under-reinforced based on the reinforcement area (As) and its corresponding steel ratio (ρ). Additionally, the rebars table is organized from the bottom of the beam upwards, facilitating the calculation of the effective moment arm of the tensile reinforcement, and ensuring that the neutral axis remains in the slab, with the flange contributing significantly to the beam's compression capacity.

T-Beams Geometry			
bf	1000	(mm)	Flanges width
bw	200	(mm)	Beam width
h	360	(mm)	Beam Height
hf	140	(mm)	Flange thickness
L	6000	(mm)	Length

Material Properties			
$\varnothing c$	0,65		
$\varnothing s$	0,85		
f'c	35	(Mpa)	Concrete Compressive Strength
fy	400	(MPa)	Steel Yield Strength
Ec	27989	(Mpa)	Concrete Elastic Modulus
Es	200000	(Mpa)	Steel Elastic Modulus
γc	2390	(kg/m3)	
$\alpha 1$	0,7975		
$\beta 1$	0,8825		

Calculations			
As	3000	(mm2)	
d - CG	418,5	(mm)	
a (pondéré)	56,2	(mm)	Neutral axis is in the slab
As min	296	(mm2)	
As max	12541	(mm2)	
rho	0,72%		
rho min	0,07%		
rho max	3,00%		
Over or under-reinforced	**Under-reinforced**		

Rebars										
			Nominal Area (mm2)	Nominal Diameter (mm)	Nb	Total Area (mm2)	d (mm)	ycg		
Bottom	Covering						20	20	10	
	Stirrup	10M	100,0	11,3				11,3	25,65	
	Rebar	25M	500,0	25,2	3	1500		25,2	43,9	456,1
	Spacing						50	50	81,5	
	Rebar	25M	500,0	25,2	3	1500		25,2	119,1	380,9

Figure B-1. Screenshot of Design Spreadsheet

Appendix C – Two and Three-dimensional Drawings

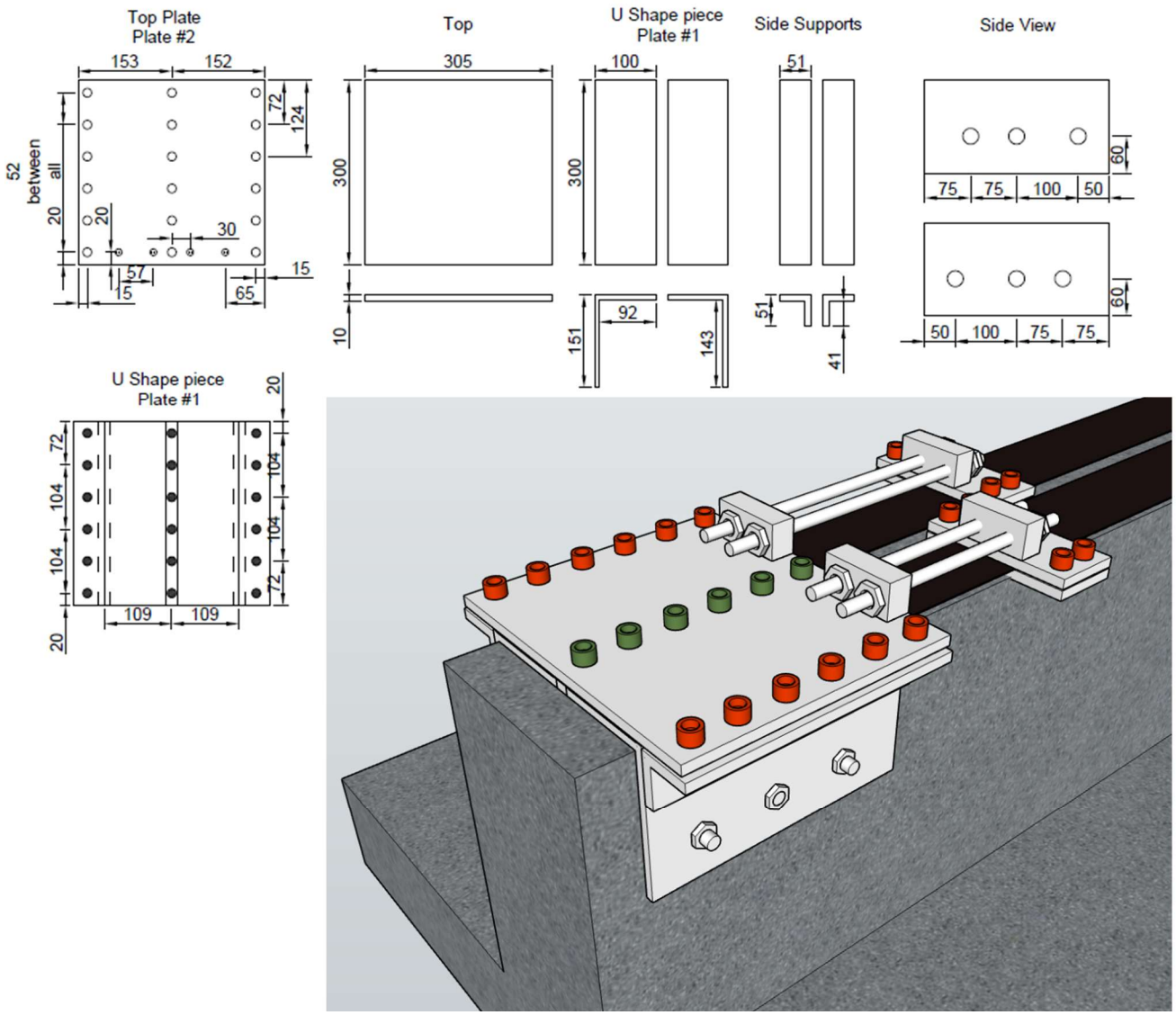

Anchors:
Single Layer Option
Version 1.1

Not to scale
All measurements are c/c when it comes to holes for bolts

Notes:

Weld extra piece between the angle iron used for the U-shape to fit the width of the beam or have a flange size to match half of the width of the beam

For Plate #2:
Dot pattern holes for tensioners. Only required on one anchor, all tapped

For Plate #1:
All holes to be tapped

Bolts used: ½" for all - adjust size of all other holes accordingly

Heavy Duty Wedge Expansion Anchor to attach the anchor system to the beam

Tensioners on a different drawing

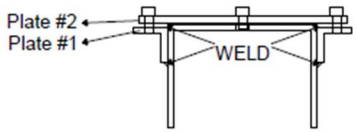

Figure C-1. Anchors' Drawings: Single Layer Option

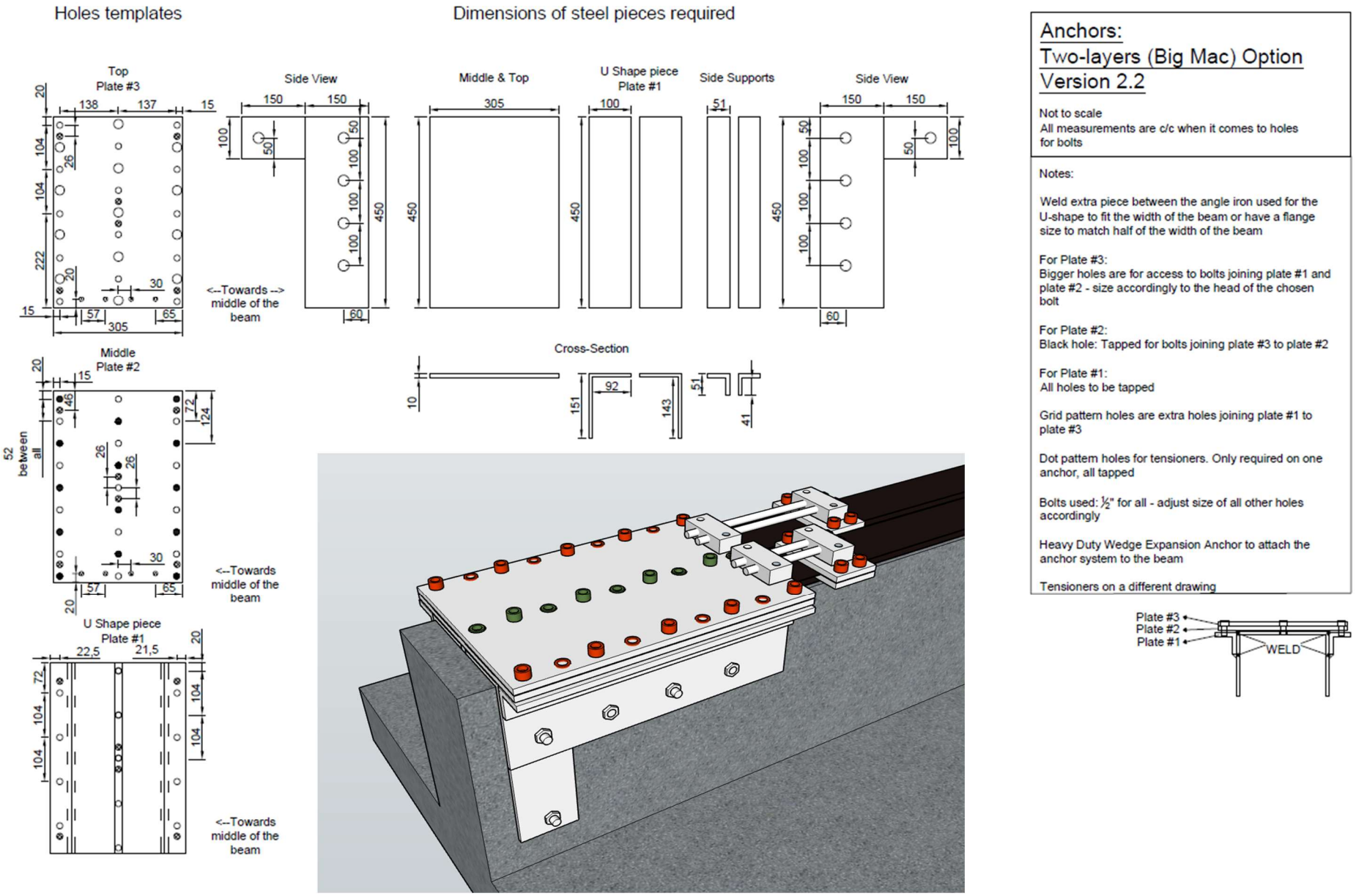

Figure C-2. Anchors' Drawings: Double-Layer Option

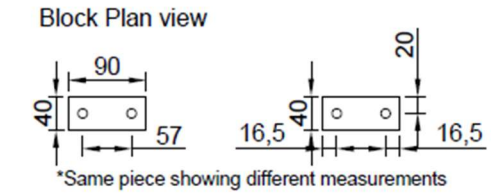

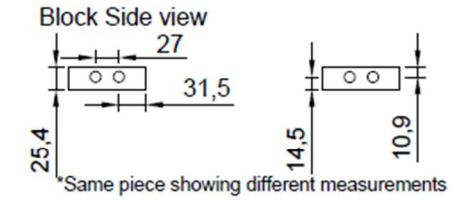

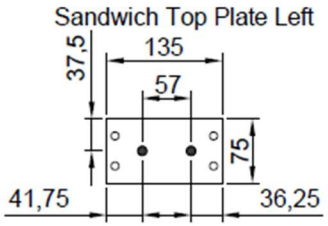

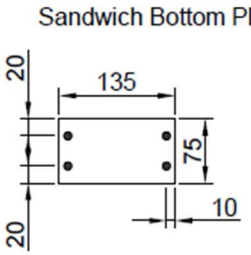

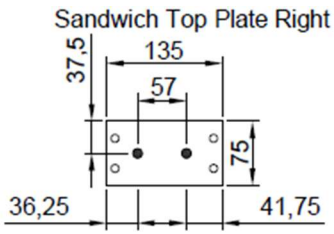

Notes:

½" high strength bolts used to join the blocks

7/16" bolts used to join the block to the sandwich/anchor

⅜" bolts used to tighten the sandwich

Two sandwiches are required, bottom plates holes to be tapped

Four blocks with the exact same hole patterns are required

Two of the block need the side view holes to be tapped (they go on the anchor, the other two go on the sandwiches)

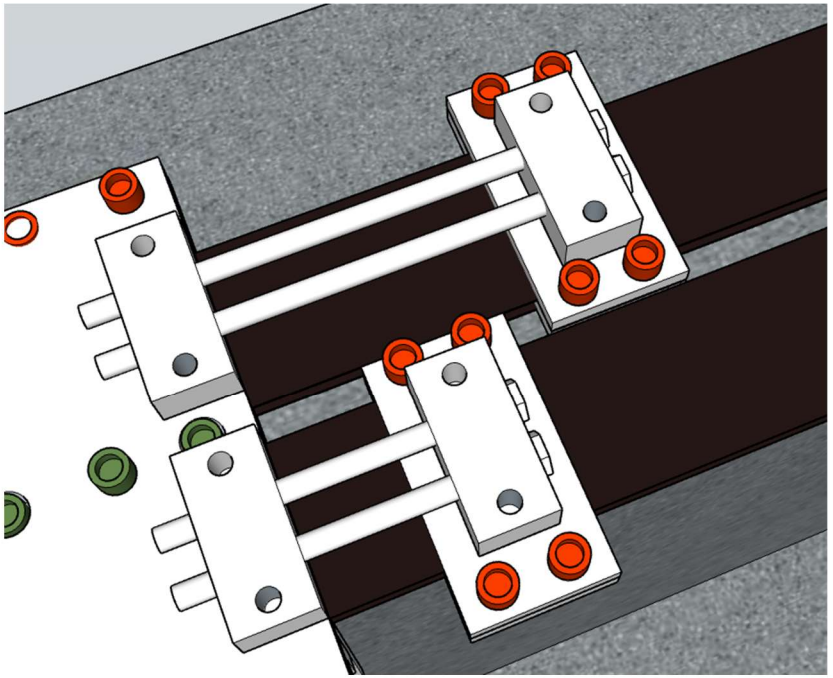

Anchors: Tensioners Version 2.1

Not to scale
All measurements are c/c when it comes to holes for bolts

Figure C-3. Anchors' Drawings: Tensioners

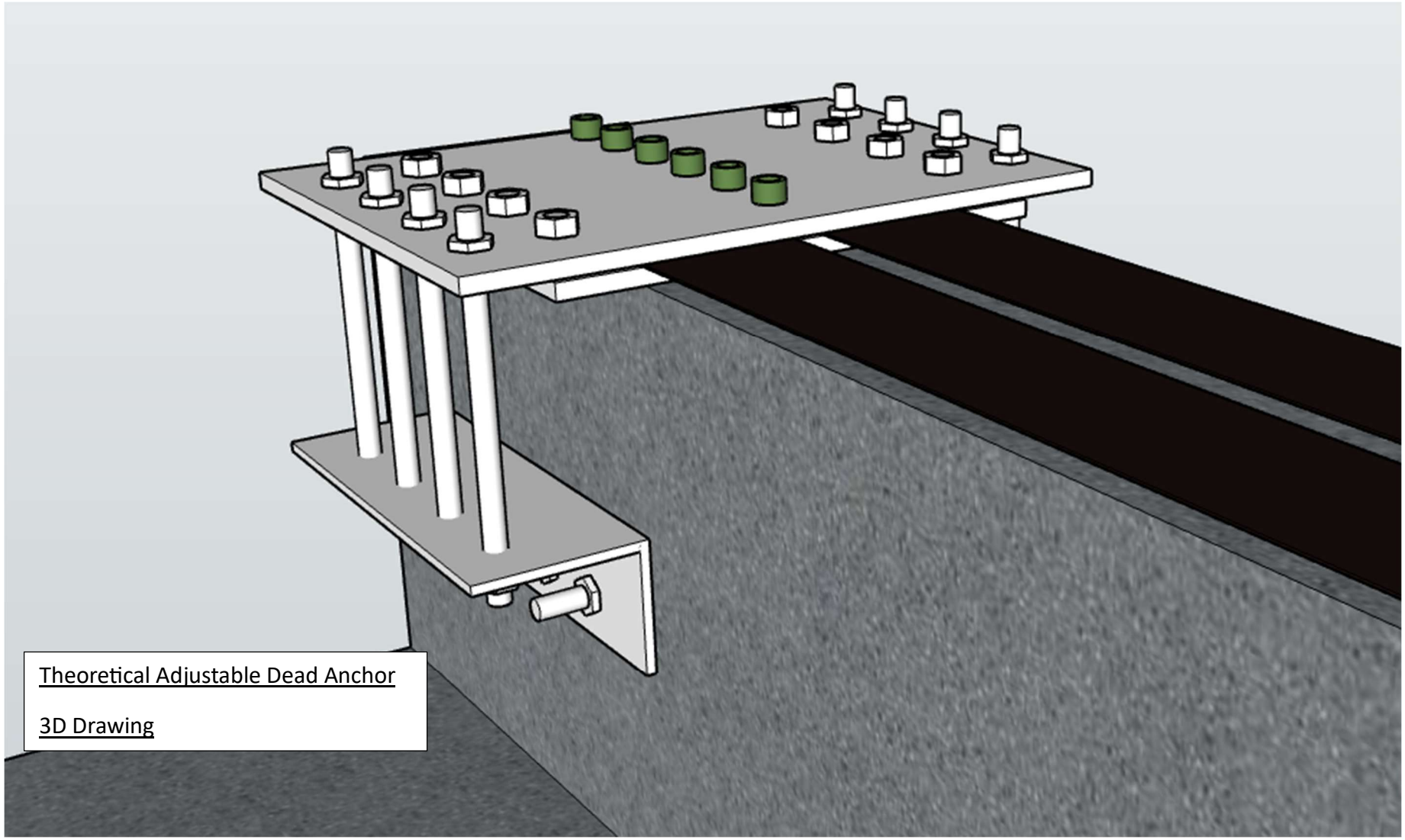

Figure C-4. Theoretical Adjustable Dead Anchor

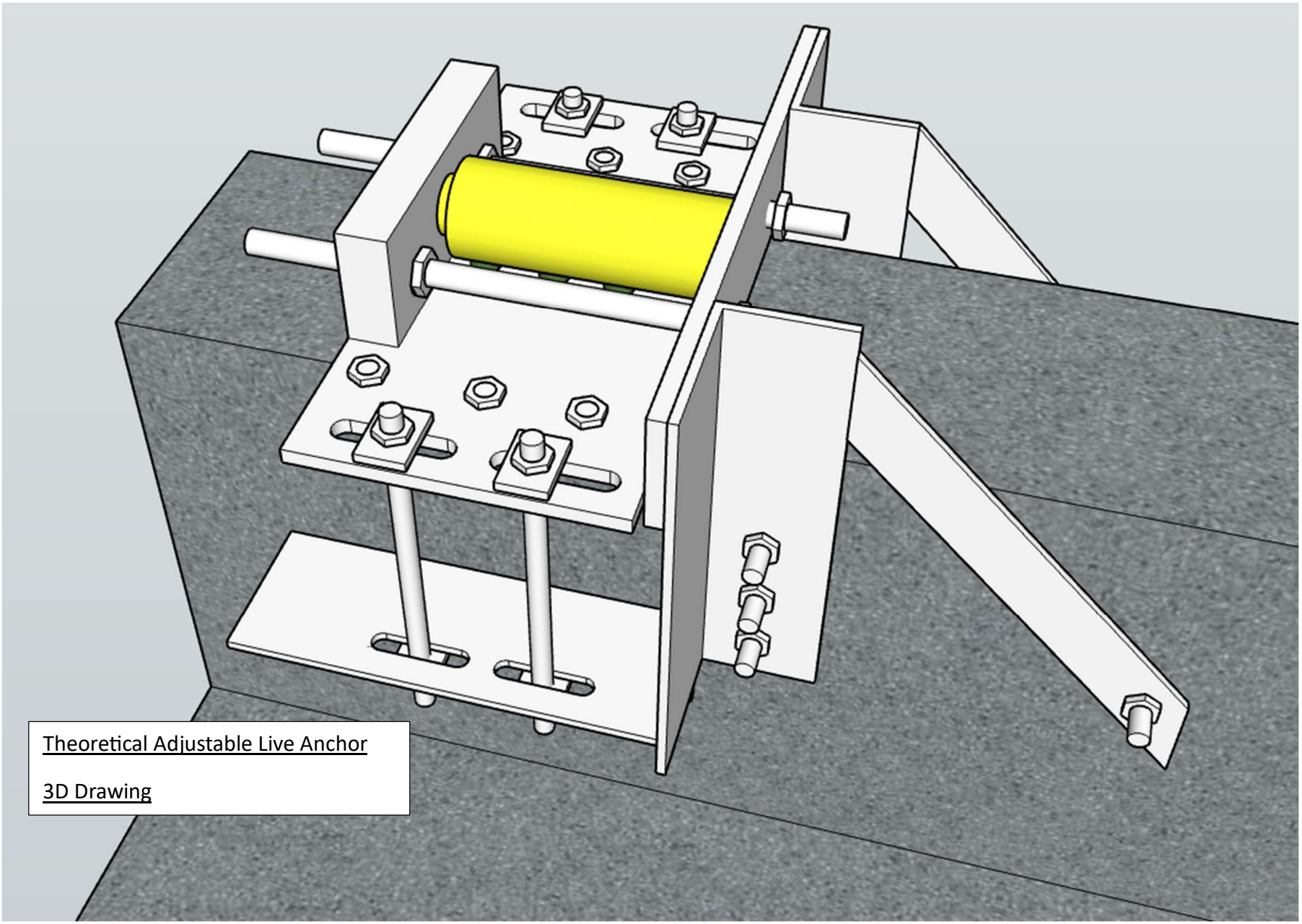

Figure C-5. Theoretical Adjustable Live Anchor

Appendix D - Supporting Details for the Moment-Curvature Predictive Model

Figure D-1 and D-2 shows the stress-strain relationship curves for steel, concrete, and CFRP which are fundamental in defining the material behaviour within the model. The values of concrete compressive strength (f'_c), strain of concrete (ε_c), tensile strength of steel (f_y), ultimate tensile strength of steel (F_u), ultimate strain of steel (ε_u), rupture strength of CFRP (f_{fu}) and rupture strain of CFRP (ε_f), circled in Figure D-3, are the basics of the curves, based on the theory of MacGregor (1988) and Collins & Mitchell (1997), for steel and concrete respectively. However, for steel, strain at hardening (ε_{sh}) was set at 0.0065 mm/mm, instead of 0.006 mm/mm from MacGregor, as per the tension test done a 25M coupons. The stress-strain relation for the curve for the CFRP is based on an estimated value of the ultimate values coming from the manufacturer as explained in Section 3.3.2 and Table 3-2.

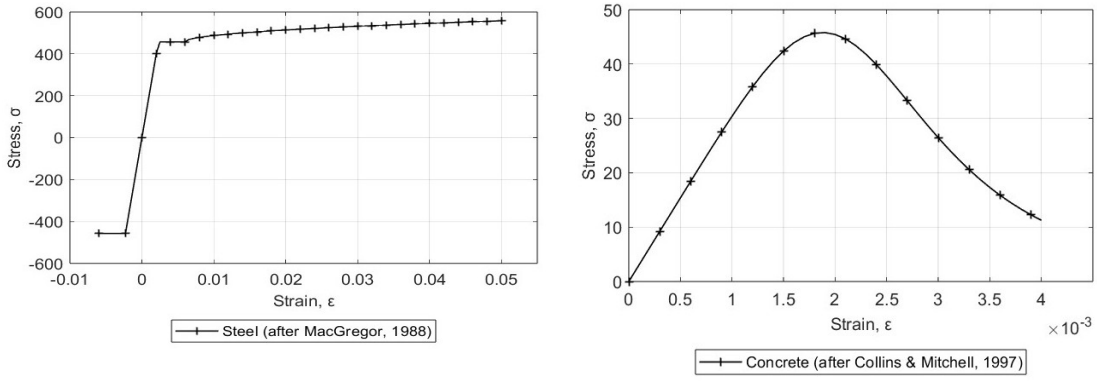

(a) Steel Stress-Strain Curve (MacGregor, 1988)

(b) Concrete Stress-Strain Curve (Collins & Mitchell, 1997)

Figure D-1. Steel and Concrete Stress-Strain Curves

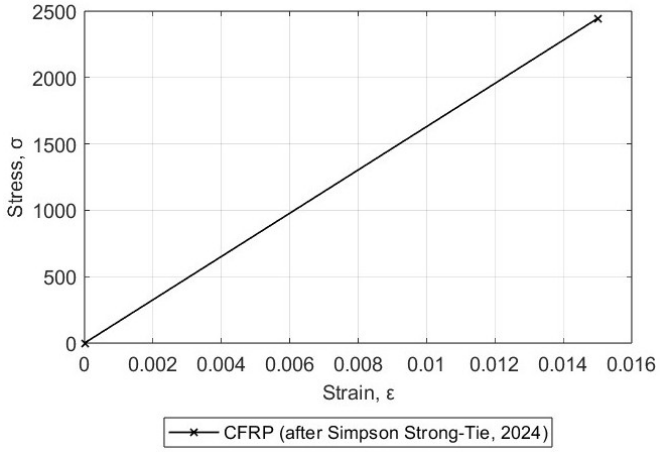

Figure D-2. CFRP Stress-Strain Curve

Details on the Predictive Model Spreadsheet – Figures D-3 & D-4

Figures D-3 and D-4 shows an example of the predictive model developed for this experiment, with the screenshot focusing specifically on SB-1.2. The design values for concrete and steel, circled in Figure D-3, are the same values used to create the stress-strain curves shown in Figure D-1. As described earlier, the ultimate stress and strain values for the CFRP were estimated.

In the model, the area of compression rebar depends on the strain assumed for the concrete. It ranges between 400 mm² and 1200 mm², varying based on whether the flange rebars contribute to the load. In the example shown in Figure D-4, ε_c strain in the concrete is set to 0.0027, which activates most of the rebars.

Each layer of concrete in compression, and up to the max tensile strength of the concrete, creates generates a corresponding force. Similarly, the steel in tension produces a force based on its area. The moment and curvature values are calculated by identifying the point where the sum of all layer forces equals zero. These values are then extracted and displayed in the output sheet, as shown in Table D-1.

Details on the Output from the Predictive Model – Table D-1

Table D-1 presents a sample output of the predictive model for SB-1.2. The "Moment" and "Phi" columns provide critical data for the load-displacement spreadsheet, referenced in Appendix E. Additionally, the theoretical neutral axis values found in Table 3-7 were calculated using the data from this output sheet, where linearity was assumed.

The table only shows values ranging from ε_c = -0.0001 to -0.0023 for clarity.

Material Resistance Factors		
$\emptyset_c$	1,00	Concrete
$\emptyset_s$	1,00	Rebar
$\emptyset_p$	1,00	Prestressing (TBD)

Concrete beam		
bf (mm)	1000	Width flange
hf (mm)	140	Depth flange
bw (mm)	200	Width web
hw (mm)	360	Depth web

I	3977964780	Inertia (mm4)
Icr	2831000000	Inertia (mm4)

Layers (for moment calcs)		
t (mm)	10	Thickness of layers
nb layers	50	
a	85,3	mm
c	100,658	mm

Design Factors - Steel Rebars		
fy	457	(MPa)
Es	200000	(MPa)
epsilon s	0,00229	
f's	-178,0877778	(MPa)
epsilon's	-0,002133498	
n	6,293665305	

Design Factors - Concrete		
f'c	49	(MPa)
Gamma	2390	(kg/m3)
Ec	31778	(MPa)
Cover	20	(mm)
Spacing	50	(mm)
epsilon c	0,0038	(mm/mm)
Alpha 1	0,7765	
Beta 1	0,8475	
Tensile Strength	4,2	
epsilon tension	0,000132167	

epsilon top	-0,00081	
epsilon bottom	0,002656197	

L	6000	(mm)

Sum	9744,191853	
epsilon t - epsilon b	-0,003466197	
per layer	-6,93239E-05	

Rebars Stress-Strain Curve		
Fu	557,54	(MPa)
Epsilon sh	0,0065	(mm/mm)
Epsilon u	0,05	(mm/mm)
Epsilon y	0,002285	(mm/mm)

Design Factors - CFRP & Epoxy		
E	163000	(MPa)
t	1,4	(mm)
Nb of layers	1	
epsilon f	0,015	(mm/mm)
ffu	2445	(MPa)
df		(mm)
w	180	(mm)
epsilon fe	0,0065079	(mm/mm)
epsilon fu	0,015	(mm/mm)
epsilon bi	0,0005	(mm/mm)

Omega	0,6666667	
Omege cr	0,474447	
Omega u	0,25	

n	5,1293372	

Figure D-3. Screenshot of Predictive Model Spreadsheet – Tombstone Data

Layer	b (mm)	thickness (mm)	top	bottom	centroid - d* (mm)	A conc (mm2)	epsilon c	sigma c (Mpa)	As (mm2)	epsilon s	sigma s (Mpa)	Afe (mm2)	epsilon fe	ffe (Mpa)	Ffrp (N)	Fc (N)	Fs (N)	M	ϕ
0							-0,0027												3,95537E-05
1	1070	10	0	10	5	10700	-0,002502232	-37,797304								-404431,151		-2,022155755	
2	1070	10	10	20	15	10700	-0,001908926	-45,78764								-489927,7449		-7,348916174	
3	1070	10	20	30	25	10700	-0,001513389	-42,37655								-453429,085		-11,33572713	
4	1070	10	30	40	35	10700	-0,001117852	-33,166872	1000	-0,0011179	-223,5704717	Compression reinforcement					-223570,4717	-7,824966511	
5	1070	10	40	50	45	10700	-0,000722315	-21,477651								-229810,865		-10,34148892	
6	1070	10	50	60	55	10700	-0,000326779	-9,2251153								-98708,73355		-5,428980345	
7	1070	10	60	70	65	10700	6,87584E-05	2,1148692								22629,10089		1,470891558	
8	1070	10	70	80	75	10700	0,000464295											0	
9	1070	10	80	90	85	10700	0,000859832											0	
10	1070	10	90	100	95	10700	0,001255369											0	
11	1070	10	100	110	105	10700	0,001650906											0	
12	1070	10	110	120	115	10700	0,002046443											0	
13	1070	10	120	130	125	10700	0,00244198											0	
14	1070	10	130	140	135	10700	0,002837517											0	
15	200	10	140	150	145	2000	0,003233054											0	
16	200	10	150	160	155	2000	0,003628591											0	
17	200	10	160	170	165	2000	0,004024127											0	
18	200	10	170	180	175	2000	0,004419664											0	
19	200	10	180	190	185	2000	0,004815201											0	
20	200	10	190	200	195	2000	0,005210738											0	
21	200	10	200	210	205	2000	0,005606275											0	
22	200	10	210	220	215	2000	0,006001812											0	
23	200	10	220	230	225	2000	0,006397349											0	
24	200	10	230	240	235	2000	0,006792886											0	
25	200	10	240	250	245	2000	0,007188423											0	
26	200	10	250	260	255	2000	0,00758396											0	
27	200	10	260	270	265	2000	0,007979497											0	
28	200	10	270	280	275	2000	0,008375033											0	
29	200	10	280	290	285	2000	0,00877057											0	
30	200	10	290	300	295	2000	0,009166107											0	
31	200	10	300	310	305	2000	0,009561644											0	
32	200	10	310	320	315	2000	0,009957181											0	
33	200	10	320	330	325	2000	0,010352718											0	
34	200	10	330	340	335	2000	0,010748255											0	
35	200	10	340	350	345	2000	0,011143792											0	
36	200	10	350	360	355	2000	0,011539329											0	
37	200	10	360	370	365	2000	0,011934866											0	
38	200	10	370	380	375	2000	0,012330403											0	
39	200	10	380	390	385	2000	0,01272594		1500	0,0127259	496,3020262	Top row of tension reinforcement					744453,0394	286,6144202	
40	200	10	390	400	395	2000	0,013121476											0	
41	200	10	400	410	405	2000	0,013517013											0	
42	200	10	410	420	415	2000	0,01391255											0	
43	200	10	420	430	425	2000	0,014308087											0	
44	200	10	430	440	435	2000	0,014703624											0	
45	200	10	440	450	445	2000	0,015099161											0	
46	200	10	450	460	455	2000	0,015494698		1500	0,0154947	503,7037224	Bottom row of tension reinforcement					755555,5836	343,7777905	
47	200	10	460	470	465	2000	0,015890235											0	
48	200	10	470	480	475	2000	0,016285772											0	
49	200	10	480	490	485	2000	0,016681309											0	
50	200	10	490	500	495	2000	0,017076846											0	
51	200	10			510		0,017670151					252	0,004542538	740,4336485	186589,2794			95,1605325	
52	200	10			520		0,018065688					252	0,004641422	756,5517775	190651,0479			95,32552397	
							0,402147631			0,0271028		504	0,00918396	1496,985426	377240,3274	-1653678,479	1276438,151	778,0469239	3,95537E-05
															0				
															Sum	0			

Figure D-4. Screenshot of Predictive Model

Table D-1. Output from the Predictive Model

Epsilon top	Epsilon Bottom	Moment	Phi	Neutral Axis	Compression Block
-0,0001	0,000226165	68,65035514	0,000652331	133,4668726	113,1131746
-0,0002	0,000603721	131,5430352	0,001607442	107,4791611	91,08858902
-0,0003	0,00092833	194,6432598	0,002456659	105,4053465	89,33103116
-0,0004	0,001200752	246,5460238	0,003201503	107,9471808	91,4852357
-0,0006	0,0019	388,0740343	0,005	103,5	87,71625
-0,0007	0,002173462	442,4156271	0,005746923	105,1238749	89,09248398
-0,0008	0,002590829	508,7934752	0,006781657	101,6687382	86,16425558
-0,0009	0,002989502	539,8083457	0,007779004	99,62644446	84,43341168
-0,0011	0,004316667	581,0895482	0,010833333	86,88461538	73,63471154
-0,0013	0,0062	602,8558088	0,015	73,5	62,29125
-0,0014	0,00735	584,9224601	0,0175	67,5	57,20625
-0,0015	0,00808393	596,3855652	0,019167859	65,93040072	55,87601461
-0,0017	0,01017988	625,5153573	0,023759759	59,89459138	50,76066619
-0,0018	0,011116667	635,9852466	0,025833333	58,20967742	49,33270161
-0,0019	0,011863672	644,6198337	0,027527344	57,62005106	48,83299327
-0,002	0,012789142	653,855995	0,029578283	56,35545889	47,76125141
-0,0021	0,014274975	666,0407084	0,03274995	53,21001139	45,09548465
-0,0023	0,0162	683,4001092	0,037	51,44594595	43,60043919

Appendix E - Supporting Details for the Load-Deflection Predictive Model

Figure E-1 presents the approach used to relate moment-curvature to load-deflection, following the methodologies outlined by Collins and Mitchell (1997) and Wight (1998). And using Equation 2 presented in Section 3.5.2 for the integration.

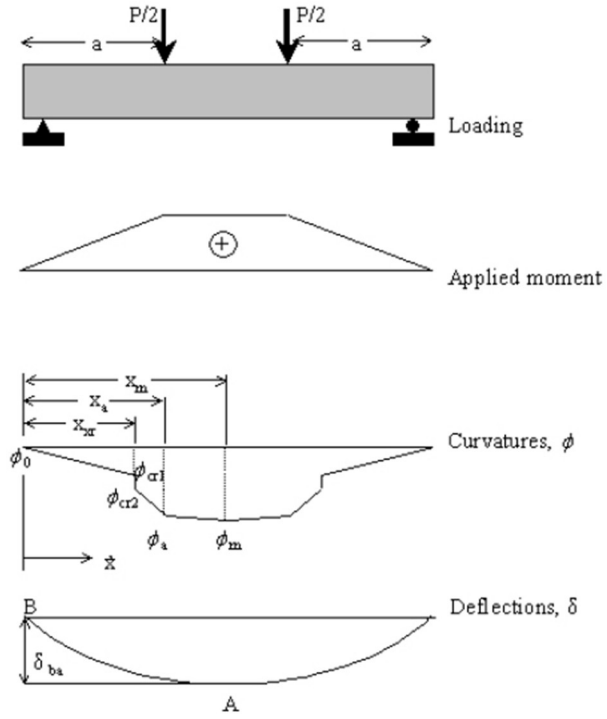

Figure E-1. Estimating deflections using curvatures (adapted from Collins and Mitchell, 1997 and Wight, 1998)

In the example spreadsheet shown in Figure E-2, loads (column C) were randomly selected within a specified range, and then multiplied by the moment arm at a chosen interval of 0.1 m to calculate the corresponding moments (D). These calculated moments were then compared against the list of moments extracted from the predictive model (A). For moments not explicitly listed, the corresponding curvature was interpolated using the moment-curvature data (A) (B). The interpolated curvatures (E) were integrated along the beam to determine deflections (F) at specific locations, resulting in 29 terms for the integration. By summing these deflections, the total mid-span displacement for a given load was approximated (G). While the model is simplified, it provides a basic representation of the expected behavior under loading conditions.

Note that the excerpt displayed below displays only two of the 29 moments arms required to compute the total displacement.

The two columns below are calculated from the Moment-Curvature model				1st Sect			2nd Sect			
Mom	Curv	Mom Arm (m)	P (kN)	M (kNm)	Curv	Disp (m)	M (kNm)	Curv	Disp (m)	Total Disp (mm)
				0,1			0,2			
0	0		0	0	0	0	0	0	0	0
68,65035514	0,000652		15	0,75	7,12666E-06	1,78167E-07	1,5	1,42533E-05	4,63233E-07	0,585419654
131,5430352	0,001607		30	1,5	1,42533E-05	3,56333E-07	3	2,85066E-05	9,26466E-07	1,170839308
194,6432598	0,002457		45	2,25	2,138E-05	5,345E-07	4,5	4,276E-05	1,3897E-06	1,756258961
246,5460238	0,003202		60	3	2,85066E-05	7,12666E-07	6	5,70133E-05	1,85293E-06	2,385198499
388,0740343	0,005		75	3,75	3,56333E-05	8,90833E-07	7,5	7,12666E-05	2,31617E-06	3,198448707
442,4156271	0,005747		100	5	4,75111E-05	1,18778E-06	10	9,50222E-05	3,08822E-06	4,662443655
508,7934752	0,006782		120	6	5,70133E-05	1,42533E-06	12	0,000114027	3,70586E-06	5,827851454
539,8083457	0,007779		140	7	6,65155E-05	1,66289E-06	14	0,000133031	4,32351E-06	6,958831492
581,0895482	0,010833		160	8	7,60177E-05	1,90044E-06	16	0,000152035	4,94115E-06	8,084739324
602,8558088	0,015		180	9	8,55199E-05	2,138E-06	18	0,00017104	5,5588E-06	9,237667508
584,9224601	0,0175		210	10,5	9,97733E-05	2,49433E-06	21	0,000199547	6,48526E-06	10,95431525
596,3855652	0,019168		240	12	0,000114027	2,85066E-06	24	0,000228053	7,41173E-06	12,59157625
625,5153573	0,02376		270	13,5	0,00012828	3,207E-06	27	0,00025656	8,33819E-06	14,20609758
635,9852466	0,025833		300	15	0,000142533	3,56333E-06	30	0,000285066	9,26466E-06	15,80695065
644,6198337	0,027527		330	16,5	0,000156787	3,91966E-06	33	0,000313573	1,01911E-05	17,42506557
653,855995	0,029578		360	18	0,00017104	4,276E-06	36	0,00034208	1,11176E-05	19,08907075
666,0407084	0,03275		390	19,5	0,000185293	4,63233E-06	39	0,000370586	1,20441E-05	20,8457376
683,4001092	0,037		420	21	0,000199547	4,98866E-06	42	0,000399093	1,29705E-05	22,84696743
687,4979177	0,038597		450	22,5	0,0002138	5,345E-06	45	0,0004276	1,3897E-05	26,32308068
695,3037103	0,040796		480	24	0,000228053	5,70133E-06	48	0,000456106	1,51091E-05	37,51980116
698,3254617	0,041979		510	25,5	0,000242307	6,05766E-06	51	0,000484613	1,64192E-05	55,01429584
702,6646989	0,043502		530	26,5	0,000251809	6,29522E-06	53	0,000503617	1,72926E-05	64,79956742
710,7777343	0,046614		550	27,5	0,000261311	6,53277E-06	55	0,000522622	1,81661E-05	78,24798288
713,7696738	0,047874		560	28	0,000266062	6,65155E-06	56	0,000532124	1,86028E-05	86,57733435
715,9235052	0,049		570	28,5	0,000270813	6,77033E-06	57	0,000541626	1,90395E-05	94,3988962
723,5083243	0,051306		580	29	0,000275564	6,88911E-06	58	0,000551129	1,94762E-05	103,111666
729,163055	0,054072		590	29,5	0,000280315	7,00788E-06	59	0,000560631	1,99129E-05	112,4009477
730,26173	0,055									
(A)	(B)		(C)	(D)	(E)	(F)				(G)

Figure E-2. Excerpt of Load-Displacement Spreadsheet